POLITECNICO DI TORINO

Master's Degree in Physics of Complex Systems

Master's Degree Thesis

Numerical schemes for dynamical mean-field theory on finitely-connected graphs

Supervisor

Prof. Luca DALL'ASTA

Candidate

Lorenzo DEMICHELIS

December 2024

Acknowledgements

I would like to express my deepest gratitude to those who have supported me throughout this journey. First and foremost, I am profoundly thankful to my family and my friends for their unwavering support and encouragement, which have been my anchor during both the challenging and rewarding moments of this endeavor.

I owe special thanks to Professor Luca Dall'Asta, whose guidance and patience have been fundamental for this work. I am also thankful to Mattia Tarabolo, who contributed to this thesis with his insight and effective suggestions.

Lorenzo

Abstract

The cavity method is an effective technique born to analyze classical system defined on graphs, and then also quantum systems, at equilibrium; by exploiting graphical models, it is indeed possible to derive self-consistent equations for one-site cavity marginals that, if obtained, allow for the computation of full one-site marginals, so that local observables can be easily computed. At equilibrium, and especially in the case of quantum systems, the results obtained with the cavity method provide a starting point for the application of the dynamical mean-field theory approach: this allows for a description of a many-body problem as a one-body problem by means of a set of effective quantities that have to be computed self-consistently. The dynamical mean-field theory approach has proven its effectiveness in many-body quantum mechanics for the analysis of both fermionic (F-DMFT) and bosonic (B-DMFT) systems. The approach based on the cavity method and on dynamical mean-field theories for the analysis of classical and quantum systems at equilibrium can be extended to out-of-equilibrium classical systems; these can be defined as a set of stochastic differential equations on a graph, each of them describing the behavior of a degree of freedom associated to a node subjected to a local term, to the interactions with the neighbors and to an additive noise. Again with the help of graphical models, it is possible to apply the dynamic cavity method to derive a set of self-consistent equations for the cavity marginals and then for the full marginals; by performing a large connectivity expansion typical of the dynamical mean-field theory approach, one is able to obtain a set of effective stochastic differential equations, one for each degree of freedom, where the interaction term gets substituted by a set of terms involving cavity mean functions, cavity correlation functions and cavity response functions. The set of effective equations can be reduced to a single effective equation, with a single cavity mean function, a single cavity correlation function and a single response function, if one considers regular graphs, like a Bethe lattice; it is also possible to analyze disordered systems with this approach by performing configurational averages. The goal of this thesis is the development of an algorithm aimed at computing the cavity mean function, the cavity correlation function and the cavity response function appearing in the effective stochastic differential equation of a generic dynamics defined on a Bethe lattice with linear interactions and additive noise. From a conceptual point of view the structure of the algorithm is the following: the cavity quantities are initialized, then they are used to generate a certain number of trajectories according to the effective equation of the dynamics, which in turn are used to update the cavity quantities in an iterative fashion until convergence is reached. After convergence, the cavity quantities can be plugged into the effective

equation of the dynamics, so that trajectories can be generated in order to perform a statistical analysis of the dynamics under exam.

Table of Contents

List of Figures

Chapter 1

The cavity method

1.1 Introduction

The purpose of this chapter is to present the cavity method for classical systems[1] and quantum systems[2][3][4]. The physical model that allows to easily show the ideas behind this approach is nothing but the Ising model on a Bethe lattice for the classical case, which is then promoted to a system of quantum spins in a transverse field for the quantum case on the same underlying graph. Starting from the classical case, the cavity method is presented in its simplest form, then it is generalized to deal with the heterogeneity of the couplings and fields; to apply the method to the quantum system, the Suzuki-Trotter procedure is introduced, which has proven to be an extremely effective technique able to transform any quantum system into a classical system with an extra dimension; once the classical counterpart is obtained, it is possible to apply the same ideas developed for the classical system. However, the formal complexity of the quantum system turned classical have prompted the derivation of simplified, but still effective, techniques, like the projected cavity mapping approach and the cavity mean-field approximation.

1.2 The classical cavity method

1.2.1 The cavity method on a Bethe lattice

The cavity method is a powerful tool in the field of statistical physics, as it allows to analyze various types of systems; it was introduced to treat classical spin models characterized by disorder, but it has been proven effective also to deal with complex optimization problem and in the field of condensed matter physics.

The simplest way to present the classical cavity method is by means of a practical example[1]; therefore, let us consider an Ising system with nearest neighbor

interactions on a Bethe lattice, that is a tree-like graph $G = (V, E)$, with V being the node set and E being the edge set, characterized by the following Hamiltonian:

$$H(\underline{\sigma}) = -J \sum_{\langle i,j \rangle} \sigma_i \sigma_j - h \sum_i \sigma_i \tag{1.1}$$

where $J > 0$ is the coupling constant, h is the external field and $\underline{\sigma} = \left\{\sigma_i \in \{-1,1\} : i \in V\right\}$ is a configuration of simple spin variables.

The Boltzmann-Gibbs measure is simply given by:

$$c(\underline{\sigma}) = \frac{1}{\mathcal{Z}} e^{-\beta H(\underline{\sigma})} \tag{1.2}$$

with $\mathcal{Z} = \sum_{\underline{\sigma}} e^{-\beta H(\underline{\sigma})}$ being the partition function and β being the inverse temperature.

The cavity method takes advantage of the natural recursive structure of the underlying infinite tree on which the system is defined; it is useful to introduce the following two quantities:

- $\mathcal{Z}_{i\to j}(\sigma_i)$: it is the partial partition function associated to the directed edge (i, j) for the subtree rooted in i, excluded the branch directed toward j

- $\mathcal{Z}_i(\sigma_i)$: it is the partition function of the whole tree, with a fixed value of σ_i

For these quantities it is possible to derive simple recursive relations:

$$\mathcal{Z}_{i\to j}(\sigma_i) = e^{\beta h \sigma_i} \prod_{k \in \partial i \setminus j} \left(\sum_{\sigma_k} \mathcal{Z}_{k\to i}(\sigma_k) e^{\beta J \sigma_i \sigma_k} \right) \tag{1.3}$$

$$\mathcal{Z}_i(\sigma_i) = e^{\beta h \sigma_i} \prod_{k \in \partial i} \left(\sum_{\sigma_k} \mathcal{Z}_{k\to i}(\sigma_k) e^{\beta J \sigma_i \sigma_k} \right) \tag{1.4}$$

with ∂i being the neighborhood of node i, that is $\partial i = \{j \in V : (i, j) \in E\}$.

The partial partition functions defined above can be used to derive the following probability distributions:

$$c_{i\to j}(\sigma_i) = \frac{\mathcal{Z}_{i\to j}(\sigma_i)}{\sum_{\sigma'} \mathcal{Z}_{i\to j}(\sigma')} = \tag{1.5a}$$

$$= \frac{1}{z_{i\to j}} e^{\beta h \sigma_i} \prod_{k \in \partial i \setminus j} \left(\sum_{\sigma_k} c_{k\to i}(\sigma_k) e^{\beta J \sigma_i \sigma_k} \right) \tag{1.5b}$$

$$c_i(\sigma_i) = \frac{\mathcal{Z}_i(\sigma_i)}{\sum_{\sigma'} \mathcal{Z}_i(\sigma')} = \tag{1.6a}$$

$$= \frac{1}{z_i} e^{\beta h \sigma_i} \prod_{k \in \partial i} \left(\sum_{\sigma_k} c_{k \to i}(\sigma_k) e^{\beta J \sigma_i \sigma_k} \right) \tag{1.6b}$$

with $z_{i \to j}$ and z_i being simple normalization constants.

It is worth to mention that it is possible to deal with this type of recursive equations by means of factor graphs. Indeed, the Boltzmann-Gibbs measure of the model under exam can be rewritten as a product of factors:

$$c(\underline{\sigma}) = \frac{1}{\mathcal{Z}} e^{-\beta H(\underline{\sigma})} = \frac{1}{\mathcal{Z}} \prod_{\langle i,j \rangle} \psi_{ij}(\sigma_i, \sigma_j) \prod_i \psi_i(\sigma_i) \tag{1.7}$$

with $\psi_{ij}(\sigma_i, \sigma_j) = e^{\beta J \sigma_i \sigma_j}$ and $\psi_i(\sigma_i) = e^{\beta h \sigma_i}$. If the graph G on which the Ising model is defined is a tree, then also the corresponding factor graph is a tree; an example of tree-like factor graph for the Ising model is represented in figure 1.1, where factor nodes are represented using white rectangles and variable nodes are represented using black dots.

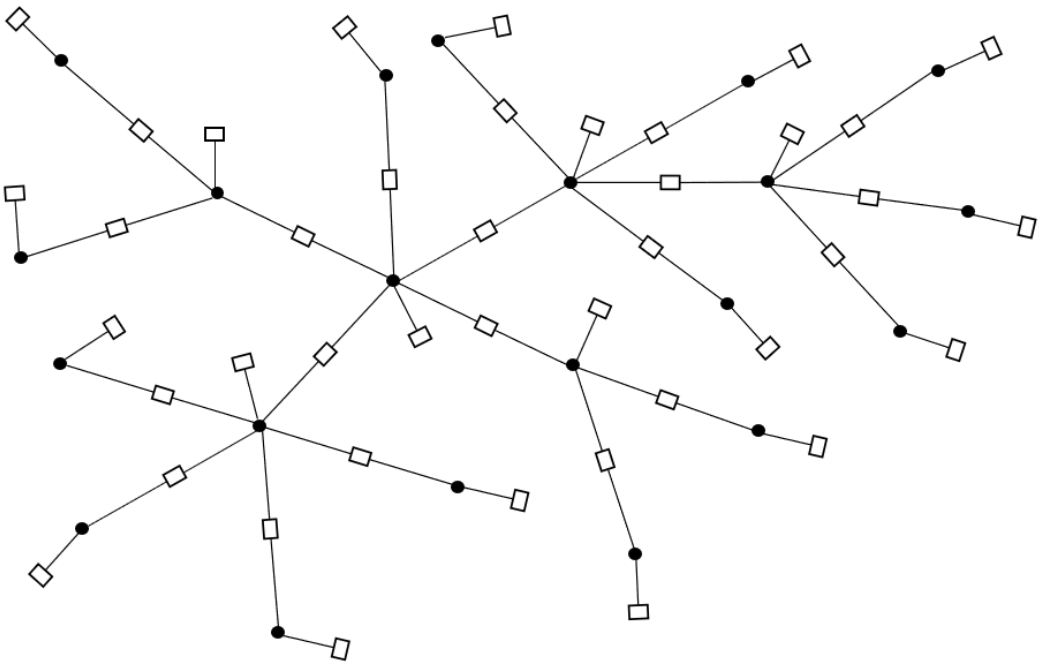

Figure 1.1: Example of factor graph for the Ising model defined on a tree.

If the graph G is a finite tree, the set of recursive equations has a single solution, which can be obtained by propagating the recursion starting from the leaves of the tree. The recursive step is represented pictorially in figure 1.2.

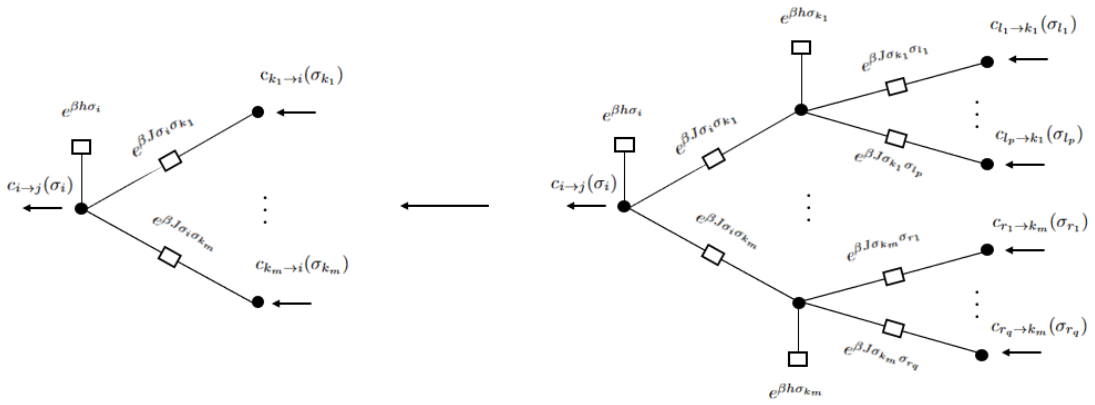

Figure 1.2: Pictorial representation of the recursive relation.

Once the probability distributions $\{c_{i\to j}(\sigma_i), c_{j\to i}(\sigma_j)\}_{(i,j)\in E}$ have been computed, it is possible to get the set of the other distributions $\{c_i(\sigma_i)\}_{i\in V}$, which are nothing but the marginal Boltzmann-Gibbs distributions; indeed, it is possible to write:

$$c_i(\sigma_i) = \sum_{\underline{\sigma}\setminus\{\sigma_i\}} c(\underline{\sigma}) \tag{1.8}$$

with $\underline{\sigma}$ indicating a specific configuration of the set of spin variables; the knowledge of the distribution $c_i(\sigma_i)$ allows for the computation of local observables, which can be obtained as $\langle O_i\rangle = \sum_{\sigma_i} O_i(\sigma_i)c_i(\sigma_i)$.

The cavity method can be applied also on graphs which are not tree-like, although in these situations the distributions that are obtained are just approximations of the real ones.

It is interesting to consider what happens on a Bethe lattice, that is on an infinite tree in which each node has exactly the same connectivity K; on such a graph, the quantities $c_{i\to j}$ become the same on all edges, hence, it is convenient to replace them with the common quantity $c_{cav}(\sigma)$. For $c_{cav}(\sigma)$ it is possible to write the following self-consistent equation:

$$c_{cav}(\sigma) = \frac{1}{z_{cav}} e^{\beta h\sigma} \sum_{\sigma_1,\ldots,\sigma_{K-1}} c_{cav}(\sigma_1)\ldots c_{cav}(\sigma_{K-1}) e^{\beta J\sigma(\sigma_1+\ldots+\sigma_{K-1})} \tag{1.9}$$

with z_{cav} being a simple normalization constant.

The full Boltzmann-Gibbs distribution of a spin variable can be recovered as:

$$c(\sigma) = \frac{1}{z} e^{\beta h \sigma} \sum_{\sigma_1,\ldots,\sigma_K} c_{cav}(\sigma_1)...c_{cav}(\sigma_{K-1}) e^{\beta J \sigma(\sigma_1+\ldots+\sigma_K)} \tag{1.10}$$

where all the neighbors of a node are taken into account and where z is just another normalization constant.

It is worth noticing that the system can be described in an even simpler way by introducing a cavity field h_{cav} and an effective field h_{eff}; this comes from the fact that, since a spin variable σ can take just two values, both the distributions $c_{cav}(\sigma)$ and $c(\sigma)$ can be parametrized with a single quantity. The best suited parametrization is the following one:

$$c_{cav}(\sigma) = \frac{e^{\beta h_{cav} \sigma}}{2cosh(\beta h_{cav})} \tag{1.11}$$

$$c(\sigma) = \frac{e^{\beta h_{eff} \sigma}}{2cosh(\beta h_{eff})} \tag{1.12}$$

By plugging the expressions above into the equation for c_{cav} and c and by performing the required computations, the following expressions for the cavity field and for the effective field are obtained:

$$h_{cav} = h + \frac{K-1}{\beta} \operatorname{atanh}[\tanh(\beta J) \tanh(\beta h_{cav})] \tag{1.13}$$

$$h_{eff} = h + \frac{K}{\beta} \operatorname{atanh}[\tanh(\beta J) \tanh(\beta h_{cav})] \tag{1.14}$$

It is not hard to see that, in the absence of an external field ($h = 0$), the expected behavior of the system is recovered: a phase transition at a critical temperature β_c separates a low temperature phase, in which h_{cav} and h_{eff} are both different from zero, from a high temperature phase in which both h_{cav} and h_{eff} vanish; the critical temperature of the Ising model defined on a Bethe lattice is obtained from the self-consistent equation for the effective field and it is equal to $\beta_c = \frac{1}{J} \operatorname{atanh}(\frac{1}{K})$.

The one that has been discussed up to now is just a simplified presentation of the cavity method; its power emerges if the magnetic fields associated to the vertices and the couplings associated to the edges of the underlying graph are allowed to be heterogeneous. This increased freedom in the parameters of the system is responsible for a much richer physical picture, but it is also responsible for a more complex mathematical description.

At this point the generalization of the cavity method to a system with heterogeneous parameters can be presented; for convenience the graph on which the system is defined is still a Bethe lattice, in order to exploit once again the recursive structure of the tree and the fixed degree of each node. The coupling of each edge is sampled independently from a distribution $P(J_{ij})$ and the same can be done for the external magnetic fields with some distribution $P(h_i)$.

On a finite graph, for a single realization of the entire set of couplings and of the external fields, the cavity method reduces to a message-passing algorithm that allows for the computation of the distributions $\{c_{i\to j}(\sigma_i)\}_{(i,j)\in E}$ and $\{c_i(\sigma_i)\}_{i\in V}$. The expressions of this algorithm are nothing but the recursive relations that have already been presented, corrected to account for heterogeneous couplings and fields:

$$c_{i\to j}(\sigma_i) = \frac{1}{z_{i\to j}} e^{\beta h_i \sigma_i} \prod_{k\in\partial i\setminus j} \left(\sum_{\sigma_k} c_{k\to i}(\sigma_k) e^{\beta J_{ik}\sigma_i\sigma_k} \right) \tag{1.15}$$

$$c_i(\sigma_i) = \frac{1}{z_{i\to j}} e^{\beta h_i \sigma_i} \prod_{k\in\partial i} \left(\sum_{\sigma_k} c_{k\to i}(\sigma_k) e^{\beta J_{ik}\sigma_i\sigma_k} \right) \tag{1.16}$$

If the graph is a tree the system of equations defined above has a unique fixed point; if instead loops are present, the landscape of fixed points is more complex and this can create issues for what concerns the convergence of the system of self-consistent equations.

1.2.2 Generalization to the case of heterogeneous couplings and fields

In the case of heterogeneous couplings it is still possible to perform a parametrization of both distributions $c_{i\to j}(\sigma_i)$ and $c_i(\sigma_i)$; this time the parametrization is achieved by introducing a "local cavity field" $h_{i\to j,cav}$ associated to the removal of each directed edge (i,j) and a "local effective field" $h_{i,eff}$ for each node i. The parametrized distributions read:

$$c_{i\to j}(\sigma_i) = \frac{e^{\beta h_{i\to j,cav}\sigma_i}}{2cosh(\beta h_{i\to j,cav})} \tag{1.17}$$

$$c_i(\sigma_i) = \frac{e^{\beta h_{i,eff}\sigma}}{2cosh(\beta h_{i,eff})} \tag{1.18}$$

If we now exploit once again the recursive relations for the distributions $c_{i\to j}(\sigma_i)$ and $c_i(\sigma_i)$ in the case of a finite tree and plug in those the parametrized distributions introduced above, we obtain the following relations for the parameters:

$$h_{i\to j,cav} = h_i + \frac{1}{\beta}\sum_{k\in\partial i\setminus j} \text{atanh}[\tanh(\beta J_{ik})\tanh(\beta h_{k\to i,cav})] \tag{1.19}$$

$$h_{i,eff} = h_i + \frac{1}{\beta}\sum_{k\in\partial i} \text{atanh}[\tanh(\beta J_{ik})\tanh(\beta h_{k\to i,cav})] \tag{1.20}$$

By solving all these equations one obtains the set of cavity fields $\{h_{i\to j,cav}\}_{(i,j)\in E}$ and the set of effective fields $\{h_{i,eff}\}_{i\in V}$, which allow to describe the behavior of the entire system and to compute observables. This approach based on the parametrization of the distributions is essentially equivalent to that based on the set of recursive relations for the distributions: in both cases one ends up with the entire set of distributions, so that observables can then be easily computed. There is however an important shortcoming for both approaches: they both hold for a single realization of the couplings and of the external fields, while it could be interesting to analyze the physics of the system independently from the specific realization of the parameters. With this idea in mind, the focus can now be shifted to derive a probability distribution for the cavity field h_{cav} and for the effective field h_{eff} by averaging over all the possible realizations of the couplings and of the external fields.

If the system is defined on a Bethe lattice with connectivity K, it is possible to consider a generic node i on the lattice and exploit some simple rules of probability[2][4]; in the following we can enumerate the neighbors of the node i from 1 to K, with the node K being the one disconnected for the cavity case. Starting from the equations (1.19) and (1.20), we can write the following self-consistent equations for $P(h_{cav})$, the distribution of the local cavity field, and $P(h_{eff})$, the distribution for the local effective field:

$$P(h_{cav}) = \int dh P(h) \prod_{q=1}^{K-1} dJ_q P(J_q) \prod_{q=1}^{K-1} dh_{q,cav} P(h_{q,cav}) \times \\ \times \delta\left(h_{cav} - h - \sum_{q=1}^{K-1} \frac{1}{\beta}\,\text{atanh}\left(\tanh(\beta J_q)\tanh(\beta h_{q,cav})\right)\right) \tag{1.21}$$

$$P(h_{eff}) = \int dh P(h) \prod_{q=1}^{d} dJ_q P(J_q) \prod_{q=1}^{K} dh_{q,cav} P(h_{q,cav}) \times \\ \times \delta\left(h_{eff} - h - \sum_{q=1}^{K} \frac{1}{\beta}\,\text{atanh}\left(\tanh(\beta J_q)\tanh(\beta h_{q,cav})\right)\right) \tag{1.22}$$

where the index i has been dropped from the external field and the couplings, since the specific node under exam is irrelevant being the graph a Bethe lattice.

The equations above are nothing but self-consistent equations for the distributions $P(h_{cav})$ and $P(h_{eff})$ respectively. To solve such equations it is necessary to exploit numerical methods(like the population dynamics algorithm[2]...), as an analytical solution is, in general, too difficult to get.

It is interesting to notice that, while in the case of homogeneous couplings the role of order parameter is played by the cavity field and by the effective field, in the heterogeneous case this role is played by the corresponding distributions, where the different phases of the system can be identified by monitoring the moments of the distributions themselves.

It is important to point out that such an equation can be derived for the Bethe lattice, which is an idealized perfectly recursive tree with vertices indistinguishable from each other, while for a generic tree with an heterogeneous structure each vertex is can in principle be different from all the others. In these kind of situations the method has to be generalized to account for the variable number of neighbors of each node.

1.2.3 Brief presentation of the population dynamics algorithm

To conclude this section about the classical cavity method it is worthy to show how to derive a distribution like that of the cavity field, on a Bethe lattice of connectivity K, defined by an equation of the type (1.21). The idea is to represent the distribution $P(h_{cav})$ by means of a population of field $h^1_{cav}, ..., h^M_{cav}$, with $M >> 1$; this population is then updated using the equation relating the cavity field on one node with the ones on its neighbors and the probability distributions of the couplings and of the external magnetic fields.

Once the population $h^1_{cav}, ..., h^M_{cav}$ has been initialized in some way, it is possible to perform the following iterative step:

1. choose $K-1$ indices $r_1, ..., r_{K-1} \in \{1, ..., M\}$ randomly uniformly
2. generate $K-1$ couplings $J_1, ..., J_{K-1}$ from the distribution $P(J)$, where we have assumed that the distribution of the coupling is the same on every edge
3. generate an external magnetic field h from the distribution $P(h)$, where we have assumed the distribution of the external magnetic field to be the same on every node
4. compute a new cavity field h^{new}_{cav} according to $h^{new}_{cav} = h + \\ + \frac{1}{\beta} \sum_{l=1}^{K-1} \text{atanh}\left(\tanh(\beta J_l)\tanh(\beta h^{r_l}_{cav})\right)$

5. choose an index $j \in \{1, ..., M\}$ and replace h^j_{cav} with the new value h^{new}_{cav} that just been computed

The convergence of the algorithm presented above can be monitored by checking the moments of the distribution $P(h_{cav})$, where the rth moment is defined as $\frac{1}{M}\sum_{i=1}^{M} {h^i_{cav}}^r$. If M is large enough, the population $h^1_{cav}, ..., h^M_{cav}$ provides a good approximation of the probability distribution $P(h_{cav})$.

1.3 The quantum cavity method

1.3.1 The Suzuki-Trotter procedure

In this section the quantum cavity method is presented[2][3][4]; for simplicity, the system under consideration is once again a spin system, but this time standard spin variables are replaced by quantum operators. Hence, the Hamiltonian operator reads:

$$\hat{H}(\sigma^z_1, ..., \sigma^z_N, \sigma^x_1, ..., \sigma^x_N) = -J \sum_{\langle i,j \rangle} \sigma^z_i \sigma^z_j - h \sum_i \sigma^x_i \tag{1.23}$$

where h is the external transverse field, J is the coupling constant between nearest neighbors and the underlying graph $G = (V, E)$ for the moment is a finite tree with N nodes.

Such an Hamiltonian operator describes a set of interacting spins subjected to an external transverse magnetic field; σ^z_i is the Pauli matrix associated to the direction z and to the site i on the graph, while σ^x_i is the Pauli matrix associated to the direction x and to the site i.

The Hilbert space of the system is spanned by the basis of 2^N vectors of the form $|\underline{\sigma}\rangle = |\sigma_1, ..., \sigma_N\rangle$, where $\sigma_i \in \{1, -1\}$ is representatives of the two possible eigenstates of the operator σ^z_i, $|\uparrow\rangle_i, |\downarrow\rangle_i$, associated to the eigenvalues 1 and -1 respectively.

It is convenient to recall the anti-commutation relations between the operators appearing in $\hat{H}$:

$$[\sigma^z_i, \sigma^z_j] = 0 \tag{1.24a}$$
$$[\sigma^x_i, \sigma^x_j] = 0 \tag{1.24b}$$
$$[\sigma^z_i, \sigma^x_j] = 2i\delta_{i,j}\sigma^y_i \tag{1.24c}$$

and also the action of the operators on the states of the basis:

$$\sigma_i^z|\sigma_1,...,\sigma_N\rangle = \sigma_i|\sigma_1,...,\sigma_N\rangle \tag{1.25a}$$
$$\sigma_i^x|\sigma_1,...,\sigma_i,...,\sigma_N\rangle = |\sigma_1,...,-\sigma_i,...,\sigma_N\rangle \tag{1.25b}$$

with $\sigma_i \in \{1,-1\}$.

Before applying the cavity method as it has been presented in the previous section, it is necessary to obtain an equivalent classical system by means of the Suzuki-Trotter approach; this is a well know method which allows to transform a quantum system in D-dimensions into a classical system in (D+1)-dimensions, where the extra dimension is that of imaginary time. This is achieved by exploiting the following trick for the partition function:

$$\mathcal{Z} = Tr[e^{-\beta\hat{H}}] = \lim_{N_s\to+\infty} Tr[(e^{-\frac{\beta}{N_s}\hat{H}})^{N_s}] = \lim_{N_s\to+\infty}\sum_{\underline{\sigma}}\langle\underline{\sigma}|(e^{-\frac{\beta}{N_s}\hat{H}})^{N_s}|\underline{\sigma}\rangle \tag{1.26}$$

The idea here is to split the imaginary time axis, which is closed on itself like a ring, into an infinite number of smaller intervals; then, it is possible to associate to each of these intervals an identity operator $\mathcal{I}$, so that it is possible to evaluate explicitly the expectation value of each operator $e^{-\frac{\beta}{N_s}\hat{H}}$.

Hence, if $\mathcal{I}^\alpha = \sum_{\underline{\sigma}^\alpha}|\underline{\sigma}^\alpha\rangle\langle\underline{\sigma}^\alpha|$ ($\alpha \in \{1,...,N_s\}$) is the identity operator associated to the time interval α, with $|\underline{\sigma}^\alpha\rangle = |\sigma_1^\alpha,...,\sigma_N^\alpha\rangle$, the partition function reads:

$$\mathcal{Z} = \lim_{N_s\to+\infty}\sum_{\underline{\sigma}}\langle\underline{\sigma}|\mathcal{I}^1 e^{-\frac{\beta}{N_s}\hat{H}}\mathcal{I}^2...\mathcal{I}^{N_s}e^{-\frac{\beta}{N_s}\hat{H}}|\underline{\sigma}\rangle \tag{1.27a}$$

$$= \lim_{N_s\to+\infty}\sum_{\underline{\sigma}^1,...,\underline{\sigma}^{N_s}}\prod_{\alpha=1}^{N_s}\langle\underline{\sigma}^\alpha|e^{-\frac{\beta}{N_s}\hat{H}}|\underline{\sigma}^{\alpha+1}\rangle \tag{1.27b}$$

where $\underline{\sigma}^\alpha \in \{-1,1\}^N$ is the configuration of the N spins in the time interval α.

Note that $\underline{\sigma}^1 = \underline{\sigma}^{N_s+1}$; this comes from the reorganization of the terms, which leads to the presence of the scalar product $\langle\underline{\sigma}|\underline{\sigma}^1\rangle = \delta_{\underline{\sigma},\underline{\sigma}^1}$ and to the identification $|\underline{\sigma}^{N_s+1}\rangle = |\underline{\sigma}\rangle$. This is the reason why it is said that the imaginary time axis is closed on itself as a ring.

At this point it is convenient to analyze each expectation value $\langle\underline{\sigma}^\alpha|e^{-\frac{\beta}{N_s}\hat{H}}|\underline{\sigma}^{\alpha+1}\rangle$ separately:

$$\langle\underline{\sigma}^\alpha|e^{-\frac{\beta}{N_s}\hat{H}}|\underline{\sigma}^{\alpha+1}\rangle = \langle\underline{\sigma}^\alpha|e^{\frac{\beta}{N_s}\sum_{\langle i,j\rangle}J\sigma_i^z\sigma_j^z+\frac{\beta h}{N_s}\sum_i\sigma_i^x}|\underline{\sigma}^{\alpha+1}\rangle = \tag{1.28a}$$

$$= e^{\frac{\beta}{N_s}\sum_{\langle i,j\rangle}J\sigma_i^\alpha\sigma_j^\alpha}\langle\underline{\sigma}^\alpha|e^{\frac{\beta h}{N_s}\sum_i\sigma_i^x}|\underline{\sigma}^{\alpha+1}\rangle = \tag{1.28b}$$

$$= e^{\frac{\beta}{N_s}\sum_{\langle i,j\rangle}J\sigma_i^\alpha\sigma_j^\alpha}\prod_{i=1}^{N}\langle\sigma_i^\alpha|e^{\frac{\beta h}{N_s}\sigma_i^x}|\sigma_i^{\alpha+1}\rangle \tag{1.28c}$$

This result has been obtained by neglecting the term of order $O\left(\frac{1}{N_s^2}\right)$ and smaller, which is reasonable since $N_s \to +\infty$.

In order to evaluate $\langle \sigma_i^\alpha | e^{\frac{\beta h}{N_s}\sigma_i^x} | \sigma_i^{\alpha+1} \rangle$, the exponential operator can be expanded in series:

$$e^{\frac{\beta h}{N_s}\sigma_i^x} = \sum_{k=0}^{\infty} \left(\frac{\beta h}{N_s}\right)^k (\sigma_i^x)^k = \tag{1.29a}$$

$$= \mathcal{I} + \frac{\beta h}{N_s}\sigma_i^x + \frac{1}{2}\left(\frac{\beta h}{N_s}\right)^2 (\sigma_i^x)^2 + \frac{1}{3!}\left(\frac{\beta h}{N_s}\right)^3 (\sigma_i^x)^3 + ... = \tag{1.29b}$$

$$= \mathcal{I} + \frac{\beta h}{N_s}\sigma_i^x + \frac{1}{2}\left(\frac{\beta h}{N_s}\right)^2 \mathcal{I} + \frac{1}{3!}\left(\frac{\beta h}{N_s}\right)^3 \sigma_i^x + ... \tag{1.29c}$$

$$\tag{1.29d}$$

where the properties of the Pauli matrices have been exploited, as $(\sigma_i^x)^k = \mathcal{I}$ if k is even and $(\sigma_i^x)^k = \sigma_i^x$ if k is odd.

By grouping the terms associated to the identity operator $\mathcal{I}$ and the terms associated to the spin operator σ_i^x, the exponential operator $e^{\frac{\beta h}{N_s}\sigma_i^x}$ can finally be rewritten as:

$$e^{\frac{\beta h}{N_s}\sigma_i^x} = \left(1 + \frac{1}{2}\left(\frac{\beta h}{N_s}\right)^2 + ...\right)\mathcal{I} + \left(\frac{\beta h}{N_s} + \frac{1}{3!}\left(\frac{\beta h}{N_s}\right)^3 + ...\right)\sigma_i^x = \tag{1.30a}$$

$$= \cosh\left(\frac{\beta h}{N_s}\right)\mathcal{I} + \sinh\left(\frac{\beta h}{N_s}\right)\sigma_i^x \tag{1.30b}$$

Now the computation of the expectation value $\langle \sigma_i^\alpha | e^{\frac{\beta h}{N_s}\sigma_i^x} | \sigma_i^{\alpha+1} \rangle$ is trivial:

$$\langle \sigma_i^\alpha | e^{\frac{\beta h}{N_s}\sigma_i^x} | \sigma_i^{\alpha+1} \rangle = \cosh\left(\frac{\beta h}{N_s}\right)\langle \sigma_i^\alpha | \mathcal{I} | \sigma_i^{\alpha+1} \rangle + \sinh\left(\frac{\beta h}{N_s}\right)\langle \sigma_i^\alpha | \sigma_i^x | \sigma_i^{\alpha+1} \rangle = \tag{1.31a}$$

$$= \cosh\left(\frac{\beta h}{N_s}\right)\delta_{\sigma_i^\alpha, \sigma_i^{\alpha+1}} + \sinh\left(\frac{\beta h}{N_s}\right)\delta_{\sigma_i^\alpha, -\sigma_i^{\alpha+1}} \tag{1.31b}$$

Such an expression can be recast by introducing the following parametrization:

$$\langle \sigma_i^\alpha | e^{\frac{\beta h}{N_s}\sigma_i^x} | \sigma_i^{\alpha+1} \rangle = e^{\Gamma \sigma_i^\alpha \sigma_i^{\alpha+1}} \tag{1.32}$$

The parameter Γ can be determined by solving the following system of equations:

$$\begin{cases} e^{\Gamma} = \cosh\left(\frac{\beta h}{N_s}\right) \\ e^{-\Gamma} = \sinh\left(\frac{\beta h}{N_s}\right) \end{cases} \tag{1.33}$$

which results in $\Gamma = \frac{1}{2\beta}\log\coth\left(\frac{\beta h}{N_s}\right)$.

All these results can be put together to derive the final expression of the partition function $\mathcal{Z}$:

$$\mathcal{Z} = \lim_{N_s\to+\infty} \sum_{\underline{\sigma}^1,\ldots,\underline{\sigma}^{N_s}} \prod_{\alpha=1}^{N_s} e^{\frac{\beta}{N_s}\sum_{\langle i,j\rangle} J\sigma_i^\alpha\sigma_j^\alpha + \beta\Gamma\sum_i \sigma_i^\alpha\sigma_i^{\alpha+1}} = \tag{1.34a}$$

$$= \lim_{N_s\to+\infty} \sum_{\underline{\sigma}^1,\ldots,\underline{\sigma}^{N_s}} e^{-\beta H_{ST}} \tag{1.34b}$$

with $H_{ST} = -\frac{1}{N_s}\sum_{\alpha=1}^{N_s}\sum_{\langle i,j\rangle} J\sigma_i^\alpha\sigma_j^\alpha - \Gamma\sum_{\alpha=1}^{N_s}\sum_i \sigma_i^\alpha\sigma_i^{\alpha+1}$ being the so-called Suzuki-Trotter Hamiltonian.

The system of N quantum spins has been transformed, by means of the Suzuki-Trotter approach, into a system of $N \times N_s$ classical spins, or, equivalently, into a system of N spin trajectories in imaginary time, where a spin trajectory can be thought of as a vector that can take 2^{N_s} possible values. In order to explicitate the fact that the Hamiltonian H_{ST} involves spin trajectories, the sum appearing in the partition function can be rewritten as:

$$\mathcal{Z} = \lim_{N_s\to+\infty} \sum_{\substack{\{\sigma_i^\alpha\}_{i\in1,\ldots,N}^{\alpha\in\{1,\ldots,N_s\}}}} e^{-\beta H_{ST}} \tag{1.35}$$

It is worth to remember that the Suzuki-Trotter approach that has been used to derive a classical representation of a quantum system is part of a set of approaches, characterized by a similar methodology, which are widely used in quantum statistical mechanics to analyze many-body systems at equilibrium. The most important of these techniques consists in writing the partition function as:

$$\mathcal{Z} = Tr[e^{-\beta\hat{H}}] = \lim_{N_s\to+\infty} Tr[(e^{-\frac{\beta}{N_s}\hat{H}})^{N_s}] \tag{1.36}$$

exactly as it has been done at the beginning of our derivation, starting from a second quantization Hamiltonian operator. Then it is common to use a number N_s of identity operators, represented using fermionic or bosonic coherent states depending on the kind of system that is being analyzed, to evaluate the expectation values of the operators $e^{-\frac{\beta}{N_s}\hat{H}}$, in a way which is completely analogous to what has been done for the system of quantum spins. In the end, one gets an expression of the

partition function analogous to that of a classical system, with the extra perk that, if the limit of N_s that goes to infinity is explicitely taken, one obtains in general a functional representation of the partition function; this becomes particularly important for system that can then be analyzed by means of the standard techniques of classical statistical field theory, like the renormalization group. This approach allows to transform any quantum system at equilibrium in D-dimensions into a classical system in $(D+1)$-dimensions, where the extra dimension is that of imaginary time, which is always closed on itself as a ring as a consequence of the system under exam being at equilibrium.

After this brief digression, the analysis of the system of quantum spins can resume, starting from the Hamiltonian:

$$\beta H_{ST} = -\frac{\beta}{N_s} \sum_{\alpha=1}^{N_s} \sum_{\langle i,j \rangle} J \sigma_i^\alpha \sigma_j^\alpha - \beta\Gamma \sum_{\alpha=1}^{N_s} \sum_i \sigma_i^\alpha \sigma_i^{\alpha+1} \tag{1.37}$$

From this expression we can notice two important things related to the interaction between spin trajectories:

1. the first term in the Hamiltonian tells us that the original graph on which the system has been defined is preserved by the Suzuki-Trotter procedure, as each spin trajectory $\{\sigma_i^\alpha\}^{\alpha\in\{1,...,N_s\}}$ interacts with all the other spin trajectories $\{\sigma_j^\alpha\}_{j\in\partial i}^{\alpha\in\{1,...,N_s\}}$ which are in its neighborhood on the original underlying graph

2. the second term of the Hamiltonian is instead describing a "ferromagnetic" interaction between a spin and itself along the imaginary time axis, as $\Gamma > 1$ for $h \neq 0$; if instead $h = 0$, then $\Gamma = 0$ and the quantum system reduces to a classical one, as it is reasonable to expect once the non triviality associated to the non zero commutator $[\sigma_i^z, \sigma_i^x]$ of each site in the graph is lost

The fact that the quantum system has been transformed into a classical one in which the original interaction graph is preserved is crucial for the application of the cavity method. This time, instead of considering a distribution associated to a single spin variable σ_i, like in the classical case, it is necessary to consider a distribution for the entire spin trajectory, which can be indicated with the notation $\underline{\sigma}_i = \{\sigma_i^1, ..., \sigma_i^{N_s}\}$.

To write down the equations for the distributions associated to the spin trajectories it is convenient to consider the factor graph associated to the Suzuki-Trotter Hamiltonian: the resulting factor graph develops in three dimensions, where the extra dimension comes from the fact that in the Suzuki-Trotter procedure imaginary time has been added, so that each variable σ_i^α couples also with $\sigma_i^{\alpha+1}$ and $\sigma_i^{\alpha-1}$. The resulting factor graph is represented in figure 1.3, where a spin trajectory is now a "rod" parallel to the imaginary time axis.

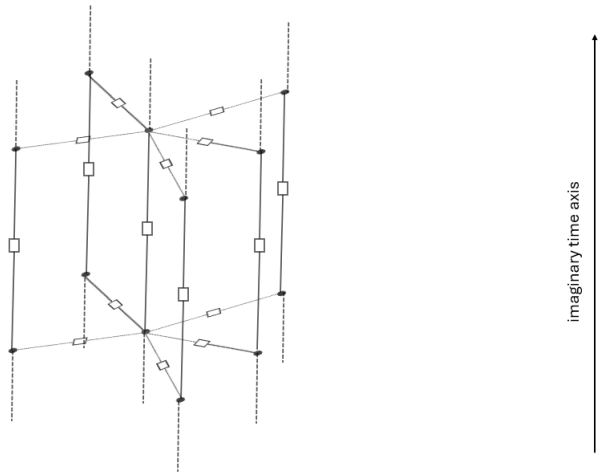

Figure 1.3: Example of factor graph resulting from the Suzuki-Trotter procedure.

Hence, in a way similar to what has been done for the classical case, the following quantities can be introduced:

- $\mathcal{Z}_{i\to j}(\underline{\sigma}_i)$: it is the partial partition function associated to the trajectory $\underline{\sigma}_i$ with the rod associated to $\underline{\sigma}_j$ removed

- $\mathcal{Z}_i(\underline{\sigma}_i)$: it is the partition function of the whole system with the trajectory $\underline{\sigma}_i$ kept fixed

For both partition functions it is possible to exploit the recursive structure of the original underlying tree to write the recursive equations:

$$\mathcal{Z}_{i\to j}(\underline{\sigma}_i) = e^{\beta\Gamma\sum_{\alpha=1}^{N_s}\sigma_i^\alpha\sigma_i^{\alpha+1}} \prod_{k\in\partial i\setminus j}\left(\sum_{\underline{\sigma}_k}\mathcal{Z}_{k\to i}(\underline{\sigma}_k)e^{\frac{\beta J}{N_s}\sum_{\alpha=1}^{N_s}\sigma_i^\alpha\sigma_k^\alpha}\right) \tag{1.38}$$

$$\mathcal{Z}_i(\underline{\sigma}_i) = e^{\beta\Gamma\sum_{\alpha=1}^{N_s}\sigma_i^\alpha\sigma_i^{\alpha+1}} \prod_{k\in\partial i}\left(\sum_{\underline{\sigma}_k}\mathcal{Z}_{k\to i}(\underline{\sigma}_k)e^{\frac{\beta J}{N_s}\sum_{\alpha=1}^{N_s}\sigma_i^\alpha\sigma_k^\alpha}\right) \tag{1.39}$$

The corresponding distributions are readily obtained:

$$c_{i\to j}(\underline{\sigma}_i) = \frac{\mathcal{Z}_{i\to j}(\underline{\sigma}_i)}{\sum_{\underline{\sigma}'}\mathcal{Z}_{i\to j}(\underline{\sigma}')} = \tag{1.40a}$$

$$= \frac{1}{z_{i\to j}} e^{\beta\Gamma\sum_{\alpha=1}^{N_s}\sigma_i^\alpha\sigma_i^{\alpha+1}} \prod_{k\in\partial i\setminus j}\left(\sum_{\underline{\sigma}_k}c_{k\to i}(\underline{\sigma}_k)e^{\frac{\beta J}{N_s}\sum_{\alpha=1}^{N_s}\sigma_i^\alpha\sigma_k^\alpha}\right) \tag{1.40b}$$

$$c_i(\underline{\sigma}_i) = \frac{\mathcal{Z}_i(\underline{\sigma}_i)}{\sum_{\underline{\sigma}'} \mathcal{Z}_i(\underline{\sigma}')} = \tag{1.41a}$$

$$= \frac{1}{z_i} e^{\beta\Gamma \sum_{\alpha=1}^{N_s} \sigma_i^\alpha \sigma_i^{\alpha+1}} \prod_{k \in \partial i} \left(\sum_{\underline{\sigma}_k} c_{k\to i}(\underline{\sigma}_k) e^{\frac{\beta J}{N_s} \sum_{\alpha=1}^{N_s} \sigma_i^\alpha \sigma_k^\alpha} \right) \tag{1.41b}$$

with $z_{i\to j}$ and z_i being the normalization constants.

The set of recursive equations that characterize the quantum cavity method is now clear:

$$c_{i\to j}(\underline{\sigma}_i) = \frac{1}{z_{i\to j}} e^{\beta\Gamma \sum_{\alpha=1}^{N_s} \sigma_i^\alpha \sigma_i^{\alpha+1}} \prod_{k \in \partial i \setminus j} \left(\sum_{\underline{\sigma}_k} c_{k\to i}(\underline{\sigma}_k) e^{\frac{\beta J}{N_s} \sum_{\alpha=1}^{N_s} \sigma_i^\alpha \sigma_k^\alpha} \right) \tag{1.42}$$

$$c_i(\underline{\sigma}_i) = \frac{1}{z_i} e^{\beta\Gamma \sum_{\alpha=1}^{N_s} \sigma_i^\alpha \sigma_i^{\alpha+1}} \prod_{k \in \partial i} \left(\sum_{\underline{\sigma}_k} c_{k\to i}(\underline{\sigma}_k) e^{\frac{\beta J}{N_s} \sum_{\alpha=1}^{N_s} \sigma_i^\alpha \sigma_k^\alpha} \right) \tag{1.43}$$

The structure of these recursive equations is similar to that of the classical cavity method, but the fact that spin trajectories now replace simple spin variables makes the problem much more complex.

Again, if the graph G is a Bethe lattice of connectivity K, a slight simplification is possible, as it is enoughe to consider a single distribution $c_{cav}(\underline{\sigma})$ in place of all the $\{c_{i\to j}(\underline{\sigma}_i)\}_{(ij)\in E}$ and a single $c(\underline{\sigma})$ in place of all the $\{c_i(\underline{\sigma}_i)\}_{i\in V}$; therefore the recursive equations take the form:

$$c_{cav}(\underline{\sigma}) = \frac{1}{z_{cav}} e^{\beta\Gamma \sum_{\alpha=1}^{N_s} \sigma^\alpha \sigma^{\alpha+1}} \times \\ \times \sum_{\underline{\sigma}_1, \dots, \underline{\sigma}_{K-1}} c_{cav}(\underline{\sigma}_1) \dots c_{cav}(\underline{\sigma}_{K-1}) e^{\frac{\beta J}{N_s} \sum_{\alpha=1}^{N_s} \sigma^\alpha (\sigma_1^\alpha + \dots + \sigma_{K-1}^\alpha)} \tag{1.44}$$

$$c(\underline{\sigma}) = \frac{1}{z} e^{\beta\Gamma \sum_{\alpha=1}^{N_s} \sigma^\alpha \sigma^{\alpha+1}} \times \\ \times \sum_{\underline{\sigma}_1, \dots, \underline{\sigma}_K} c_{cav}(\underline{\sigma}_1) \dots c_{cav}(\underline{\sigma}_K) e^{\frac{\beta J}{N_s} \sum_{\alpha=1}^{N_s} \sigma^\alpha (\sigma_1^\alpha + \dots + \sigma_K^\alpha)} \tag{1.45}$$

The distribution $c(\underline{\sigma})$ can then be used to compute local observable[3], as it is nothing but the marginal distribution of a generic spin trajectory; however, the fact that the system under exam is a quantum system makes the computation more involved. Let $\hat{O}_i$ be the operator corresponding to some local observable computed

at site i in the lattice; then the value of the observable associated to the operator $\hat{O}_i$ is obtained as:

$$\langle \hat{O}_i \rangle = \frac{1}{\mathcal{Z}} Tr[\hat{O}_i e^{-\beta \hat{H}}] = \frac{Tr[\hat{O}_i e^{-\beta \hat{H}}]}{Tr[e^{-\beta \hat{H}}]} \tag{1.46}$$

as defined by the laws of quantum statistical mechanics.

In order to get an explicit expression for $\langle \hat{O}_i \rangle$ which exploits the distribution $c(\underline{\sigma})$, it is convenient to apply again the Suzuki-Trotter procedure and write:

$$Tr[\hat{O}_i e^{-\beta \hat{H}}] = \lim_{N_s \to +\infty} Tr[\hat{O}_i (e^{-\beta \frac{\hat{H}}{N_s}})^{N_s}] = \tag{1.47a}$$

$$= \lim_{N_s \to +\infty} \sum_{\underline{\sigma}} \langle \underline{\sigma} | \hat{O}_i (e^{-\beta \frac{\hat{H}}{N_s}})^{N_s} | \underline{\sigma} \rangle = \tag{1.47b}$$

$$= \lim_{N_s \to +\infty} \sum_{\underline{\sigma}} \langle \underline{\sigma} | \hat{O}_i \mathcal{I}^1 e^{-\frac{\beta}{N_s} \hat{H}} \mathcal{I}^2 ... \mathcal{I}^{N_s} e^{-\frac{\beta}{N_s} \hat{H}} | \underline{\sigma} \rangle \tag{1.47c}$$

Note that, in the expression above, $\hat{O}_i$ can be placed anywhere in the productory of the operators, thanks to the cyclic invariance of the trace. Therefore, the previous expression becomes:

$$Tr[\hat{O}_i e^{-\beta \hat{H}}] = \lim_{N_s \to +\infty} \sum_{\underline{\sigma}^1, ..., \underline{\sigma}^{N_s}} \langle \underline{\sigma}^{\alpha'} | \hat{O}_i e^{-\frac{\beta}{N_s} \hat{H}} | \underline{\sigma}^{\alpha'+1} \rangle \times$$

$$\times \prod_{\alpha=1, \alpha \neq \alpha'}^{N_s} \langle \underline{\sigma}^{\alpha} | e^{-\frac{\beta}{N_s} \hat{H}} | \underline{\sigma}^{\alpha+1} \rangle \tag{1.48}$$

with α' that can take any value in $\{1, ..., N_s\}$.

It is now convenient to multiplicate and divide by $\langle \underline{\sigma}^{\alpha'} | e^{-\frac{\beta}{N_s} \hat{H}} | \underline{\sigma}^{\alpha'+1} \rangle$:

$$Tr[\hat{O}_i e^{-\beta \hat{H}}] = \lim_{N_s \to +\infty} \sum_{\underline{\sigma}^1, ..., \underline{\sigma}^{N_s}} \frac{\langle \underline{\sigma}^{\alpha'} | \hat{O}_i e^{-\frac{\beta}{N_s} \hat{H}} | \underline{\sigma}^{\alpha'+1} \rangle}{\langle \underline{\sigma}^{\alpha'} | e^{-\frac{\beta}{N_s} \hat{H}} | \underline{\sigma}^{\alpha'+1} \rangle} \times$$

$$\times \prod_{\alpha=1}^{N_s} \langle \underline{\sigma}^{\alpha} | e^{-\frac{\beta}{N_s} \hat{H}} | \underline{\sigma}^{\alpha+1} \rangle \tag{1.49}$$

By noticing that $\langle \underline{\sigma}^{\alpha'} | \hat{O}_i e^{-\frac{\beta}{N_s} \hat{H}} | \underline{\sigma}^{\alpha'+1} \rangle = O_i(\sigma_i^{\alpha'}) \langle \underline{\sigma}^{\alpha'} | e^{-\frac{\beta}{N_s} \hat{H}} | \underline{\sigma}^{\alpha'+1} \rangle$, the explicit expression for $\langle \hat{O}_i \rangle$ reads:

$$\langle \hat{O}_i \rangle = \frac{1}{\mathcal{Z}} \lim_{N_s \to +\infty} \sum_{\underline{\sigma}^1, ..., \underline{\sigma}^{N_s}} O_i(\sigma_i^{\alpha'}) \prod_{\alpha=1}^{N_s} \langle \underline{\sigma}^{\alpha} | e^{-\frac{\beta}{N_s} \hat{H}} | \underline{\sigma}^{\alpha+1} \rangle = \tag{1.50a}$$

$$= \frac{1}{\mathcal{Z}} \lim_{N_s \to +\infty} \sum_{\underline{\sigma}^1, ..., \underline{\sigma}^{N_s}} O_i(\sigma_i^{\alpha'}) e^{-\beta H_{ST}} \tag{1.50b}$$

$$= \frac{1}{\mathcal{Z}} \lim_{N_s \to +\infty} \sum_{\{\sigma_j^{\alpha}\}_{j \in 1, ..., N}^{\alpha \in \{1, ..., N_s\}}} O_i(\sigma_i^{\alpha'}) e^{-\beta H_{ST}} \tag{1.50c}$$

Therefore, we can conclude that:

$$\langle \hat{O}_i \rangle = \lim_{N_s \to +\infty} \sum_{\{\sigma_i^{\alpha}\}^{\alpha \in \{1, ..., N_s\}}} O_i(\sigma_i^{\alpha'}) c_i(\underline{\sigma}_i) \tag{1.51}$$

Since α' can take any value in $\{1, ..., N_s\}$, the expectation value of $\hat{O}_i$ can be recasted as:

$$\langle \hat{O}_i \rangle = \lim_{N_s \to +\infty} \sum_{\underline{\sigma}_i} c_i(\underline{\sigma}_i) \frac{1}{N_s} \sum_{\alpha'=1}^{N_s} O_i(\sigma_i^{\alpha'}) \tag{1.52}$$

The fact that the system of quantum spins has been defined on a Bethe lattice with an homogeneous transverse field and an homogeneous coupling constant allows us to drop the index i and to identify the marginal $c_i(\underline{\sigma}_i)$ with the distribution $c(\underline{\sigma})$ obtained with the quantum cavity method; hence, it is possible to write:

$$\langle \hat{O} \rangle = \lim_{N_s \to +\infty} \sum_{\underline{\sigma}} c(\underline{\sigma}) \frac{1}{N_s} \sum_{\alpha'=1}^{N_s} O(\sigma^{\alpha'}) \tag{1.53}$$

The fact that the index i has been dropped also from the observable $\hat{O}$ simply means that it is a local quantity which does not depend on the specific site of the lattice.

1.3.2 Generalization of the quantum cavity method in the case of heterogeneous couplings and fields

As for the classical case, the results that have been obtained from the Suzuki-Trotter procedure can be generalized to a case in which both the couplings and the external fields are heterogeneous and sampled independently from some distributions $P(J_{ij})$ and $P(h_i)$. The quantum Hamiltonian for the heterogeneous case is:

$$\hat{H}(\sigma_1^z, ..., \sigma_N^z, \sigma_1^x, ..., \sigma_N^x) = -\sum_{\langle i,j \rangle} J_{ij} \sigma_i^z \sigma_j^z - \sum_i h_i \sigma_i^x \tag{1.54}$$

By carrying all the required computation one finds the partition function for the heterogeneous case, which reads:

$$\mathcal{Z} = \lim_{N_s \to +\infty} \sum_{\underline{\sigma}^1, \ldots, \underline{\sigma}^{N_s}} e^{-\beta H_{ST}^{het}} \tag{1.55}$$

with $H_{ST}^{het} = -\frac{1}{N_s} \sum_{\alpha=1}^{N_s} \sum_{\langle i,j \rangle} J_{ij} \sigma_i^\alpha \sigma_j^\alpha - \sum_{\alpha=1}^{N_s} \sum_i \Gamma_i \sigma_i^\alpha \sigma_i^{\alpha+1}$ being the Suzuki-Trotter Hamiltonian for the heterogeneous system, with $\Gamma_i = \frac{1}{2\beta} \log \coth(\frac{\beta h_i}{N_s})$.

In this context it is possible to generalize the recursive equations for the distributions $c_{i \to j}(\underline{\sigma}_i)$ and $c_i(\underline{\sigma}_i)$ that have already been defined for the homogeneous case; these now reads:

$$c_{i \to j}(\underline{\sigma}_i) = \frac{1}{z_{i \to j}} e^{\beta \sum_{\alpha=1}^{N_s} \Gamma_i \sigma_i^\alpha \sigma_i^{\alpha+1}} \prod_{k \in \partial i \setminus j} \left(\sum_{\underline{\sigma}_k} c_{k \to i}(\underline{\sigma}_k) e^{\frac{\beta}{N_s} \sum_{\alpha=1}^{N_s} J_{ik} \sigma_i^\alpha \sigma_k^\alpha} \right) \tag{1.56}$$

$$c_i(\underline{\sigma}_i) = \frac{1}{z_i} e^{\beta \sum_{\alpha=1}^{N_s} \Gamma_i \sigma_i^\alpha \sigma_i^{\alpha+1}} \prod_{k \in \partial i} \left(\sum_{\underline{\sigma}_k} c_{k \to i}(\underline{\sigma}_k) e^{\frac{\beta}{N_s} \sum_{\alpha=1}^{N_s} J_{ik} \sigma_i^\alpha \sigma_k^\alpha} \right) \tag{1.57}$$

If solved on a finite graph, these equations provide all the required distributions to compute the observables of the system; however, such a solution holds only for a specific realization of the couplings and of the external fields. To go beyond the single realization of couplings and fields, it is necessary to introduce a relatively complex object, that is a distribution of distributions. While in the classical case the cavity field is replaced by a distribution when switching to the heterogeneous case, in the quantum case the cavity distribution is replaced by a distribution of distributions. Such complex objects can be defined by means of a functional self-consistent equation, in complete analogy to what has been done to derive the self-consistent equation for the distribution of the fields in the classical case.

To write down the equations it is convenient to consider again a Bethe lattice with a certain connectivity K, focus on a generic node i and delete one of the edges connecting i to some neighbor; the neighbors of the node i can be enumerated from 1 to K, with the neighbor K being the one which is disconnected. The self-consistent equations for the distributions of distributions then read:

$$\begin{aligned} P[c_{cav}(\underline{\sigma})] = \int \prod_{q=1}^{K-1} Dc_{q,cav}(\underline{\sigma}_q) P[c_{q,cav}(\underline{\sigma}_q)] \prod_{q=1}^{K-1} dJ_q P(J_K) dh P(h) \times \\ \times \delta \Bigg(c_{cav}(\underline{\sigma}) - \frac{1}{z_{cav}} e^{\beta \sum_{\alpha=1}^{N_s} \Gamma \sigma^\alpha \sigma^{\alpha+1}} \times \\ \times \prod_{q=1}^{K-1} \left(\sum_{\underline{\sigma}_q} c_{q,cav}(\underline{\sigma}_q) e^{\frac{\beta}{N_s} \sum_{\alpha=1}^{N_s} J_q \sigma^\alpha \sigma_q^\alpha} \right) \Bigg) \end{aligned} \tag{1.58}$$

$$P[c(\underline{\sigma})] = \int \prod_{q=1}^{K} Dc_{q,cav}(\underline{\sigma}_q) P[c_{q,cav}(\underline{\sigma}_q)] \prod_{q=1}^{K} dJ_q P(J_q) dh P(h) \times$$
$$\times \delta \Bigg(c_{cav}(\underline{\sigma}) - \frac{1}{z_{cav}} e^{\beta \sum_{\alpha=1}^{N_s} \Gamma \sigma^\alpha \sigma^{\alpha+1}} \times$$
$$\times \prod_{q=1}^{K} \Bigg(\sum_{\underline{\sigma}_q} c_{q,cav}(\underline{\sigma}_q) e^{\frac{\beta}{N_s} \sum_{\alpha=1}^{N_s} J_q \sigma^\alpha \sigma_q^\alpha} \Bigg) \Bigg) \quad (1.59)$$

where the index i has been dropped in both the expressions above, since it is irrelevant to consider the specific node i or any other node, being the underlying graph a Bethe lattice.

1.3.3 The projected cavity mapping

An alternative approach to deal with quantum spin systems is that of the projected cavity mapping[2]; to present this method a Bethe lattice is considered once again, with homogeneous couplings and external fields, so that it is possible to exploit its useful properties. Here the focus is on a single node and on its K neighbors; let v_0 be the central node and let the nodes v_1, v_2,..., v_K be its neighbors, as pictured in figure 1.4.

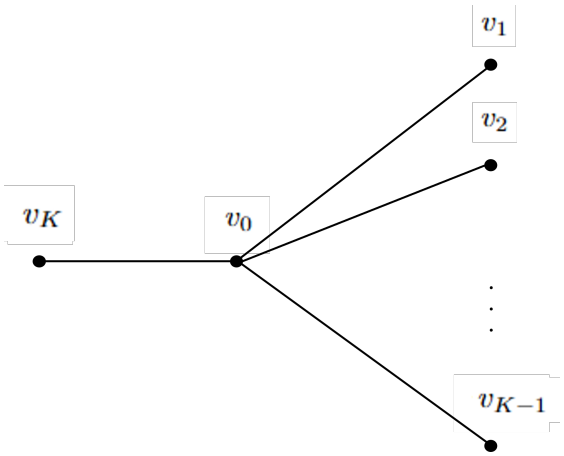

Figure 1.4: Node of the Bethe lattice under exam with its neighbors.

The projected cavity mapping focuses on node v_0, with the link between v_0 itself and v_K removed, and assumes that each node v_i, with $i \in \{1, ..., K-1\}$, can be described by an Hamiltonian operator $\hat{H}_i^{cav} = -h\sigma_i^x - h^{cav}\sigma_i^z$: here h is the usual external magnetic field, while h^{cav} plays the role of the cavity field.

The system of spin 0 with its remaining $K-1$ neighbors can be described by the following Hamiltonian operator:

$$\hat{H}_0 = -h\sigma_0^x - \sum_{i=1}^{K-1} \left(h\sigma_i^x + h^{cav}\sigma_i^z + J\sigma_0^z\sigma_i^z \right) \tag{1.60}$$

However, since the neighbors of v_0 are described by an Hamiltonian operator of the type $\hat{H}_i^{cav}$ and since we are considering a Bethe lattice, it is reasonable to assume that also the node v_0 can be described by an Hamiltonian operator $\hat{H}_0^{cav} = -h\sigma_0^x - h^{cav}\sigma_0^z$ when the focus switches on the node v_K and on its neighbors, exploiting once again the recursive tree-like structure of the underlying graph. The field h^{cav} can be computed by imposing that the magnetization of node v_0, defined as $m_0 = \langle \sigma_0^z \rangle$, computed with $\hat{H}_0$ is compatible with the one computed with $\hat{H}_0^{cav}$.

Hence, we can start by computing m_0 for the case with $\hat{H}_0$, which is obtained as:

$$m_0 = \frac{Tr[\sigma_0^z e^{-\beta\hat{H}_0}]}{Tr[e^{-\beta\hat{H}_0}]} = \frac{\sum_{\sigma_0,...,\sigma_{K-1}} \langle \sigma_0, ..., \sigma_{K-1} | \sigma_0^z e^{-\beta\hat{H}_0} | \sigma_0, ..., \sigma_{K-1} \rangle}{\sum_{\sigma_0,...,\sigma_{K-1}} \langle \sigma_0, ..., \sigma_{K-1} | e^{-\beta\hat{H}_0} | \sigma_0, ..., \sigma_{K-1} \rangle} \tag{1.61}$$

where the vectors of the basis used to compute the trace are of the form $|\sigma_0, ..., \sigma_{K-1}\rangle$, with each $\sigma_i \in \{-1,1\}$ being representative of the two possible eigenvalues associated to the operator σ_i^z.

Obtaining explicitly the result of this expression is non trivial, due to the fact that it is necessary to compute $e^{-\beta\hat{H}_0}|\sigma_0, ..., \sigma_{K-1}\rangle$. The best strategy here is to diagonalize the Hamiltonian operator $\hat{H}_0$ and then use the results to compute the trace of the exponential operator $e^{-\beta\hat{H}_0}$.

At this point it is necessary to compute $\langle \sigma_0^z \rangle$ with the Hamiltonian $\hat{H}_0^{cav}$; this is given by:

$$\langle \sigma_0^z \rangle = \frac{Tr[\sigma_0^z e^{-\beta\hat{H}_0^{cav}}]}{Tr[e^{-\beta\hat{H}_0^{cav}}]} = \frac{\sum_{\sigma_0} \langle \sigma_0 | \sigma_0^z e^{-\beta\hat{H}_0^{cav}} | \sigma_0 \rangle}{\sum_{\sigma_0} \langle \sigma_0 | e^{-\beta\hat{H}_0^{cav}} | \sigma_0 \rangle} = \tag{1.62a}$$

$$= \frac{\langle 1 | e^{-\beta\hat{H}_0^{cav}} | 1 \rangle - \langle -1 | e^{-\beta\hat{H}_0^{cav}} | -1 \rangle}{\langle 1 | e^{-\beta\hat{H}_0^{cav}} | 1 \rangle + \langle -1 | e^{-\beta\hat{H}_0^{cav}} | -1 \rangle} \tag{1.62b}$$

This time, since the Hamiltonian operator $\hat{H}_0^{cav}$ involves only the spin operators of node v_0, it is possible to compute the trace by using the basis of vectors of the form $|\sigma_0\rangle$, with $\sigma_0 \in \{-1,1\}$.

Now, in order to compute the expectation values of the operator $e^{-\beta\hat{H}_0^{cav}}$, it is convenient to diagonalize the matrix $-\beta H_0^{cav}$ and then use the results to compute

the matrix $e^{-\beta H_0^{cav}}$; once the exponential matrix has been computed, its diagonal elements can be plugged into the expression $\langle \sigma_0^z \rangle$ written above. In conclusion, one arrives to the following equation for the cavity field h^{cav}:

$$m_0 = \frac{h^{cav}}{\sqrt{h^{cav\,2} + h^2}} \tanh \beta \sqrt{h^{cav\,2} + h^2} \tag{1.63}$$

The projected cavity mapping can be generalized to the case of heterogeneous couplings and external magnetic fields sampled respectively from some distributions $P(J_{ij})$ and $P(h_i)$. If the graph is still a Bethe lattice and the focus is once again the node v_0 and its neighbors apart from v_K, as represented in figure 1.4, it is possible to associate to each of the nodes v_1,...,v_{K-1} an Hamiltonian operator $\hat{H}_i^{cav} = -h_i \sigma_i^x - h_i^{cav} \sigma_i^z$, where now h_i^{cav} is the local cavity field; the Hamiltonian operator that is now associated to the central spin on node v_0 is given by:

$$\hat{H}_0 = -h_0 \sigma_0^x - \sum_{i=1}^{d-1} \left(h_i \sigma_i^x + h_i^{cav} \sigma_i^z + J_{0i} \sigma_0^z \sigma_i^z \right) \tag{1.64}$$

The self-consistency of the approach is achieved by assuming that also the behavior of the spin on node v_0 can be described by an Hamiltonian operator which is analogous to that of its neighbors, that is $\hat{H}_0^{cav}$, and by imposing that the expectation value of σ_0^z computed with $\hat{H}_0$ is compatible with the one computed with $\hat{H}_0^{cav}$, exactly like it has been done in the case of homogeneous couplings and fields. By repeating similar computation to those done for the homogeneous case, one arrives at the following equation:

$$m_0 = \frac{h_0^{cav}}{\sqrt{h_0^{cav\,2} + h_0^2}} \tanh \beta \sqrt{h_0^{cav\,2} + h_0^2} \tag{1.65}$$

where m_0 is nothing but the expectation value of σ_0^z computed with the Hamiltonian operator $\hat{H}_0$, which now contains all the information about the couplings $J_{01}, ..., J_{0K-1}$ and the local cavity fields $h_1^{cav}, ..., h_{K-1}^{cav}$ of the neighbors of node v_0.

Since it is more interesting to make our results independent on the single realization of the couplings and of the external magnetic fields, it would be reasonable to average over all the possible realizations of the parameters using the distributions $P(J_{ij})$ and $P(h_i)$; however, in the case of the projected cavity mapping, this is not so easy to do, as the parameters of the neighbors do not appear explicitly in m_0. Formally, it is still possible to write down a self-consistent equation for the probability distribution associated to the local cavity field $P(h^{cav})$ as:

$$P(h^{cav}) = \int \prod_{i=0}^{K-1} dh_i P(h_i) \prod_{i=1}^{K-1} dJ_{0i} P(J_{0i}) \prod_{i=1}^{K-1} dh_i^{cav} P(h_i^{cav}) \times$$
$$\times \delta \Bigg(m_0 \Big(\{h_i\}_{i=0,\dots,K-1}, \{J_{0i}\}_{i=1,\dots,K-1}, \{h_i^{cav}\}_{i=1,\dots,K-1} \Big) + \\ - \frac{h^{cav}}{\sqrt{h^{cav\,2} + h_0^2}} \tanh \beta \sqrt{h^{cav\,2} + h_0^2} \Bigg) \quad (1.66)$$

The projected cavity mapping approach provides a simplified way to treat systems of quantum spins: indeed, it allows to replace the entire spin trajectory resulting from the Suzuki-Trotter procedure with a single number, or better, by means of a probability distribution associated to such a parameter. The population dynamics algorithm can be used to compute the distribution $P(h^{cav})$, which here becomes the natural order parameter for the system, as it happened also in the classical case; however, the computation of the distribution is heavier, from a numerical point of view, with respect to the classical case, due to the fact that the derivation of m_0 is not straightforward.

1.3.4 The cavity mean-field approximation

As an improvement to the projected cavity mapping approach, the cavity mean-field approximation has been introduced[2]. To present this method it is convenient to consider once again a Bethe lattice with connectivity K and to start from the case of homogeneous couplings and external magnetic fields. If the portion of Bethe lattice pictured in figure 1.4 is taken as a reference, it is possible to focus on the node v_0 and on its neighbors, apart from the node v_K.

The Hamiltonian operators associated to the neighbors are the same that have been introduced for the projected cavity mapping, that is $\hat{H}_i^{cav} = -h\sigma_i^x - h^{cav}\sigma_i^z$; for what concerns the Hamiltonian operator of the spin on node v_0, it reads instead $\hat{H}_0^{cav-MF} = -h\sigma_0^x - \sigma_0^z \sum_{i=1}^{K-1} J\langle\sigma_i^z\rangle$. This choice implies that $h^{cav} = \sum_{i=1}^{d-1} J\langle\sigma_i^z\rangle$ and it directly provides us with a self-consistent equation for the cavity field h^{cav}. The quantity $\langle\sigma_i^z\rangle$ can be computed as:

$$\langle\sigma_i^z\rangle = \frac{Tr[\sigma_i^z e^{-\beta H_i^{cav}}]}{Tr[e^{-\beta H_i^{cav}}]} \quad (1.67)$$

To find the result of the expression above it is possible to exploit what has already been computed while analyzing the projected cavity mapping, where it was found that:

$$\langle \sigma_i^z \rangle = \frac{h^{cav}}{\sqrt{h^{cav\,2} + h^2}} \tanh \beta \sqrt{h^{cav\,2} + h^2} \tag{1.68}$$

Therefore, the self-consistent equation for the cavity field reads:

$$h^{cav} = \sum_{i=1}^{K-1} J \frac{h^{cav}}{\sqrt{h^{cav\,2} + h^2}} \tanh \beta \sqrt{h^{cav\,2} + h^2} \tag{1.69}$$

which reduces to:

$$h^{cav} = (K-1) J \frac{h^{cav}}{\sqrt{h^{cav\,2} + h^2}} \tanh \beta \sqrt{h^{cav\,2} + h^2} \tag{1.70}$$

The generalization to the heterogeneous case is straightforward; in this case the Hamiltonian operators associated to the nodes v_1,...,v_{K-1} take the form $\hat{H}_i^{cav} = -h_i \sigma_i^x - h_i^{cav} \sigma_i^z$, where h_i^{cav} is the usual local cavity field, while the Hamiltonian operator describing the behavior on the spin on the node v_0 is $\hat{H}_0^{cav-MF} = -h_0 \sigma_0^x - \sigma_0^z \sum_{i=1}^{K-1} J_{0i} \langle \sigma_i^z \rangle$. The equation relating the local cavity fields of the nodes v_1,...,v_{K-1} to the local cavity field on the node v_0 is simply given by:

$$h_0^{cav} = \sum_{i=1}^{K-1} J_{0i} \frac{h_i^{cav}}{\sqrt{h_i^{cav\,2} + h_i^2}} \tanh \beta \sqrt{h_i^{cav\,2} + h_i^2} \tag{1.71}$$

This result holds for a specific realization of the couplings and of the external magnetic fields; to make the results general, it is possible to follow the same procedure that has already been used a few times to derive a distribution for the local cavity field. This time the self-consistent equation for the distribution reads:

$$P(h^{cav}) = \int \prod_{i=1}^{K-1} dh_i P(h_i) \prod_{i=0}^{K-1} dJ_{0i} P(J_{0i}) \prod_{i=1}^{K-1} dh_i^{cav} P(h_i^{cav}) \times \\ \times \delta \left(h^{cav} - \sum_{i=1}^{K-1} J_{0i} \frac{h_i^{cav}}{\sqrt{h_i^{cav\,2} + h_i^2}} \tanh \beta \sqrt{h_i^{cav\,2} + h_i^2} \right) \tag{1.72}$$

The cavity mean-field approximation in the heterogeneous case defines once again a probability distribution for the local cavity field. From a practical point of view, the desired distribution can be obtained by means of the population dynamics algorithm, like in the case of the projected cavity mapping; this time however, it should be a little bit simpler, since the update of the local cavity field in the algorithm is simply given by (1.71).

Chapter 2

Relation between the cavity method and dynamical mean-field theory

2.1 Introduction

This chapter focuses on the relation between the cavity method and the approach of dynamical mean-field theory. In the previous chapter the classical cavity method has been presented, together with a simple, but still practically complex, version of the quantum cavity method for spin systems. Here the procedure to turn a quantum system into a classical system is analyzed further: in particular, the approach which allows to go from the second quantization Hamiltonian of a many-body system to an equivalent classical field theory is presented in details, with a brief review of bosonic coherent states. The procedure is implemented for the Bose-Hubbard model on a Bethe lattice, with the aim to derive a cavity distribution and a full marginal distribution, in a way similar to what has been done for the system of quantum spins in a transverse field in the previous chapter. The choice of the model to examine has fallen on the Bose-Hubbard model so that the equations of bosonic dynamical mean field theory[3][5][6][7] can be derived directly from the expressions obtained via the cavity method, showing the strong relation that exists between the methodology of the cavity method and that of dynamical mean-field theory.

2.2 Application of the cavity method for the analysis of the Bose-Hubbard model

2.2.1 Presentation of the model and brief review of bosonic coherent states

Let us start by recalling that the Hamiltonian operator of the Bose-Hubbard model[1] on a graph with N nodes is given by:

$$\hat{H} = -J \sum_{\langle \alpha,\gamma \rangle} (\hat{a}_\alpha^\dagger \hat{a}_\gamma + \hat{a}_\gamma^\dagger \hat{a}_\alpha) + \frac{U}{2} \sum_{\alpha=1}^{N} \hat{a}_\alpha^\dagger \hat{a}_\alpha^\dagger \hat{a}_\alpha \hat{a}_\alpha - \mu \sum_{\alpha=1}^{N} \hat{a}_\alpha^\dagger \hat{a}_\alpha \tag{2.1}$$

where $\hat{a}_\alpha$ is the usual annihilation operator associated to site α, while $\hat{a}_\alpha^\dagger$ is the usual creation operator associated to site α; these operators are characterized by the following commutation relations:

$$[\hat{a}_\alpha, \hat{a}_\gamma] = 0 \tag{2.2a}$$
$$[\hat{a}_\alpha^\dagger, \hat{a}_\gamma^\dagger] = 0 \tag{2.2b}$$
$$[\hat{a}_\alpha, \hat{a}_\gamma^\dagger] = \delta_{\alpha,\gamma} \tag{2.2c}$$

and the action of these operators on Fock states is simply given by:

$$\hat{a}_\alpha |n_\alpha\rangle = \sqrt{n_\alpha} |n_\alpha - 1\rangle \tag{2.3a}$$
$$\hat{a}_\alpha^\dagger |n_\alpha\rangle = \sqrt{n_\alpha + 1} |n_\alpha + 1\rangle \tag{2.3b}$$
$$\hat{a}_\alpha^\dagger \hat{a}_\alpha |n_\alpha\rangle = \hat{n}_\alpha |n_\alpha\rangle = n_\alpha |n_\alpha\rangle \tag{2.3c}$$

where $\hat{n}_\alpha = \hat{a}_\alpha^\dagger \hat{a}_\alpha$ is the usual number operator associated to the site α.

The first term of the Hamiltonian, weighted by the hopping amplitude J, is associated to the hopping of bosons between nearest neighbors; the second term is instead a term associated to the on-site interactions, whose strength is measured by U; the third term is simply fixing the particle density by means of the chemical potential μ.

In the following, bosonic coherent states will be used to derive the field theory of the Bose-Hubbard model, so it is convenient to review their main properties[8]. It is possible to start by remembering that a Fock state can be expressed in terms of creation operators acting on the vacuum; for a graph with N sites, it can be written:

$$|n_1, ..., n_N\rangle = \prod_{\alpha=1}^{N} \frac{(\hat{a}_\alpha^\dagger)^{n_\alpha}}{n_\alpha!} |0\rangle \tag{2.4}$$

The set of Fock states $\{|n_1, ..., n_N\rangle\}_{\left\{n_1,...,n_N \in \{0,1,2,..\}\right\}}$ can be used as a basis on which a generic coherent state $|\Phi\rangle$ can be expanded:

$$|\Phi\rangle = \sum_{n_1}^{+\infty} ... \sum_{n_N}^{+\infty} \Phi_{n_1,...,n_N} |n_1, ..., n_N\rangle \tag{2.5}$$

Coherent states are defined as the eigenstates of the annihilation operators; therefore, for a generic site α, it is possible to write:

$$\hat{a}_\alpha |\Phi\rangle = \Phi_\alpha |\Phi\rangle \tag{2.6}$$

where Φ_α is the eigenvalue associates to the operator $\hat{a}_\alpha$, with $\alpha \in \{1, ..., N\}$.

By exploiting this information, the structure of the coefficients $\{\Phi_{n_1,..,n_N}\}$ appearing in the expansion can be obtained. For simplicity, the case with a single mode is considered; the action of the annihilation operator $\hat{a}$ on the coherent state $|\Phi\rangle$ is:

$$\hat{a}|\Phi\rangle = \hat{a} \sum_{n=0}^{+\infty} \Phi_n |n\rangle = \sum_{n=0}^{+\infty} \Phi_n \hat{a}|n\rangle = \sum_{n=0}^{+\infty} \Phi_n \sqrt{n}|n-1\rangle = \tag{2.7a}$$

$$= \sum_{n=1}^{+\infty} \Phi_n \sqrt{n}|n-1\rangle = \sum_{n=0}^{+\infty} \Phi_{n+1} \sqrt{n+1}|n\rangle = \tag{2.7b}$$

$$= \Phi|\Phi\rangle = \Phi \sum_{n=0}^{+\infty} \Phi_n |n\rangle \tag{2.7c}$$

From this expression it is possible to obtain a sort of recursive equation for the coefficients:

$$\Phi_{n+1} = \frac{\Phi}{\sqrt{n+1}} \Phi_n \tag{2.8}$$

or equivalently:

$$\Phi_n = \frac{\Phi}{\sqrt{n}} \Phi_{n-1} \tag{2.9}$$

By iterating this recursion, it is possible to derive the generic structure of a coefficient Φ_n, given the initial coefficient Φ_0:

$$\Phi_n = \frac{(\Phi)^n}{\sqrt{n!}} \Phi_0 \tag{2.10}$$

Therefore, the expression of a coherent state, in the case of a single mode, becomes:

$$|\Phi\rangle = \Phi_0 \sum_{n=0}^{+\infty} \frac{(\Phi)^n}{\sqrt{n!}}|n\rangle = \Phi_0 \sum_{n=0}^{+\infty} \frac{(\Phi)^n(\hat{a}^\dagger)^n}{\sqrt{n!}}|0\rangle \tag{2.11}$$

The initial value Φ_0 can be obtained from the normalization procedure; indeed, by imposing that $\langle\Phi|\Phi\rangle = 1$:

$$\rightarrow |\Phi_0|^2 \sum_{n=0}^{+\infty}\sum_{m=0}^{+\infty} \frac{(\Phi)^n(\Phi^*)^m}{\sqrt{n!m!}}\langle m|n\rangle = 1 \tag{2.12}$$

which results in:

$$|\Phi_0|^2 \sum_{n=0}^{+\infty} \frac{|\Phi|^{2n}}{n!} = 1 \rightarrow |\Phi_0|^2 e^{|\Phi|^2} = 1 \rightarrow \Phi_0 = e^{-\frac{|\Phi|^2}{2}} \tag{2.13}$$

Hence, the final expression for a single mode coherent state is given by:

$$|\Phi\rangle = e^{-\frac{|\Phi|^2}{2}} \sum_{n=0}^{+\infty} \frac{(\Phi)^n}{\sqrt{n!}}|n\rangle \tag{2.14}$$

It is worth to recall that it is quite common to find bosonic coherent states as unnormalized, as in that case they can be compactly written as:

$$|\Phi\rangle = \sum_{n=0}^{+\infty} \frac{(\Phi)^n}{\sqrt{n!}}|n\rangle = \sum_{n=0}^{+\infty} \frac{(\Phi)^n(\hat{a}^\dagger)^n}{\sqrt{n!}}|0\rangle = e^{\Phi\hat{a}^\dagger}|0\rangle \tag{2.15}$$

Another important expression is that of the identity operator, which in the single mode case takes the form:

$$\mathcal{I} = \int \frac{d\Phi d\Phi^*}{2\pi i} e^{-|\Phi|^2}|\Phi\rangle\langle\Phi| \tag{2.16}$$

It is important to remember that this expression of the identity operator has to be used when dealing with not normalized coherent states. If that is not the case, the correct form of the identity operator becomes the following one:

$$\mathcal{I} = \int \frac{d\Phi d\Phi^*}{2\pi i} |\Phi\rangle\langle\Phi| \tag{2.17}$$

A result which will be useful later is that of the scalar product between two bosonic coherent states:

$$\langle\Psi|\Phi\rangle = \left(e^{-\frac{|\Psi|^2}{2}}\sum_{m=0}^{+\infty}\frac{(\Psi^*)^m}{\sqrt{m!}}\langle m|\right)\left(e^{-\frac{|\Phi|^2}{2}}\sum_{n=0}^{+\infty}\frac{(\Phi)^n}{\sqrt{n!}}|n\rangle\right) = \tag{2.18a}$$

$$= e^{-\frac{|\Psi|^2}{2}}e^{-\frac{|\Phi|^2}{2}}\sum_{m=0}^{\infty}\sum_{n=0}^{\infty}\frac{(\Psi^*)^m(\Phi^n)}{\sqrt{n!m!}}\langle m|n\rangle = \tag{2.18b}$$

$$= e^{-\frac{|\Psi|^2}{2}}e^{-\frac{|\Phi|^2}{2}}\sum_{n=0}^{\infty}\frac{(\Psi^*\Phi)^n}{n!} = \tag{2.18c}$$

$$= e^{-\frac{|\Psi|^2}{2}}e^{-\frac{|\Phi|^2}{2}}e^{\Psi^*\Phi} \tag{2.18d}$$

If the states are not normalized, the result simply becomes:

$$\langle\Psi|\Phi\rangle = e^{\Psi^*\Phi} \tag{2.19}$$

With a reasoning similar to the one that has just been carried out, it is possible to derive the coherent states for a multi mode case. The expansion on the Fock state basis now reads:

$$|\Phi\rangle = \prod_{\alpha=1}^{N}\sum_{n_\alpha=0}^{+\infty}\frac{(\Phi_\alpha)^{n_\alpha}}{\sqrt{n_\alpha!}}|n_\alpha\rangle = e^{\sum_\alpha \Phi_\alpha \hat{a}_\alpha^\dagger} \tag{2.20}$$

The action of the creation and annihilation operators on the bra $\langle\Phi|$ and on the ket $|\Phi\rangle$ can be summarized as:

$$\hat{a}_\alpha|\Phi\rangle = \Phi_\alpha|\Phi\rangle \tag{2.21a}$$

$$\hat{a}_\alpha^\dagger|\Phi\rangle = \partial_{\Phi_\alpha}|\Phi\rangle \tag{2.21b}$$

$$\langle\Phi|\hat{a}_\alpha = \partial_{\Phi_\alpha}\langle\Phi| \tag{2.21c}$$

$$\langle\Phi|\hat{a}_\alpha^\dagger = \langle\Phi|\Phi_\alpha^* \tag{2.21d}$$

This brief summary of the properties of the bosonic coherent states can be concluded with the expression of the identity operator for the multi mode case to be used with normalized coherent states:

$$\mathcal{I} = \int\prod_{\alpha=1}^{N}\frac{d\Phi_\alpha d\Phi_\alpha^*}{2\pi i}e^{-\sum_\alpha \Phi_\alpha^*\Phi_\alpha}|\Phi\rangle\langle\Phi| \tag{2.22}$$

The expression to be used with not normalized coherent states is instead:

$$\mathcal{I} = \int\prod_{\alpha=1}^{N}\frac{d\Phi_\alpha d\Phi_\alpha^*}{2\pi i}|\Phi\rangle\langle\Phi| \tag{2.23}$$

The scalar product between multi mode coherent states simply reads:

$$\langle\Psi|\Phi\rangle = e^{-\sum_\alpha \frac{|\Psi^*_\alpha|^2}{2}} e^{-\sum_\alpha \frac{|\Phi_\alpha|^2}{2}} e^{\sum_\alpha \Psi^*_\alpha \Phi_\alpha} \tag{2.24}$$

If instead not normalized states are considered, the scalar product simply becomes:

$$\langle\Psi|\Phi\rangle = e^{\sum_\alpha \Psi^*_\alpha \Phi_\alpha} \tag{2.25}$$

2.2.2 Derivation of the field theory and quantum cavity method

Now that the properties of bosonic coherent states have been reviewed, it is possible to present the technique which allows to derive a classical field theory, with the usual extra dimension of imaginary time, starting directly from the Hamiltonian operator of the model under consideration[1][5][6][7]. The starting point is exactly the same of the Suzuki-Trotter procedure, that is the partition function rewritten as:

$$\mathcal{Z} = Tr[e^{-\beta\hat{H}}] = \lim_{N_s\to+\infty} Tr[(e^{-\frac{\beta}{N_s}\hat{H}})^{N_s}] \tag{2.26}$$

In this particular case, it is convenient to separate the two terms of the Hamiltonian as:

$$\hat{H} = \hat{H}_{hop} + \hat{H}_{loc} \tag{2.27a}$$

$$\hat{H}_{hop} = -J \sum_{\langle\alpha,\gamma\rangle} (\hat{a}^\dagger_\alpha \hat{a}_\gamma + \hat{a}^\dagger_\alpha \hat{a}_\gamma) \tag{2.27b}$$

$$\hat{H}_{loc} = \sum_{\alpha=1}^{N} \left[\frac{U}{2} \left(\hat{a}^\dagger_\alpha \hat{a}^\dagger_\alpha \hat{a}_\alpha \hat{a}_\alpha \right) - \mu \hat{a}^\dagger_\alpha \hat{a}_\alpha \right] \tag{2.27c}$$

With this separation in mind, the partition function can be rewritten as:

$$\mathcal{Z} = \lim_{N_s\to+\infty} Tr[(e^{-\frac{\beta}{N_s}\hat{H}_{hop}} e^{-\frac{\beta}{N_s}\hat{H}_{loc}})^{N_s}] \tag{2.28}$$

where the fact that $e^{-\frac{\beta}{N_s}\hat{H}} = e^{-\frac{\beta}{N_s}\hat{H}_{hop}} e^{-\frac{\beta}{N_s}\hat{H}_{loc}}$ comes from the fact that, since $N_s \to +\infty$, the commutator between $\hat{H}_{loc}$ and $\hat{H}_{hop}$ can be approximated as $[\hat{H}_{loc}, \hat{H}_{hop}] \approx 0$.

Formally, the procedure presented here is almost analogous to the one that has already been implemented for the system of quantum spins: an imaginary time axis can be introduced and a set of identity operators, this time expressed in the

basis of bosonic coherent states, can be used to evaluate the expectation values of the operator $e^{-\frac{\beta}{N_s}\hat{H}_{hop}}e^{-\frac{\beta}{N_s}\hat{H}_{loc}}$.

Therefore, one has:

$$\mathcal{Z} = \lim_{N_s\to+\infty}\sum_{n_1,...,n_N=0}^{+\infty}\langle n_1,..,n_N|(e^{-\frac{\beta}{N_s}\hat{H}_{hop}}e^{-\frac{\beta}{N_s}\hat{H}_{loc}})\mathcal{I}\times \tag{2.29a}$$

$$\times ...\mathcal{I}(e^{-\frac{\beta}{N_s}\hat{H}_{hop}}e^{-\frac{\beta}{N_s}\hat{H}_{loc}})\mathcal{I}|n_1,...,n_N\rangle = \tag{2.29b}$$

$$= \lim_{N_s\to+\infty}\sum_{n_1,...,n_N=0}^{+\infty}\int\prod_{\alpha=1}^{N}\frac{d{\Phi_\alpha}^{N_s}d{\Phi_\alpha^*}^{N_s}}{2\pi i}e^{-\sum_{\alpha=1}^{N}{\Phi_\alpha}^{N_s}d{\Phi_\alpha^*}^{N_s}}\times \tag{2.29c}$$

$$\times\langle n_1,..,n_N|(e^{-\frac{\beta}{N_s}\hat{H}_{hop}}e^{-\frac{\beta}{N_s}\hat{H}_{loc}})\mathcal{I}...\mathcal{I}(e^{-\frac{\beta}{N_s}\hat{H}_{hop}}e^{-\frac{\beta}{N_s}\hat{H}_{loc}})|\Phi^{N_s}\rangle\times \tag{2.29d}$$

$$\times\langle\Phi^{N_s}|n_1,..,n_N\rangle \tag{2.29e}$$

where the superscript N_s appearing in the eigenvalues of the annihilation operators indicates that ${\Phi_\alpha}^{N_s}$ and ${\Phi_\alpha^*}^{N_s}$ are to be referred to the N_s-th sub-interval of the imaginary time axis.

Now the terms can be reorganized and, by exploiting the representation of the identity operator in the basis of Fock states $\mathcal{I} = \sum_{n_1,...,n_N=0}^{+\infty}|n_1,..,n_N\rangle\langle n_1,..,n_N|$, it is possible to write:

$$\mathcal{Z} = \lim_{N_s\to+\infty}\int\prod_{\alpha=1}^{N}\frac{d{\Phi_\alpha}^{N_s}d{\Phi_\alpha^*}^{N_s}}{2\pi i}e^{-\sum_{\alpha=1}^{N}{\Phi_\alpha^*}^{N_s}{\Phi_\alpha}^{N_s}}\times \tag{2.30a}$$

$$\times\langle\Phi^{N_s}|\left(\sum_{n_1,...,n_N=0}^{+\infty}|n_1,...,n_N\rangle\langle n_1,...,n_N|\right)\times \tag{2.30b}$$

$$\times(e^{-\frac{\beta}{N_s}\hat{H}_{hop}}e^{-\frac{\beta}{N_s}\hat{H}_{loc}})\mathcal{I}...\mathcal{I}(e^{-\frac{\beta}{N_s}\hat{H}_{hop}}e^{-\frac{\beta}{N_s}\hat{H}_{loc}})|\Phi^{N_s}\rangle = \tag{2.30c}$$

$$= \lim_{N_s\to+\infty}\int\prod_{\alpha=1}^{N}\frac{d{\Phi_\alpha}^{N_s}d{\Phi_\alpha^*}^{N_s}}{2\pi i}e^{-\sum_{\alpha=1}^{N}{\Phi_\alpha^*}^{N_s}{\Phi_\alpha}^{N_s}}\times \tag{2.30d}$$

$$\times\langle\Phi^{N_s}|(e^{-\frac{\beta}{N_s}\hat{H}_{hop}}e^{-\frac{\beta}{N_s}\hat{H}_{loc}})\mathcal{I}...\mathcal{I}(e^{-\frac{\beta}{N_s}\hat{H}_{hop}}e^{-\frac{\beta}{N_s}\hat{H}_{loc}})|\Phi^{N_s}\rangle \tag{2.30e}$$

The other identity operators appearing in the expression of the partition function can be explicitated:

$$\mathcal{Z} = \lim_{N_s\to+\infty}\int\prod_{l=1}^{N_s}\prod_{\alpha=1}^{N}\frac{d{\Phi_\alpha}^{l}d{\Phi_\alpha^*}^{l}}{2\pi i}e^{-\sum_{l=1}^{N_s}\sum_{\alpha=1}^{N}{\Phi_\alpha^*}^{l}{\Phi_\alpha}^{l}}\times$$
$$\times\prod_{l=1}^{N_s}\langle\Phi^{l}|(e^{-\frac{\beta}{N_s}\hat{H}_{hop}}e^{-\frac{\beta}{N_s}\hat{H}_{loc}})|\Phi^{l+1}\rangle \tag{2.31}$$

with the periodic boundary condition $|\Phi^{N_s+1}\rangle = |\Phi^1\rangle$, which results in a set of periodic boundary conditions for the eigenvalues $\Phi_\alpha^1 = \Phi_\alpha^{N_s}$ for each $\alpha \in \{1, .., N\}$.

The expectation value $\langle\Phi^l|(e^{-\frac{\beta}{N_s}\hat{H}_{hop}}e^{-\frac{\beta}{N_s}\hat{H}_{loc}})|\Phi^{l+1}\rangle$ can now be computed; this can be achieved by performing an expansion of both $e^{-\frac{\beta}{N_s}\hat{H}_{hop}}$ and $e^{-\frac{\beta}{N_s}\hat{H}_{loc}}$ and by retaining the terms which are first order in $\frac{\beta}{N_s}$; this can be done due to the fact the $\frac{\beta}{N_s}$ tends to zero as N_s tends to plus infinity. Hence:

$$\langle\Phi^l|(e^{-\frac{\beta}{N_s}\hat{H}_{hop}}e^{-\frac{\beta}{N_s}\hat{H}_{loc}})|\Phi^{l+1}\rangle \approx \langle\Phi^l|\Big(\mathcal{I} - \frac{\beta}{N_s}(\hat{H}_{hop} + \hat{H}_{loc})\Big)|\Phi^{l+1}\rangle = \tag{2.32a}$$

$$= \langle\Phi^l|\Phi^{l+1}\rangle - \frac{\beta}{N_s}\langle\Phi^l|(\hat{H}_{hop} + \hat{H}_{loc})|\rangle\Phi^{l+1}\rangle = \tag{2.32b}$$

$$= e^{\sum_{\alpha=1}^{N}\Phi_\alpha^{*\,l}\Phi_\alpha{}^{l+1}}\left(1 - \frac{\beta}{N_s}H(\{\Phi_\alpha^{*\,l}\}_{\alpha\in\{1,..,N\}}, \{\Phi_\alpha{}^{l+1}\}_{\alpha\in\{1,...,N\}})\right) \tag{2.32c}$$

where $H(\{\Phi_\alpha^{*\,l}\}_{\alpha\in\{1,..,N\}}, \{\Phi_\alpha{}^{l+1}\}_{\alpha\in\{1,...,N\}})$ is given by:

$$\begin{aligned} H(\{\Phi_\alpha^{*\,l}\}_{\alpha\in\{1,..,N\}}, \{\Phi_\alpha{}^{l+1}\}_{\alpha\in\{1,...,N\}}) = \\ = -J\sum_{\langle\alpha,\gamma\rangle}(\Phi_\alpha^{*\,l}\Phi_\gamma{}^{l+1} + \Phi_\alpha^{*\,l}\Phi_\gamma{}^{l+1}) \\ + \sum_{\alpha=1}^{N}\left(\frac{U}{2}(\Phi_\alpha^{*\,l}\Phi_\alpha^{*\,l}\Phi_\alpha{}^{l+1}\Phi_\alpha{}^{l+1}) - \mu\Phi_\alpha^{*\,l}\Phi_\alpha{}^{l+1}\right) \end{aligned} \tag{2.33}$$

By exploiting the fact that $\frac{\beta}{N_s}$ is small in the limit of $N_s \to +\infty$, the expectation value $\langle\Phi^l|(e^{-\frac{\beta}{N_s}\hat{H}_{hop}}e^{-\frac{\beta}{N_s}\hat{H}_{loc}})|\Phi^{l+1}\rangle$ can finally be approximated as:

$$\begin{aligned} \langle\Phi^l|(e^{-\frac{\beta}{N_s}\hat{H}_{hop}}e^{-\frac{\beta}{N_s}\hat{H}_{loc}})|\Phi^{l+1}\rangle \approx e^{\sum_{\alpha=1}^{N}\Phi_\alpha^{*\,l}\Phi_\alpha{}^{l+1}}\times \\ \times\, e^{-\frac{\beta}{N_s}H(\{\Phi_\alpha^{*\,l}\}_{\alpha\in\{1,..,N\}},\{\Phi_\alpha{}^{l+1}\}_{\alpha\in\{1,...,N\}})} \end{aligned} \tag{2.34}$$

This result can be plugged back into the expression of the partition function, which becomes:

$$\begin{aligned} \mathcal{Z} = \lim_{N_s\to+\infty}\int\prod_{l=1}^{N_s}\prod_{\alpha=1}^{N}\frac{d\Phi_\alpha{}^l d\Phi_\alpha^{*\,l}}{2\pi i}e^{-\sum_{l=1}^{N_s}\sum_{\alpha=1}^{N}\Phi_\alpha^{*\,l}\Phi_\alpha{}^l}\times \\ \times\, e^{\sum_{l=1}^{N_s}\sum_{\alpha=1}^{N}\Phi_\alpha^{*\,l}\Phi_\alpha{}^{l+1}}e^{-\frac{\beta}{N_s}\sum_{l=1}^{N_s}H(\{\Phi_\alpha^{*\,l}\}_{\alpha\in\{1,..,N\}},\{\Phi_\alpha{}^{l+1}\}_{\alpha\in\{1,...,N\}})} \end{aligned} \tag{2.35}$$

Now, the length of the small time interval can be renamed as $\delta = \frac{\beta}{N_s}$ and the terms of the partition function can be reorganized as:

$$\mathcal{Z} = \lim_{\delta \to 0} \int \prod_{l=1}^{N_s} \prod_{\alpha=1}^{N} \frac{d{\Phi_\alpha}^l d{\Phi^*_\alpha}^l}{2\pi i} \times \\ \times e^{-\delta \sum_{l=1}^{N_s} \left(\sum_{\alpha=1}^{N} {\Phi^*_\alpha}^l \frac{{\Phi_\alpha}^l - {\Phi_\alpha}^{l+1}}{\delta} + H(\{{\Phi^*_\alpha}^l\}_{\alpha \in \{1,..,N\}}, \{{\Phi_\alpha}^{l+1}\}_{\alpha \in \{1,...,N\}}) \right)} \tag{2.36}$$

The limit of $\delta \to 0$ can be formally taken at this step: this requires to replace the discrete variable with continuous time-dependent functions for each site of the lattice; moreover, discrete differences become derivatives and sums become integrals. Therefore, the partition function can be rewritten as:

$$\mathcal{Z} = \int \prod_{\alpha=1}^{N} D\Phi_\alpha(\tau) D\Phi^*_\alpha(\tau) \exp\left\{ - \int_0^\beta d\tau \Big\{ \sum_{\alpha=1}^{N} \left(\Phi^*_\alpha(\tau) \Big(\frac{\partial}{\partial \tau} - \mu \Big) \Phi_\alpha(\tau) + \right. \right. \\ \left. \left. + \frac{U}{2} \Phi^2_\alpha(\tau) {\Phi^*_\alpha}^2(\tau) \right) - J \sum_{\langle \alpha, \gamma \rangle} (\Phi^*_\alpha(\tau) \Phi_\gamma(\tau) + \Phi^*_\gamma(\tau) \Phi_\alpha(\tau)) \Big\} \right\} \tag{2.37}$$

where τ is the imaginary time.
Hence, the action of the Bose-Hubbard model reads:

$$S[\{\Phi_\alpha(\tau)\}_{\alpha \in \{1,..,N\}}, \{\Phi^*_\alpha(\tau)\}_{\alpha \in \{1,..,N\}}] = \\ = \int_0^\beta d\tau \Big\{ \sum_{\alpha=1}^{N} \left(\Phi^*_\alpha(\tau) \Big(\frac{\partial}{\partial \tau} - \mu \Big) \Phi_\alpha(\tau) + \frac{U}{2} \Phi^2_\alpha(\tau) \Phi^*_\alpha(\tau)^2 \right) + \\ - J \sum_{\langle \alpha, \gamma \rangle} (\Phi^*_\alpha(\tau) \Phi_\gamma(\tau) + \Phi^*_\gamma(\tau) \Phi_\alpha(\tau)) \Big\} \tag{2.38}$$

To understand why the integral in imaginary time goes from 0 to β, let us consider again the initial expression of the partition function as the trace of the operator $e^{-\beta \hat{H}}$:

$$\mathcal{Z} = \sum_{n_1, ..., n_N}^{+\infty} \langle n_1, ..., n_N | e^{-\beta \hat{H}} | n_1, ..., n_N \rangle \tag{2.39}$$

The expectation value $\langle n_1, ..., n_N | e^{-\beta \hat{H}} | n_1, ..., n_N \rangle$ can be reinterpreted, from a purely quantum mechanical point of view, as the probability amplitude for the

state $|n_1, ..., n_N\rangle$ to evolve into itself after an imaginary time interval of length β: this is a consequence of the fact that the operator $e^{-\beta\hat{H}}$ in nothing but the time evolution operator over the time interval $[0, \beta]$; the fact that the time is considered imaginary is a consequence of the usual definition of the propagators, which is characterized by the presence of the imaginary unit in the exponent. Under this light, the practical meaning of the Suzuki-Trotter procedure becomes evident: the imaginary time axis $[0, \beta]$ is split into an infinite number of time intervals whose length tend to zero; then the evolution of the system over all these time intervals is evaluated by introducing all the identity operators associated to the different time intervals and this leads to the derivation of an effective action for the quantum system under exam. As a last remark, it is crucial to remember that periodic boundary conditions hold; as a consequence, the imaginary time axis is actually closed on itself as a ring; moreover, the following periodic conditions hold for the bosonic functions:

$$\Phi_\alpha(0) = \Phi_\alpha(\beta) \tag{2.40a}$$
$$\Phi^*_\alpha(0) = \Phi^*_\alpha(\beta) \tag{2.40b}$$

for each $\alpha \in \{1, .., N\}$.

Since the partition function of the Bose-Hubbard model has now been computed for a generic lattice, it is possible to apply, at least from a theoretical point of view, the cavity method. Let us then consider a Bethe lattice with connectivity K; by looking at the expression of the partition function, it is possible to identify a portion of the measure which is local and a portion of the measure which is instead associated to the edges connecting the sites; therefore, it is reasonablee to put forward the following ansatz for the cavity distribution, due to the regularity of the Bethe lattice and due to the fact that U and μ are the same on all sites while J is the same for all the edges:

$$\begin{aligned} c_{cav}(\Phi(\tau), \Phi^*(\tau)) = \frac{1}{z_{cav}} e^{-\int_0^\beta d\tau \left\{ \Phi^*(\tau)(\frac{\partial}{\partial\tau} - \mu)\Phi(\tau) + \frac{U}{2}\Phi^2(\tau)\Phi^{*2}(\tau) \right\}} \times \\ \times \int \prod_{i=1}^{K-1} D\Phi_i(\tau) D{\Phi_i}^*(\tau) c_{cav}(\Phi_i(\tau), \Phi_i^*(\tau)) \times \\ \times e^{J\int_0^\beta d\tau \left\{ \Phi^*(\tau)\sum_{i=1}^{K-1}\Phi_i(\tau) + \Phi(\tau)\sum_{i=1}^{K-1}\Phi_i^*(\tau) \right\}} \end{aligned} \tag{2.41}$$

where z_{cav} is just the normalization constant fixed by:

$$z_{cav} = \int D\Phi(\tau) D\Phi^*(\tau) e^{-\int_0^\beta d\tau \left\{ \Phi^*(\tau)(\frac{\partial}{\partial\tau} - \mu)\Phi(\tau) + \frac{U}{2}\Phi^2(\tau)\Phi^{*2}(\tau) \right\}} \times$$
$$\times \int \prod_{i=1}^{K-1} D\Phi_i(\tau) D\Phi_i{}^*(\tau) c_{cav}(\Phi_i(\tau), \Phi_i^*(\tau)) \times$$
$$\times e^{J\int_0^\beta d\tau \left\{ \Phi^*(\tau) \sum_{i=1}^{K-1} \Phi_i(\tau) + \Phi(\tau) \sum_{i=1}^{K-1} \Phi_i^*(\tau) \right\}} \quad (2.42)$$

Note that the index of the site α has been dropped from the functions on which c_{cav} depends on, as the actual site taken under exam to write the ansatz is indistinguishable from all the others, being the model defined on a Bethe lattice; the index i appearing in the expression has instead been introduced just for practical purposes, to enumerate the quantities associated to the various neighbors of the site taken as a reference.

Similar expressions can be obtained for the full marginal distribution if all the neighbors are taken into account:

$$c(\Phi(\tau), \Phi^*(\tau)) = \frac{1}{z} e^{-\int_0^\beta d\tau \left\{ \Phi^*(\tau)(\frac{\partial}{\partial\tau} - \mu)\Phi(\tau) + \frac{U}{2}\Phi^2(\tau)\Phi^{*2}(\tau) \right\}} \times$$
$$\times \int \prod_{i=1}^{K} D\Phi_i(\tau) D\Phi_i{}^*(\tau) c_{cav}(\Phi_i(\tau), \Phi_i^*(\tau)) \times$$
$$\times e^{J\int_0^\beta d\tau \left\{ \Phi^*(\tau) \sum_{i=1}^{K} \Phi_i(\tau) + \Phi(\tau) \sum_{i=1}^{K} \Phi_i^*(\tau) \right\}} \quad (2.43)$$

where z is the usual normalization constant:

$$z = \int D\Phi(\tau) D\Phi^*(\tau) e^{-\int_0^\beta d\tau \left\{ \Phi^*(\tau)(\frac{\partial}{\partial\tau} - \mu)\Phi(\tau) + \frac{U}{2}\Phi^2(\tau)\Phi^{*2}(\tau) \right\}} \times$$
$$\times \int \prod_{i=1}^{K} D\Phi_i(\tau) D\Phi_i{}^*(\tau) c_{cav}(\Phi_i(\tau), \Phi_i^*(\tau)) \times$$
$$\times e^{J\int_0^\beta d\tau \left\{ \Phi^*(\tau) \sum_{i=1}^{K} \Phi_i(\tau) + \Phi(\tau) \sum_{i=1}^{K} \Phi_i^*(\tau) \right\}} \quad (2.44)$$

From a formal point of view, the expressions defined above could have been obtained following the usual recipe: starting from the discrete-time version of

the partition function, one could have defined a factor graph similar to that used for the presentation of the quantum cavity method for spin systems; then, by grouping together the variables associated to a site in pairs of trajectories, such as $\{{\Phi_\alpha}^l, \Phi_\alpha^{*l}\}_{l\in\{1,\dots,N_s\}}$, the standard cavity method could have been applied to derive the equations for $c_{cav}(\Phi(\tau), \Phi^*(\tau))$ and for $c(\Phi(\tau), \Phi^*(\tau))$ presented above.

2.2.3 Connection with B-DMFT

It is interesting to show the connection between the approach of the cavity method applied after the computation of the partition function of the Bose-Hubbard model by means of the coherent-states path integral formulation and the approach of bosonic dynamical mean-field theory(B-DMFT)[1].

B-DMFT was introduced after its counterpart for fermionic systems with the goal of studying strongly correlated bosonic systems defined on lattices, while taking into account both the normal phase and the condensate phase of bosons. The general idea of B-DMFT is to isolate a single site of the lattice and treat the interactions of this site with the rest of the system as interactions with two reservoirs, one of normal bosons and one for condensate bosons, whose properties are encoded in specific functions to be determined self-consistently[5][6][7]. It is important to remember that the expressions obtained with this approach include all the local and dynamical correlations of the system under exam and are exact on lattices with an infinite connectivity, which is equivalent to having infinite dimensions. This last statement is explicative of the mean-field character of the approach, hence the name of dynamical mean-field theory.

To derive the action of the Bose-Hubbard model in the contest of B-DMFT it is possible to proceed in two not so different ways: the first starts directly from the full action (2.38), where a single site of the lattice is isolated and where the properties of the reservoirs are determined by means of an expansion of the portion of the action describing the hopping between the different sites; the second instead starts from the expression of the normalization constant of the full marginal distribution (2.44) and proceeds with a large connectivity expansion of the exponential term resulting from the hopping term of the Hamiltonian. In the following this second approach will be analyzed in details, but first, it is necessary to do two things: to perform the large connectivity expansion, it is convenient to redefine the coupling constant as $J = \frac{\mathcal{J}}{K}$, with K being the connectivity of the lattice; to make the results consistent with those found in the literature, it is necessary to make some simple change to the expression of the normalization constant of (2.44).

In order to obtain the desired expression for the normalization constant which will be used to perform the large connectivity expansion, it is necessary to symmetrize the term associated to the imaginary time derivative appearing in the action (2.38): this can be achieved by performing the coherent-states path integral formulation

with normalized coherent states and with the corresponding expression of the identity operator. To clarify this step, it is possible to start from the expression of the partition function obtained during the computations of the previous section:

$$\mathcal{Z} = \lim_{N_s \to +\infty} \int \prod_{l=1}^{N_s} \prod_{\alpha=1}^{N} \frac{d{\Phi_\alpha}^l d{\Phi^*_\alpha}^l}{2\pi i} e^{-\sum_{l=1}^{N_s} \sum_{\alpha=1}^{N} {\Phi^*_\alpha}^l {\Phi_\alpha}^l} \times \\ \times \prod_{l=1}^{N_s} \langle \Phi^l | (e^{-\frac{\beta}{N_s} \hat{H}_{hop}} e^{-\frac{\beta}{N_s} \hat{H}_{loc}}) | \Phi^{l+1} \rangle \quad (2.45)$$

If normalized coherent states are used, this expression becomes:

$$\mathcal{Z} = \lim_{N_s \to +\infty} \int \prod_{l=1}^{N_s} \prod_{\alpha=1}^{N} \frac{d{\Phi_\alpha}^l d{\Phi^*_\alpha}^l}{2\pi i} \prod_{l=1}^{N_s} \langle \Phi^l | (e^{-\frac{\beta}{N_s} \hat{H}_{hop}} e^{-\frac{\beta}{N_s} \hat{H}_{loc}}) | \Phi^{l+1} \rangle \quad (2.46)$$

The term $\langle \Phi^l | (e^{-\frac{\beta}{N_s} \hat{H}_{hop}} e^{-\frac{\beta}{N_s} \hat{H}_{loc}}) | \Phi^{l+1} \rangle$ now becomes:

$$\langle \Phi^l | (e^{-\frac{\beta}{N_s} \hat{H}_{hop}} e^{-\frac{\beta}{N_s} \hat{H}_{loc}}) | \Phi^{l+1} \rangle \approx e^{\sum_{\alpha=1}^{N} {\Phi^*_\alpha}^l {\Phi_\alpha}^{l+1}} e^{-\frac{1}{2} \sum_{\alpha=1}^{N} {\Phi^*_\alpha}^l {\Phi_\alpha}^l} \times \\ \times e^{-\frac{1}{2} \sum_{\alpha=1}^{N} {\Phi^*_\alpha}^{l+1} {\Phi_\alpha}^{l+1}} e^{-\frac{\beta}{N_s} H(\{{\Phi^*_\alpha}^l\}_{\alpha \in \{1,..,N\}}, \{{\Phi_\alpha}^{l+1}\}_{\alpha \in \{1,...,N\}})} \quad (2.47)$$

The expression of the partition function then becomes:

$$\mathcal{Z} = \lim_{N_s \to +\infty} \int \prod_{l=1}^{N_s} \prod_{\alpha=1}^{N} \frac{d{\Phi_\alpha}^l d{\Phi^*_\alpha}^l}{2\pi i} e^{\sum_{l=1}^{N_s} \sum_{\alpha=1}^{N} {\Phi^*_\alpha}^l {\Phi_\alpha}^{l+1}} e^{-\frac{1}{2} \sum_{l=1}^{N_s} \sum_{\alpha=1}^{N} {\Phi^*_\alpha}^l {\Phi_\alpha}^l} \times \\ \times e^{-\frac{1}{2} \sum_{l=1}^{N_s} \sum_{\alpha=1}^{N} {\Phi^*_\alpha}^{l+1} {\Phi_\alpha}^{l+1}} e^{-\frac{\beta}{N_s} \sum_{l=1}^{N_s} H(\{{\Phi^*_\alpha}^l\}_{\alpha \in \{1,..,N\}}, \{{\Phi_\alpha}^{l+1}\}_{\alpha \in \{1,...,N\}})} \quad (2.48)$$

By setting once again $\delta = \frac{\beta}{N_s}$, the partition function can be rewritten as:

$$\mathcal{Z} = \lim_{\delta \to 0} \int \prod_{l=1}^{N_s} \prod_{\alpha=1}^{N} \frac{d{\Phi_\alpha}^l d{\Phi^*_\alpha}^l}{2\pi i} \exp \left\{ -\delta \sum_{l=1}^{N_s} \left(\frac{1}{2} \sum_{\alpha=1}^{N} {\Phi^*_\alpha}^l \frac{{\Phi_\alpha}^l - {\Phi_\alpha}^{l+1}}{\delta} + \right. \right. \\ \left. \left. + \frac{1}{2} \sum_{\alpha=1}^{N} {\Phi_\alpha}^{l+1} \frac{{\Phi^*_\alpha}^{l+1} - {\Phi^*_\alpha}^l}{\delta} \right) + \sum_{l=1}^{N_s} H(\{{\Phi^*_\alpha}^l\}_{\alpha \in \{1,..,N\}}, \{{\Phi_\alpha}^{l+1}\}_{\alpha \in \{1,...,N\}}) \right\} \quad (2.49)$$

By explicitely taking the limit of $\delta \to 0$, we obtain the expression of the partition function in continous time:

$$\mathcal{Z} = \int \prod_{\alpha=1}^{N} D\Phi_\alpha(\tau) D\Phi_\alpha^*(\tau) \exp\Bigg\{ - \int_0^\beta d\tau \Big\{ \sum_{\alpha=1}^{N} \Bigg(\frac{1}{2}\Phi_\alpha^*(\tau)\Big(\frac{\partial}{\partial\tau} - \mu\Big)\Phi_\alpha(\tau) + \frac{1}{2}\Phi_\alpha(\tau)\Big(- \frac{\partial}{\partial\tau} - \mu\Big)\Phi_\alpha^*(\tau) + \frac{U}{2}\Phi_\alpha^2(\tau)\Phi_\alpha^{*\,2}(\tau)\Bigg) + - J \sum_{\langle\alpha,\gamma\rangle} (\Phi_\alpha^*(\tau)\Phi_\gamma(\tau) + \Phi_\gamma^*(\tau)\Phi_\alpha(\tau))\Big\}\Bigg\} \quad (2.50)$$

Therefore, the symmetrized action of the Bose-Hubbard model reads:

$$\begin{aligned} &S[\{\Phi_\alpha(\tau)\}_{\alpha\in\{1,..,N\}}, \{\Phi_\alpha^*(\tau)\}_{\alpha\in\{1,..,N\}}] = \\ &= \int_0^\beta d\tau \Big\{ \sum_{\alpha=1}^{N} \Bigg(\frac{1}{2}\Phi_\alpha^*(\tau)\Big(\frac{\partial}{\partial\tau} - \mu\Big)\Phi_\alpha(\tau) + \frac{1}{2}\Phi_\alpha(\tau)\Big(- \frac{\partial}{\partial\tau} - \mu\Big)\Phi_\alpha^*(\tau) + \\ &\quad + \frac{U}{2}\Phi_\alpha^2(\tau)\Phi_\alpha^*(\tau)^2\Bigg) - J \sum_{\langle\alpha,\gamma\rangle} (\Phi_\alpha^*(\tau)\Phi_\gamma(\tau) + \Phi_\gamma^*(\tau)\Phi_\alpha(\tau))\Big\} \end{aligned} \quad (2.51)$$

At this point it is straightforward to derive the desired expression for the normalization constant z of the full marginal distribution to be used for the large connectivity expansion, which is given by:

$$\begin{aligned} z = \int D\Phi(\tau) D\Phi^*(\tau) e^{-\int_0^\beta d\tau \left\{ \frac{1}{2}\Phi^*(\tau)(\frac{\partial}{\partial\tau} - \mu)\Phi(\tau) + \frac{1}{2}\Phi(\tau)(-\frac{\partial}{\partial\tau} - \mu)\Phi^*(\tau) + \frac{U}{2}\Phi^2(\tau)\Phi^{*\,2}(\tau) \right\}} \times \\ \times \prod_{i=1}^{K} \int D\Phi_i(\tau) D\Phi_i{}^*(\tau) c_{cav}(\Phi_i(\tau), \Phi_i^*(\tau)) \times \\ \times e^{\frac{\mathcal{J}}{K}\int_0^\beta d\tau \left\{ \Phi^*(\tau)\Phi_i(\tau) + \Phi(\tau)\Phi_i^*(\tau) \right\}} \end{aligned} \quad (2.52)$$

where the coupling constant has now been correctly rescaled.

To perform the large connectivity expansion, it is possible to start from the exponential associated to the hopping between sites:

$$e^{\frac{\mathcal{J}}{K}\int_0^\beta d\tau\left\{\Phi^*(\tau)\Phi_i(\tau)+\Phi(\tau)\Phi_i^*(\tau)\right\}} = \tag{2.53a}$$

$$= 1+\frac{\mathcal{J}}{K}\int_0^\beta d\tau\left\{\Phi^*(\tau)\Phi_i(\tau)+\Phi(\tau)\Phi_i^*(\tau)\right\}+\frac{\mathcal{J}^2}{2K^2}\int_0^\beta d\tau_1\int_0^\beta d\tau_1\times \tag{2.53b}$$

$$\times\left\{\Phi^*(\tau_1)\Phi_i(\tau_1)+\Phi(\tau_1)\Phi_i^*(\tau_1)\right\}\left\{\Phi^*(\tau_2)\Phi_i(\tau_2)+\Phi(\tau_2)\Phi_i^*(\tau_2)\right\}+ \tag{2.53c}$$

$$+o\left(\frac{1}{K^2}\right)= \tag{2.53d}$$

$$= 1+\frac{\mathcal{J}}{K}\int_0^\beta d\tau\left\{\Phi^*(\tau)\Phi_i(\tau)+\Phi(\tau)\Phi_i^*(\tau)\right\}+\frac{\mathcal{J}^2}{K^2}\int_0^\beta d\tau_1\int_0^\beta d\tau_1\times \tag{2.53e}$$

$$\times\Big\{\Phi^*(\tau_1)\Phi_i(\tau_1)\Phi^*(\tau_2)\Phi_i(\tau_2)+\Phi^*(\tau_1)\Phi_i(\tau_1)\Phi(\tau_2)\Phi_i^*(\tau_2)+ \tag{2.53f}$$

$$+\Phi(\tau_1)\Phi_i^*(\tau_1)\Phi^*(\tau_2)\Phi_i(\tau_2)+\Phi(\tau_1)\Phi_i^*(\tau_1)\Phi(\tau_2)\Phi_i^*(\tau_2)\Big\}+o\left(\frac{1}{K^2}\right) \tag{2.53g}$$

It is useful to define a cavity average for a generic observable $O(\Phi_i(\tau),\Phi_i^*(\tau))$ as:

$$\langle O(\Phi_i(\tau),\Phi_i^*(\tau))\rangle_{cav} = \\ = \int D\Phi_i(\tau)D\Phi_i^*(\tau)c_{cav}(\Phi_i(\tau),\Phi_i^*(\tau))O(\Phi_i(\tau),\Phi_i^*(\tau)) \tag{2.54}$$

By exploiting this definition, one can write:

$$\int D\Phi_i(\tau)D\Phi_i^*(\tau)c_{cav}(\Phi_i(\tau),\Phi_i^*(\tau))e^{\frac{\mathcal{J}}{K}\int_0^\beta d\tau\left\{\Phi^*(\tau)\Phi_i(\tau)+\Phi(\tau)\Phi_i^*(\tau)\right\}} = \tag{2.55a}$$

$$= 1+\frac{\mathcal{J}}{K}\int_0^\beta d\tau\left\{\Phi^*(\tau)\langle\Phi_i(\tau)\rangle_{cav}+\Phi(\tau)\langle\Phi_i^*(\tau)\rangle_{cav}\right\}+ \tag{2.55b}$$

$$+\frac{\mathcal{J}^2}{2K^2}\int_0^\beta d\tau_1\int_0^\beta d\tau_2\Big\{\Phi^*(\tau_1)\Phi^*(\tau_2)\langle\Phi_i(\tau_1)\Phi_i(\tau_2)\rangle_{cav}+ \tag{2.55c}$$

$$+\Phi^*(\tau_1)\Phi(\tau_2)\langle\Phi_i(\tau_1)\Phi_i^*(\tau_2)\rangle_{cav}+\Phi(\tau_1)\Phi^*(\tau_2)\langle\Phi_i^*(\tau_1)\Phi_i(\tau_2)\rangle_{cav}+ \tag{2.55d}$$

$$+\Phi(\tau_1)\Phi(\tau_2)\langle\Phi_i^*(\tau_1)\Phi_i^*(\tau_2)\rangle_{cav}\Big\}+o\left(\frac{1}{K^2}\right) \tag{2.55e}$$

To obtain the B-DMFT action of the Bose-Hubbard model it is necessary to exponentiate the last expression in the following way:

$$\int D\Phi_i(\tau)D\Phi_i^*(\tau)c_{cav}(\Phi_i(\tau),\Phi_i^*(\tau))e^{\frac{\mathcal{J}}{K}\int_0^\beta d\tau\left\{\Phi^*(\tau)\Phi_i(\tau)+\Phi(\tau)\Phi_i^*(\tau)\right\}} =$$
$$= \exp\left\{\log\left(1+\frac{\mathcal{J}}{K}\int_0^\beta d\tau\left\{\Phi^*(\tau)\langle\Phi_i(\tau)\rangle_{cav}+\Phi(\tau)\langle\Phi_i^*(\tau)\rangle_{cav}\right\}+\right.\right.$$
$$+\frac{\mathcal{J}^2}{2K^2}\int_0^\beta d\tau_1\int_0^\beta d\tau_2\left\{\Phi^*(\tau_1)\Phi^*(\tau_2)\langle\Phi_i(\tau_1)\Phi_i(\tau_2)\rangle_{cav}+\right.$$
$$+\Phi^*(\tau_1)\Phi(\tau_2)\langle\Phi_i(\tau_1)\Phi_i^*(\tau_2)\rangle_{cav}+\Phi(\tau_1)\Phi^*(\tau_2)\langle\Phi_i^*(\tau_1)\Phi_i(\tau_2)\rangle_{cav}+$$
$$\left.\left.\left.+\Phi(\tau_1)\Phi(\tau_2)\langle\Phi_i^*(\tau_1)\Phi_i^*(\tau_2)\rangle_{cav}\right\}+o\left(\frac{1}{K^2}\right)\right)\right\} \quad (2.56)$$

The logarithm at the exponent can be expanded as well, hence one gets:

$$\int D\Phi_i(\tau)D\Phi_i^*(\tau)c_{cav}(\Phi_i(\tau),\Phi_i^*(\tau))e^{\frac{\mathcal{J}}{d}\int_0^\beta d\tau\left\{\Phi^*(\tau)\Phi_i(\tau)+\Phi(\tau)\Phi_i^*(\tau)\right\}} = \quad (2.57a)$$
$$= \exp\left\{\frac{\mathcal{J}}{d}\int_0^\beta d\tau\left\{\Phi^*(\tau)\langle\Phi_i(\tau)\rangle_{cav}+\Phi(\tau)\langle\Phi_i^*(\tau)\rangle_{cav}\right\}+\right. \quad (2.57b)$$
$$+\frac{\mathcal{J}^2}{2d^2}\int_0^\beta d\tau_1\int_0^\beta d\tau_2\left\{\Phi^*(\tau_1)\Phi^*(\tau_2)\times\right. \quad (2.57c)$$
$$\times\left(\langle\Phi_i(\tau_1)\Phi_i(\tau_2)\rangle_{cav}-\langle\Phi_i(\tau_1)\rangle_{cav}\langle\Phi_i(\tau_2)\rangle_{cav}\right)+\Phi^*(\tau_1)\Phi(\tau_2)\times \quad (2.57d)$$
$$\times\left(\langle\Phi_i(\tau_1)\Phi_i^*(\tau_2)\rangle_{cav}-\langle\Phi_i(\tau_1)\rangle_{cav}\langle\Phi_i^*(\tau_2)\rangle_{cav}\right)+\Phi(\tau_1)\Phi^*(\tau_2)\times \quad (2.57e)$$
$$\times\left(\langle\Phi_i^*(\tau_1)\Phi_i(\tau_2)\rangle_{cav}-\langle\Phi_i^*(\tau_1)\rangle_{cav}\langle\Phi_i(\tau_2)\rangle_{cav}\right)+\Phi(\tau_1)\Phi(\tau_2)\times \quad (2.57f)$$
$$\left.\left.\times\left(\langle\Phi_i^*(\tau_1)\Phi_i^*(\tau_2)\rangle_{cav}-\langle\Phi_i^*(\tau_1)\rangle_{cav}\langle\Phi_i^*(\tau_2)\rangle_{cav}\right)\right\}\right\} \quad (2.57g)$$

In the expression above the first and the second moments with respect to the cavity distribution $c_{cav}(\Phi_i(\tau),\Phi_i^*(\tau))$ can be recognized. The first moments can be renamed as:

$$\Psi(\tau) = \langle\Phi_i(\tau)\rangle_{cav} \quad (2.58a)$$
$$\Psi^*(\tau) = \langle\Phi_i^*(\tau)\rangle_{cav} \quad (2.58b)$$

while the second moments can be recast as:

$$G^{11}_{cav}(\tau_1,\tau_2) = \langle \Phi_i(\tau_1)\Phi_i^*(\tau_2)\rangle_{cav} - \langle \Phi_i(\tau_1)\rangle_{cav}\langle \Phi_i^*(\tau_2)\rangle_{cav} \tag{2.59a}$$
$$G^{12}_{cav}(\tau_1,\tau_2) = \langle \Phi_i(\tau_1)\Phi_i(\tau_2)\rangle_{cav} - \langle \Phi_i(\tau_1)\rangle_{cav}\langle \Phi_i(\tau_2)\rangle_{cav} \tag{2.59b}$$
$$G^{21}_{cav}(\tau_1,\tau_2) = \langle \Phi_i^*(\tau_1)\Phi_i^*(\tau_2)\rangle_{cav} - \langle \Phi_i^*(\tau_1)\rangle_{cav}\langle \Phi_i^*(\tau_2)\rangle_{cav} \tag{2.59c}$$
$$G^{22}_{cav}(\tau_1,\tau_2) = \langle \Phi_i^*(\tau_1)\Phi_i(\tau_2)\rangle_{cav} - \langle \Phi_i^*(\tau_1)\rangle_{cav}\langle \Phi_i(\tau_2)\rangle_{cav} \tag{2.59d}$$

These expressions can be rewritten in terms of $\Psi(\tau)$ and $\Psi^*(\tau)$ as:

$$G^{11}_{cav}(\tau_1,\tau_2) = \langle \Phi_i(\tau_1)\Phi_i^*(\tau_2)\rangle_{cav} - \Psi(\tau_1)\Psi^*(\tau_2) \tag{2.60a}$$
$$G^{12}_{cav}(\tau_1,\tau_2) = \langle \Phi_i(\tau_1)\Phi_i(\tau_2)\rangle_{cav} - \Psi(\tau_1)\Psi(\tau_2) \tag{2.60b}$$
$$G^{21}_{cav}(\tau_1,\tau_2) = \langle \Phi_i^*(\tau_1)\Phi_i^*(\tau_2)\rangle_{cav} - \Psi^*(\tau_1)\Psi^*(\tau_2) \tag{2.60c}$$
$$G^{22}_{cav}(\tau_1,\tau_2) = \langle \Phi_i^*(\tau_1)\Phi_i(\tau_2)\rangle_{cav} - \Psi^*(\tau_1)\Psi(\tau_2) \tag{2.60d}$$

Finally, it is possible to write:

$$\begin{aligned}\int D\Phi_i(\tau)D\Phi_i^*(\tau)c_{cav}(\Phi_i(\tau),\Phi_i^*(\tau))e^{\frac{\mathcal{J}}{d}\int_0^\beta d\tau\left\{\Phi^*(\tau)\Phi_i(\tau)+\Phi(\tau)\Phi_i^*(\tau)\right\}} = \\ = \exp\left\{\frac{\mathcal{J}}{K}\int_0^\beta d\tau\left\{\Phi^*(\tau)\Psi(\tau)+\Phi(\tau)\Psi^*(\tau)\right\}+\right. \\ + \frac{\mathcal{J}^2}{2K^2}\int_0^\beta d\tau_1\int_0^\beta d\tau_2\left\{\Phi^*(\tau_1)\Phi^*(\tau_2)G^{12}_{cav}(\tau_1,\tau_2)+\Phi^*(\tau_1)\Phi(\tau_2)\times\right. \\ \left.\left.\times G^{11}_{cav}(\tau_1,\tau_2)+\Phi(\tau_1)\Phi^*(\tau_2)G^{22}_{cav}(\tau_1,\tau_2)+\Phi(\tau_1)\Phi(\tau_2)G^{21}_{cav}(\tau_1,\tau_2)\right\}\right\}\end{aligned} \tag{2.61}$$

Obviously, the equality holds only in the limit of d large (ideally $d \to +\infty$); for lattices with a finite connectivity, this is clearly just an approximation.

The expression for the normalization constant z then reads:

$$z = \int D\Phi(\tau) D\Phi^*(\tau) e^{-\int_0^\beta d\tau \left\{ \Phi^*(\tau)(\frac{\partial}{\partial\tau} - \mu)\Phi(\tau) + \frac{U}{2}\Phi^2(\tau)\Phi^{*2}(\tau) \right\}} \times$$
$$\times \prod_{i=1}^{K} \exp\left\{ \frac{\mathcal{J}}{d} \int_0^\beta d\tau \left\{ \Phi^*(\tau)\Psi(\tau) + \Phi(\tau)\Psi^*(\tau) \right\} + \right.$$
$$+ \frac{\mathcal{J}^2}{2K^2} \int_0^\beta d\tau_1 \int_0^\beta d\tau_2 \left\{ \Phi^*(\tau_1)\Phi^*(\tau_2) G^{12}_{cav}(\tau_1, \tau_2) + \Phi^*(\tau_1)\Phi(\tau_2) \times \right.$$
$$\left.\left. \times G^{11}_{cav}(\tau_1, \tau_2) + \Phi(\tau_1)\Phi^*(\tau_2) G^{22}_{cav}(\tau_1, \tau_2) + \Phi(\tau_1)\Phi(\tau_2) G^{21}_{cav}(\tau_1, \tau_2) \right\} \right\} \quad (2.62)$$

In the contest of B-DMFT the normalization constant z can be reinterpreted as the partition function of an isolated site, where the local action is given by:

$$S_{loc} = \int_0^\tau d\tau \left\{ \Phi^*(\tau)\Big(\frac{\partial}{\partial\tau} - \mu\Big)\Phi(\tau) + \Phi(\tau)\Big(-\frac{\partial}{\partial\tau} - \mu\Big)\Phi^*(\tau) + \frac{U}{2}\Phi^2(\tau)\Phi^{*2}(\tau) \right\} +$$
$$- \mathcal{J} \int_0^\beta d\tau \left\{ \Phi^*(\tau)\Psi(\tau) + \Phi(\tau) + \Psi^*(\tau) \right\} +$$
$$- \frac{\mathcal{J}}{2K} \int_0^\beta d\tau_1 \int_0^\beta d\tau_2 \left\{ \Phi^*(\tau_1)\Phi^*(\tau_2) G^{12}_{cav}(\tau_1, \tau_2) + \Phi^*(\tau_1)\Phi(\tau_2) \times \right.$$
$$\left. \times G^{11}_{cav}(\tau_1, \tau_2) + \Phi(\tau_1)\Phi^*(\tau_2) G^{22}_{cav}(\tau_1, \tau_2) + \Phi(\tau_1)\Phi(\tau_2) G^{21}_{cav}(\tau_1, \tau_2) \right\} \quad (2.63)$$

To complete the picture of B-DMFT, it is necessary to compute the quantities $\Psi(\tau)$, $\Psi^*(\tau)$, $G^{11}_{cav}(\tau_1, \tau_2)$, $G^{12}_{cav}(\tau_1, \tau_2)$, $G^{21}_{cav}(\tau_1, \tau_2)$ and $G^{22}_{cav}(\tau_1, \tau_2)$; since these have been defined as averages with respect to the cavity distribution $c_{cav}(\Phi(\tau), \Phi^*(\tau))$, the action which allows to self-consistently compute them is simply obtained by considering a lattice with a connectivity $K - 1$. Therefore, it is useful to consider also the following action:

$$S_{cav} = \int_0^\tau d\tau \Big\{ \Phi^*(\tau)\Big(\frac{\partial}{\partial\tau} - \mu\Big)\Phi(\tau) + \Phi(\tau)\Big(-\frac{\partial}{\partial\tau} - \mu\Big)\Phi^*(\tau) + \frac{U}{2}\Phi^2(\tau)\Phi^{*2}(\tau)\Big\} +$$
$$- \frac{\mathcal{J}}{K}(K-1)\int_0^\beta d\tau \Big\{ \Phi^*(\tau)\Psi(\tau) + \Phi(\tau) + \Psi^*(\tau)\Big\} +$$
$$- \frac{\mathcal{J}}{2K^2}(K-1)\int_0^\beta d\tau_1 \int_0^\beta d\tau_2 \Big\{ \Phi^*(\tau_1)\Phi^*(\tau_2)G^{12}_{cav}(\tau_1,\tau_2) + \Phi^*(\tau_1)\Phi(\tau_2)\times$$
$$\times G^{11}_{cav}(\tau_1,\tau_2) + \Phi(\tau_1)\Phi^*(\tau_2)G^{22}_{cav}(\tau_1,\tau_2) + \Phi(\tau_1)\Phi(\tau_2)G^{21}_{cav}(\tau_1,\tau_2)\Big\} \quad (2.64)$$

To conclude this chapter, some final considerations can be made. Starting from the many-body quantum Hamiltonian, the partition function of the system has been derived and from that, the cavity method has been applied to obtain the expressions of the cavity measure and of the one-site marginal distribution; while in the case of classical systems this is enough, for quantum spins it is necessary to go beyond to get a representation of the system which allows for numerical approaches[7]. The solution is provided by the dynamical mean-filed theory approach, which provides an effective description of the original system in terms of quantities that can be computed self-consistently. The most important takeaway of this chapter is the methodology that allowed to go from the original Hamiltonian operator of the model under exam, up to an effective action which can be analyzed using the approach of Matsubara frequencies, apart from the non-linear term associated to the same-site interaction term; indeed, such methodology can be extended to complex classical systems defined on graph to obtain effective descriptions which can be analyzed by means of numerical methods. The remaining chapters of this thesis are indeed devoted at the presentation of the extension of the methodology presented here to classical systems and to the derivation of an algorithm for the derivation of numerical results.

Chapter 3

The dynamic cavity approach for out of equilibrium systems

3.1 Introduction

While in the two previous chapters a recipe has been laid out for the analysis of classical and quantum systems at equilibrium, it would be interesting to understand whether the ideas of the cavity method and of the dynamical mean-field theory approach can be extended to study out of equilibrium problems. Starting from this premise and following the approach developed in [9], a generic dynamics defined on a graph with linear couplings is analyzed and the dynamic cavity equations are derived; from those a set of effective equations of the dynamics can be obtained by performing a large connectivity (or small coupling) expansion, with an approach similar to that of B-DMFT. The set of effective equations involves quantities that can be computed self-consistently by means of an algorithm presented in [10], whose main ideas are analyzed at the end of the chapter.

3.2 The dynamic cavity approach

3.2.1 Derivation of the dynamic cavity equations

To present the dynamic cavity approach, a set of interacting degrees of freedom defined on a graph $G = (V, E)$ is considered; these are such that their evolution is described by a set of Langevin equations and that the interactions between them are linear. Hence, for each degree of freedom $x_i(t)$, with $i \in V$, it is possible to

write:

$$\frac{dx_i}{dt} = f[x_i(t)] + \alpha \sum_{j\in\partial i} J_{ij} x_j(t) + \eta_i(t) \tag{3.1}$$

where the noise $\eta_i(t)$ is a Gaussian white noise with the following properties:

$$\langle \eta_i(t) \rangle = 0 \tag{3.2a}$$
$$\langle \eta_i(t)\eta_j(t') \rangle = 2g[x_i(t)]\delta_{i,j}\delta(t-t') \tag{3.2b}$$

In the equation above the parameter α is added, so that later a series expansion can be performed, while the parameters J_{ij} are nothing but the coupling constants between the various degrees of freedom of the system.

To derive the effective equations it is necessary to go through the path integral representation of the equations of the dynamics; this can be achieved by means of the Martin-Siggia-Rose-Janssen-De Dominicis (MSRJD) functional formalism. To this purpose, it is convenient to exploit a discrete-time formulation of the dynamics; the scheme used here is the Euler-Maruyama's one, where $t = \Delta n$ and Δ is a small time step approaching zero. Within this picture, the identification $x_i^n = x_i(t = n\Delta)$ for the trajectories and $\Delta\eta_i^n = \int_{n\Delta}^{(n+1)\Delta} dt\eta_i(t)$ for the noise(Ito convention) can be made. The discretized version of the stochastic differential equation presented at the beginning is:

$$x_i^{n+1} = x_i^n + \left(f[x_i^n] + \alpha \sum_{j\in\partial i} J_{ij} x_j^n \right) \Delta + \Delta\eta_i^n \tag{3.3}$$

with n going from 0 to $T = \mathcal{T}/\Delta$, where $\mathcal{T}$ is the time horizon of the dynamics. The properties of the noise in discrete time read:

$$\langle \Delta\eta_i^n \rangle = 0 \tag{3.4a}$$
$$\langle \Delta\eta_i^n \Delta\eta_j^{n'} \rangle = 2g[x_i^n]\delta_{i,j}\delta_{n,n'} \tag{3.4b}$$

The dynamical partition function of the MSRJD formalism is given by:

$$\mathcal{Z} = \left\langle \int D\vec{\mathbf{x}} \prod_i p_i(x_i^0) \prod_n \delta_{x_i^{n+1}, x_i^n + f[x_i^n]\Delta + \alpha\Delta \sum_{j\in\partial i} J_{ij} x_j^n + \Delta\eta_i^n} \right\rangle_{\vec{\Delta\eta}} = \tag{3.5a}$$

$$= \left\langle \int D\vec{\mathbf{x}} D\vec{\hat{\mathbf{x}}} \prod_i p_i(x_i^0) \prod_n e^{-i\hat{x}_i^n (x_i^{n+1} - x_i^n - f[x_i^n]\Delta - \alpha\Delta \sum_{j\in\partial i} J_{ij} x_j^n - \Delta\eta_i^n)} \right\rangle_{\vec{\Delta\eta}} \tag{3.5b}$$

where $\langle ... \rangle_{\vec{\Delta\eta}}$ indicates that the average is taken over all the possible realization of the noise trajectories associated to the nodes in the graph, where $p_i(x_i^0)$ is the probability distribution for the initial value of the trajectory $\mathbf{x}_i$ and where the functional measure is compactly written as $\int D\vec{\mathbf{x}} = \prod_i \int D\mathbf{x}_i = \prod_{i,n} \int dx_i^n$ and $\int D\vec{\hat{\mathbf{x}}} = \prod_i \int D\hat{\mathbf{x}}_i = \prod_{i,n} \int d\hat{x}_i^n$.

By noticing that only a part of the integrand of the functional integral depends on the noise and that this part factorizes over the nodes, we can compute the average $\langle ... \rangle_{\vec{\Delta\eta}}$ by factorizing over the nodes and by exploiting the following result:

$$\left\langle e^{i\hat{\mathbf{x}}_i^T \vec{\Delta\eta}_i} \right\rangle_{\vec{\Delta\eta}_i} = \int D\vec{\Delta\eta}_i e^{i\hat{\mathbf{x}}_i{}^T \vec{\Delta\eta}_i} P[\vec{\Delta\eta}_i] = \tag{3.6a}$$

$$= \prod_n \int d\Delta\eta_i^n e^{i\hat{x}_i^n \Delta\eta_i^n} e^{-\frac{\Delta\eta_i^{n\,2}}{2g[x_i^n]}} = \tag{3.6b}$$

$$= \prod_n e^{-\frac{\hat{x}_i^{n\,2} g[x_i^n]}{2}} = \tag{3.6c}$$

$$= e^{-\frac{1}{2} i\vec{\hat{\mathbf{x}}}_i^T G_i \vec{\hat{\mathbf{x}}}_i} \tag{3.6d}$$

where $\int D\vec{\Delta\eta}_i = \int \prod_n d\Delta\eta_i^n$, where $P[\vec{\Delta\eta}_i]$ is the probability distribution associated to the trajectory of the noise of the node i and where G_i is nothing but the covariance matrix of the Gaussian random vector $\vec{\Delta\eta}_i$ with zero mean, and it is such that $G_i^{n,n'} = \langle \Delta\eta_i^n \Delta\eta_i^{n'} \rangle - \langle \Delta\eta_i^n \rangle \langle \Delta\eta_i^{n'} \rangle = 2g[x_i^n]\Delta\delta_{n,n'}$.

The dynamical partition function can be factorized as:

$$\mathcal{Z} = \int D\vec{\mathbf{x}} D\vec{\hat{\mathbf{x}}} \prod_i \left\{ p_i(x_i^0) \prod_n e^{-i\hat{x}_i^n (x_i^{n+1} - x_i^n - f[x_i^n]\Delta) - g[x_i^n]\Delta(\hat{x}_i^n)^2} \right\} \times \tag{3.7a}$$

$$\times \prod_{i<j} \prod_n \left\{ e^{\alpha\Delta(J_{ij} i\hat{x}_i^n x_j^n + J_{ji} i\hat{x}_j^n x_i^n)} \right\} \tag{3.7b}$$

This factorization of the dynamical partition function is useful to determine the factor graph of this model, which is of great help in putting forward the following dynamic cavity equation:

$$c_{i\setminus j}[\mathbf{x}_i, \hat{\mathbf{x}}_i] = \frac{1}{Z_{ij}^{cav}} e^{\sum_n \left\{ -i\hat{x}_i^n (x_i^{n+1} - x_i^n - f[x_i^n]\Delta) - g[x_i^n]\Delta(\hat{x}_i^n)^2 \right\}} \times$$

$$\times \prod_{k \in \partial i \setminus j} \int D\mathbf{x}_k D\hat{\mathbf{x}}_k c_{ki}[\mathbf{x}_k, \hat{\mathbf{x}}_k] e^{\alpha\Delta \sum_n (J_{ki} i\hat{x}_k^n x_i^n + J_{ik} i\hat{x}_i^n x_k^n)} \tag{3.8}$$

where Z_{ij}^{cav} is nothing but a normalization constant:

$$Z_{ij}^{cav} = \int D\mathbf{x}_i D\hat{\mathbf{x}}_i e^{\sum_n \left\{-i\hat{x}_i^n(x_i^{n+1}-x_i^n-f[x_i^n]\Delta)-g[x_i^n]\Delta(\hat{x}_i^n)^2\right\}} \times \\ \times \prod_{k\in\partial i\setminus j} \int D\mathbf{x}_k D\hat{\mathbf{x}}_k c_{ki}[\mathbf{x}_k,\hat{\mathbf{x}}_k] e^{\alpha\Delta\sum_n (J_{ki}i\hat{x}_k^n x_i^n + J_{ik}i\hat{x}_i^n x_k^n)} \quad (3.9)$$

The expression for the full marginal can be obtained by considering all the neighbors of a node:

$$c_i[\mathbf{x}_i,\hat{\mathbf{x}}_i] = \frac{1}{Z_i} e^{\sum_n \left\{-i\hat{x}_i^n(x_i^{n+1}-x_i^n-f[x_i^n]\Delta)-g[x_i^n]\Delta(\hat{x}_i^n)^2\right\}} \times \\ \times \prod_{k\in\partial i} \int D\mathbf{x}_k D\hat{\mathbf{x}}_k c_{ki}[\mathbf{x}_k,\hat{\mathbf{x}}_k] e^{\alpha\Delta\sum_n (J_{ki}i\hat{x}_k^n x_i^n + J_{ik}i\hat{x}_i^n x_k^n)} \quad (3.10)$$

where Z_i is the corresponding normalization constant:

$$Z_i = \int D\mathbf{x}_i D\hat{\mathbf{x}}_i e^{\sum_n \left\{-i\hat{x}_i^n(x_i^{n+1}-x_i^n-f[x_i^n]\Delta)-g[x_i^n]\Delta(\hat{x}_i^n)^2\right\}} \times \\ \times \prod_{k\in\partial i} \int D\mathbf{x}_k D\hat{\mathbf{x}}_k c_{ki}[\mathbf{x}_k,\hat{\mathbf{x}}_k] e^{\alpha\Delta\sum_n (J_{ki}i\hat{x}_k^n x_i^n + J_{ik}i\hat{x}_i^n x_k^n)} \quad (3.11)$$

3.2.2 Small coupling expansion

To proceed in the derivation of the effective stochastic differential equations, it is useful to perform an expansion of the exponential term that appears in (3.8); the expansion is carried out by exploiting the parameter α, which is assumed to be small for the moment; moreover, it allows to interpret this same analysis as an expansion around the non-interacting case. The expansion reads:

$$\int D\mathbf{x}_k D\hat{\mathbf{x}}_k c_{ki}[\mathbf{x}_k,\hat{\mathbf{x}}_k] e^{\alpha\Delta\sum_n (J_{ki}i\hat{x}_k^n x_i^n + J_{ik}i\hat{x}_i^n x_k^n)} = \quad (3.12a)$$

$$= \int D\mathbf{x}_k D\hat{\mathbf{x}}_k c_{ki}[\mathbf{x}_k,\hat{\mathbf{x}}_k] \Bigg(1 + \alpha\Delta\sum_n (J_{ki}i\hat{x}_k^n x_i^n + J_{ik}i\hat{x}_i^n x_k^n) + \quad (3.12b)$$

$$+ \frac{1}{2}\alpha^2\Delta^2 \sum_{n,n'} (J_{ki}^2 i\hat{x}_k^n x_i^n i\hat{x}_k^{n'} x_i^{n'} + J_{ik}^2 i\hat{x}_i^n x_k^n i\hat{x}_i^{n'} x_k^{n'} \quad (3.12c)$$

$$+ J_{ki}J_{ik} i\hat{x}_k^n x_i^n i\hat{x}_i^{n'} x_k^{n'} + J_{ik}J_{ki} i\hat{x}_i^n x_k^n i\hat{x}_k^{n'} x_i^{n'}) + o(\alpha^2)\Bigg) \quad (3.12d)$$

The cavity marginals can be used to define local statistical averages:

$$\langle \mathcal{O}[\mathbf{x}_k, \hat{\mathbf{x}}_k] \rangle_{\setminus i} = \int D\mathbf{x}_k D\hat{\mathbf{x}}_k c_{k\setminus i}[\mathbf{x}_k, \hat{\mathbf{x}}_k] \mathcal{O}[\mathbf{x}_k, \hat{\mathbf{x}}_k] \tag{3.13}$$

Hence, it is possible to define:

- the averages $\mu_{i\setminus j}(t) = \langle x_i(t) \rangle_{\setminus j}$ and $\hat{\mu}_{i\setminus j}(t) = \langle \hat{x}_i(t) \rangle_{\setminus j}$
- the connected two-times cavity correlation function $C_{i\setminus j}(t,t') = \langle x_i(t) x_i(t') \rangle_{\setminus j} - \mu_{i\setminus j}(t)\mu_{i\setminus j}(t')$
- the cavity response functions $R_{i\setminus j}(t,t') = \langle x_i(t) i\hat{x}_i(t') \rangle_{\setminus j}$ and $\tilde{B}_{i\setminus j}(t,t') = \langle i\hat{x}_i(t) i\hat{x}_i(t') \rangle_{\setminus j}$

Since the dynamics is causal, it is reasonable to expect that $\hat{\mu}_{i\setminus j}(t)$ and $\tilde{B}_{i\setminus j}(t,t')$ both vanish for all t and t'; moreover, being $R_{i\setminus j}(t,t')$ the response function, it vanishes for $t \leq t'$. Given that in the expansion we are dealing with discrete time quantities, it is convenient to set $\mu^n_{i\setminus j} = \mu_{i\setminus j}(t = \Delta n)$, $C^{n,n'}_{i\setminus j} = C_{\setminus j}(t = \Delta n, t' = \Delta n')$ and $R_{i\setminus j}(t,t') = R_{i\setminus j}(t = \Delta n, t' = \Delta n')$.

By computing the averages, one gets:

$$\int D\mathbf{x}_k D\hat{\mathbf{x}}_k c_{ki}[\mathbf{x}_k, \hat{\mathbf{x}}_k] e^{\alpha\Delta \sum_n (J_{ki} i\hat{x}^n_k x^n_i + J_{ik} i\hat{x}^n_i x^n_k)} = \tag{3.14a}$$

$$= 1 + \alpha\Delta \sum_n (J_{ki} \langle i\hat{x}^n_k \rangle_{\setminus i} x^n_i + J_{ik} i\hat{x}^n_i \langle x^n_k \rangle_{\setminus i}) + \tag{3.14b}$$

$$+ \frac{1}{2}\alpha^2\Delta^2 \sum_{n,n'} \Big(J^2_{ki} \langle i\hat{x}^n_k i\hat{x}^{n'}_k \rangle_{\setminus i} x^n_i x^{n'}_i + J^2_{ik} \langle x^n_k x^{n'}_k \rangle_i i\hat{x}^n_i i\hat{x}^{n'}_i \tag{3.14c}$$

$$+ J_{ki}J_{ik} \langle i\hat{x}^n_k x^{n'}_k \rangle_{\setminus i} x^n_i i\hat{x}^{n'}_i + J_{ik}J_{ki} \langle x^n_k i\hat{x}^{n'}_k \rangle_{\setminus i} i\hat{x}^n_i x^{n'}_i \Big) + o(\alpha^2) \tag{3.14d}$$

The expression of (3.14a) can be simplified by exploiting the consequences of causality:

$$\int D\mathbf{x}_k D\hat{\mathbf{x}}_k c_{ki}[\mathbf{x}_k, \hat{\mathbf{x}}_k] e^{\alpha\Delta(J_{ki} i\hat{x}_k^n x_i^n + J_{ik} i\hat{x}_i^n x_k^n)} = \tag{3.15a}$$

$$= 1 + \alpha\Delta \sum_n J_{ik} i\hat{x}_i^n \langle x_k^n \rangle_{\setminus i} + \frac{1}{2}\alpha^2\Delta^2 \sum_{n,n'} J_{ik}^2 \langle x_k^n x_k^{n'} \rangle_{\setminus i} i\hat{x}_i^n i\hat{x}_i^{n'} + \tag{3.15b}$$

$$+ \frac{1}{2}\alpha^2\Delta^2 \sum_{n \geq n'} 2J_{ik}J_{ki} \langle x_k^n i\hat{x}_k^{n'} \rangle_{\setminus i} i\hat{x}_i^n x_i^{n'}) + o(\alpha^2) = \tag{3.15c}$$

$$= \exp\Bigg\{ \log\Bigg(1 + \alpha\Delta \sum_n J_{ik} i\hat{x}_i^n \langle x_k^n \rangle_{\setminus i} + \frac{1}{2}\alpha^2\Delta^2 \sum_{n,n'} J_{ik}^2 \langle x_k^n x_k^{n'} \rangle_{\setminus i} i\hat{x}_i^n i\hat{x}_i^{n'} + \tag{3.15d}$$

$$+ \frac{1}{2}\alpha^2\Delta^2 \sum_{n \geq n'} 2J_{ik}J_{ki} \langle x_k^n i\hat{x}_k^{n'} \rangle_{\setminus i} i\hat{x}_i^n x_i^{n'} + o(\alpha^2) \Bigg) \Bigg\} \tag{3.15e}$$

At this point is convenient to expand the logarithm, so that one obtains an exponential which is a function of $\mathbf{x}_i$ and $\hat{\mathbf{x}}_i$:

$$\int D\mathbf{x}_k D\hat{\mathbf{x}}_k c_{ki}[\mathbf{x}_k, \hat{\mathbf{x}}_k] e^{\alpha\Delta(J_{ki} i\hat{x}_k^n x_i^n + J_{ik} i\hat{x}_i^n x_k^n)} \simeq \tag{3.16a}$$

$$\simeq \exp\Bigg(\alpha\Delta \sum_n J_{ik} i\hat{x}_i^n \langle x_k^n \rangle_{\setminus i} + \frac{1}{2}\alpha^2\Delta^2 \sum_{n,n'} J_{ik}^2 \langle x_k^n x_k^{n'} \rangle_{\setminus i} i\hat{x}_i^n i\hat{x}_i^{n'} + \tag{3.16b}$$

$$+ \frac{1}{2}\alpha^2\Delta^2 \sum_{n \geq n'} 2J_{ik}J_{ki} \langle x_k^n i\hat{x}_k^{n'} \rangle_{\setminus i} i\hat{x}_i^n x_i^{n'}) + \tag{3.16c}$$

$$- \frac{1}{2}\alpha^2\Delta^2 \sum_{n,n'} J_{ik}^2 i\hat{x}_i^n \langle x_k^n \rangle_{\setminus i} i\hat{x}_i^{n'} \langle x_k^{n'} \rangle_{\setminus i} = \tag{3.16d}$$

$$= \exp\Bigg(\alpha\Delta \sum_n J_{ik} i\hat{x}_i^n \mu_{k\setminus i}^n + \frac{1}{2}\alpha^2\Delta^2 \sum_{n,n'} J_{ik}^2 C_{k\setminus i}^{n,n'} i\hat{x}_i^n i\hat{x}_i^{n'} + \tag{3.16e}$$

$$+ \alpha^2\Delta^2 \sum_{n \geq n'} J_{ik}J_{ki} R_{k\setminus i}^{n,n'} i\hat{x}_i^n x_i^{n'} \Bigg) \tag{3.16f}$$

This result can now be substituted in the expressions of the normalization constants Z_{ij}^{cav} and Z_i:

$$Z_{ij}^{cav} = \int D\mathbf{x}_i D\hat{\mathbf{x}}_i \exp\Bigg(\sum_n \Big\{ -i\hat{x}_i^n (x_i^{n+1} - x_i^n - f[x_i^n]\Delta - g[x_i^n]\Delta(\hat{x}_i^n)^2) \Big\} + \\ + \alpha \sum_n \sum_{k\in\partial i\setminus j} J_{ik} i\hat{x}_i^n \mu_{k\setminus i}^n \Delta + \frac{1}{2}\alpha^2 \sum_{n,n'} \sum_{k\in\partial i\setminus j} J_{ik}^2 C_{k\setminus i}^{n,n'} i\hat{x}_i^n i\hat{x}_i^{n'} \Delta^2 + \\ + \alpha^2 \sum_{n\geq n'} \sum_{k\in\partial i\setminus j} J_{ik} J_{ki} R_{k\setminus i}^{n,n'} i\hat{x}_i^n x_i^{n'} \Delta^2) \Bigg) \quad (3.17)$$

$$Z_i = \int D\mathbf{x}_i D\hat{\mathbf{x}}_i \exp\Bigg(\sum_n \Big\{ -i\hat{x}_i^n (x_i^{n+1} - x_i^n - f[x_i^n]\Delta - g[x_i^n]\Delta(\hat{x}_i^n)^2) \Big\} + \\ + \alpha \sum_n \sum_{k\in\partial i} J_{ik} i\hat{x}_i^n \mu_{k\setminus i}^n \Delta + \frac{1}{2}\alpha^2 \sum_{n,n'} \sum_{k\in\partial i} J_{ik}^2 C_{k\setminus i}^{n,n'} i\hat{x}_i^n i\hat{x}_i^{n'} \Delta^2 + \\ + \alpha^2 \sum_{n\geq n'} \sum_{k\in\partial i} J_{ik} J_{ki} R_{k\setminus i}^{n,n'} i\hat{x}_i^n x_i^{n'} \Delta^2) \Bigg) \quad (3.18)$$

These expressions play a key role in the derivation of the effective equations of the dynamics: indeed, Z_i can be reinterpreted as the local dynamical partition function associated to the node i in the graph, where the interactions with the neighbors have been hidden in the quantities $\mu_{k\setminus i}$, $C_{k\setminus i}$ and $R_{k\setminus}$, with $k \in \partial i$; in a similar way, Z_{ij} can be reinterpreted as a sort of local cavity dynamical partition function. These objects play the same role of the quantities z and z_{cav} that were considered during the analysis of the B-DMFT approach; moreover, it is not hard to see the connection between that approach and the one that is being analyzed right now: in particular, apart from the derivation of the partition function, which is different in the two cases, the expansion and the approximation of the interaction term is almost analogous, showing the effectiveness of these approaches to deal with different physical systems, both classical and quantum and both at equilibrium and out of equilibrium.

Before proceeding to the derivation of the effective equations of the dynamics, it is important to discuss the fact that the assumption of small coupling required to deal with the interactions is equivalent to that of large connectivity of the graph on which the dynamics is defined. To clarify this point, it is convenient to revisit the way in which a dynamics on a graph is defined starting from an Hamiltonian describing the behavior of the degrees of freedom associated to the nodes of the graph itself. If one consider the generic noisy dynamics with linear interactions that has been used to present the dynamic cavity approach, the starting Hamiltonian would be:

$$\mathcal{H}[\{x_l(t)\}_{l\in V}] = -\sum_{l\in V} f[x_l(t)] - \sum_{l\in V}\sum_{j\in\partial l} J_{lj}x_l(t)x_l(t) \tag{3.19}$$

with $G = (V, E)$ being the graph on which the dynamics is defined.

The dynamics of the degree of freedom associated to a generic node i, as prescribed by non equilibrium statistical mechanics[8], is given by:

$$\frac{dx_i}{dt} = -\frac{\delta\mathcal{H}[\{x_l(t)\}_{l\in V}]}{\delta x_i(t)} + \eta_i(t) \tag{3.20}$$

with $\eta_i(t)$ being the noise.

If the graph on which the dynamics is defined is characterized by a large connectivity, it is customary to rescale the coupling constants to avoid divergencies, exactly as it would be done in equilibrium statistical mechanics. Therefore, the constant α that has been introduced in 3.1 to derive the dynamic cavity equations can be seen as the constant performing the necessary rescaling from a graph with a large connectivity K, namely $\alpha \propto K^{-\gamma}$ for some $\gamma \leq 0$ which depends on the dynamics under exam. In conclusion, if the coupling constants in the Hamiltonian $\mathcal{H}$ are redefined as $J'_{lj} = \alpha J_{lj}$, it becomes clear to see that requiring the couplings to be small is equivalent to requiring the connectivity to be large.

3.2.3 Derivation of the effective stochastic differential equations

The way to derive the effective equations is to apply backwards the MSRJD formalism, bur first, it is necessary to rewrite Z_{ij}^{cav} and Z_i as averages of the type $\langle ... \rangle_{\vec{\Delta\eta}}$; this can be achieved by performing backwards the Gaussian integral associated to the noise.

Therefore, let us consider the terms in the functional integrals involving products of the type $i\hat{x}_i^n i\hat{x}_i^{n'}$; in the case of Z_{ij}^{cav} we have:

$$\exp\left\{\sum_n\left[-\Delta g[x_i^n](\hat{x}_i^n)^2 - \frac{1}{2}\alpha^2\Delta^2\sum_{n'}\sum_{k\in\partial i\setminus j} J_{ik}^2 C_{k\setminus i}^{n,n'}\hat{x}_i^n\hat{x}_i^{n'}\right]\right\} = \tag{3.21a}$$

$$= \exp\left\{-\frac{1}{2}\sum_{n,n'}\hat{x}_i^n\left[2\Delta g[x_i^n] + \alpha^2\Delta^2\sum_{k\in\partial i\setminus j} J_{ik}^2 C_{k\setminus i}^{n,n'}\right]\hat{x}_i^{n'}\right\} = \tag{3.21b}$$

$$= \exp\left\{-\frac{1}{2}\hat{\mathbf{x}}_i^T G_i\hat{\mathbf{x}}_i\right\} = \left\langle e^{i\hat{\mathbf{x}}_i^T\vec{\Delta\eta}_i}\right\rangle_{\vec{\Delta\eta}_i} \tag{3.21c}$$

The partition functions can be rewritten as:

$$Z_{ij}^{cav} = \left\langle \int D\mathbf{x}_i D\hat{\mathbf{x}}_i \exp\Bigg(\sum_n \Big\{ -i\hat{x}_i^n (x_i^{n+1} - x_i^n - f[x_i^n]\Delta + \right.$$
$$\left. - \alpha \sum_{k\in\partial i\setminus j} J_{ik}\mu_{k\setminus i}^n \Delta - \alpha^2 \sum_{n':n'\le n} \sum_{k\in\partial i\setminus j} J_{ik}J_{ki} R_{k\setminus i}^{n,n'} x_i^{n'} \Delta^2 - \Delta\eta_i^n) \Big\} \Bigg) \right\rangle_{\vec{\Delta\eta}} \tag{3.22}$$

$$Z_i = \left\langle \int D\mathbf{x}_i D\hat{\mathbf{x}}_i \exp\Bigg(\sum_n \Big\{ -i\hat{x}_i^n (x_i^{n+1} - x_i^n - f[x_i^n]\Delta + \right.$$
$$\left. - \alpha \sum_{k\in\partial i} J_{ik}\mu_{k\setminus i}^n \Delta - \alpha^2 \sum_{n':n'\le n} \sum_{k\in\partial i} J_{ik}J_{ki} R_{k\setminus i}^{n,n'} x_i^{n'} \Delta^2 - \Delta\eta_i^n) \Big\} \Bigg) \right\rangle_{\vec{\Delta\eta}} \tag{3.23}$$

Finally, these two expressions can be used to derive the desired effective stochastic differential equations. Since the parameter α is no longer necessary, it can be set equal to one; however, it is important to remember that the results derived with the approach developed here holds under the assumption of weak coupling or large connectivity. The equations in discrete time are:

$$x_i^{n+1} = x_i^n + f[x_i^n]\Delta + \sum_{k\in\partial i\setminus j} J_{ik}\mu_{k\setminus i}^n \Delta + \\ + \sum_{n':n'\le n} \sum_{k\in\partial i\setminus j} J_{ik}J_{ki} R_{k\setminus i}^{n,n'} x_i^{n'} \Delta^2 + \Delta\eta_i^n \tag{3.24}$$

$$x_i^{n+1} = x_i^n + f[x_i^n]\Delta + \sum_{k\in\partial i} J_{ik}\mu_{k\setminus i}^n \Delta + \\ + \sum_{n':n'\le n} \sum_{k\in\partial i} J_{ik}J_{ki} R_{k\setminus i}^{n,n'} x_i^{n'} \Delta^2 + \Delta\eta_i^n \tag{3.25}$$

where $\vec{\Delta\eta}_i$ is a random vector such that, in the cavity case:

$$\langle \Delta\eta_i^n \rangle = 0 \tag{3.26a}$$
$$\langle \Delta\eta_i^n \Delta\eta_i^{n'} \rangle = 2g[x_i^n]\Delta\delta_{n,n'} + \sum_{k\in\partial i\setminus j} J_{ik}^2 C_{k\setminus i}^{n,n'} \Delta^2 \tag{3.26b}$$

while for the full case:

$$\langle \Delta\eta_i^n \rangle = 0 \tag{3.27a}$$
$$\langle \Delta\eta_i^n \Delta\eta_i^{n'} \rangle = 2g[x_i^n]\Delta\delta_{n,n'} + \sum_{k\in\partial i} J_{ik}^2 C_{k\setminus i}^{n,n'} \Delta^2 \tag{3.27b}$$

The equations in continuous time are easily obtained:

$$\frac{dx_i}{dt} = f[x_i(t)] + \sum_{k\in\partial i\setminus j} J_{ik}\mu_{k\setminus i}(t) + \\ + \sum_{k\in\partial i\setminus j} \int_0^t dt' J_{ik}J_{ki} R_{k\setminus i}(t,t') x_i(t') + \eta_i(t) \tag{3.28}$$

where $\eta_i(t)$ is now a colored Gaussian noise with the following moments:

$$\langle \eta_i(t) \rangle = 0 \tag{3.29a}$$
$$\langle \eta_i(t)\eta_i(t') \rangle = 2g[x_i(t)]\delta(t-t') + \sum_{k\in\partial i\setminus j} J_{ik}^2 C_{k\setminus i}(t-t') \tag{3.29b}$$

and:

$$\frac{dx_i}{dt} = f[x_i(t)] + \sum_{k\in\partial i} J_{ik}\mu_{k\setminus i}(t) + \\ + \sum_{k\in\partial i} \int_0^t dt' J_{ik}J_{ki} R_{k\setminus i}(t,t') x_i(t') + \eta_i(t) \tag{3.30}$$

where $\eta_i(t)$ is again a colored Gaussian noise with the following moments:

$$\langle \eta_i(t) \rangle = 0 \tag{3.31a}$$
$$\langle \eta_i(t)\eta_i(t') \rangle = 2g[x_i(t)]\delta(t-t') + \sum_{k\in\partial i} J_{ik}^2 C_{k\setminus i}(t-t') \tag{3.31b}$$

The only difference in the moments of the noises for the two effective equations is in the set of indices over which the sum of the second order moments runs, being $\{k \in \partial i \setminus j\}$ in (3.29*b*) and $\{k \in \partial i\}$ in (3.31*b*).

Note that the equations have been derived by considering a site i chosen arbitrarily in the graph, but the same results could have been obtained by taking any other node under consideration. In the following equations (3.28) and (3.30) will

be referred to as the equations of the dynamical mean field theory approach(DMFT), or simply as effective equations of the dynamics.

Given the quantities $\{\mu_{k\setminus i}(t)\}_{k\in\partial i\setminus j}$, $\{C_{k\setminus i}(t,t')\}_{k\in\partial i\setminus j}$ and $\{R_{k\setminus i}(t,t')\}_{k\in\partial i\setminus j}$, (3.28) describes the dynamics of $x_i(t)$ when the link with its neighbor $x_j(t)$ has been severed. The quantities appearing in the equation are unknown in principle; however, if a certain number of trajectories of the neighbors was known, it would be possible to estimate the quantities required to describe the behaviour of $x_i(t)$. This idea is the starting point for the derivation of the algorithm which allows to compute all the quantities appearing in the DMFT equations of a dynamics.

3.3 Scheme for the derivation of the DMFT equations

3.3.1 Analysis of a generic dynamics

As it has been pointed out observing equations (3.28) and (3.30), it is possible to develop an algorithm for the computation of the quantities $\{\mu_{k\setminus i}(t)\}_{k\in\partial i\setminus j}$, $\{C_{k\setminus i}(t,t')\}_{k\in\partial i\setminus j}$ and $\{R_{k\setminus i}(t,t')\}_{k\in\partial i\setminus j}$ for each node i in any given graph.

In the previous section the way to derive a set of effective equations describing a given dynamics has been presented; it is important to notice how the underlying graph of the dynamics and the coupling constants were assumed to be known. To really understand and appreciate the effectiveness of the DMFT approach, it would be interesting to consider a situation in which the couplings are sampled from some distribution $P(J_{ij})$ and in which the underlying graph is regular with connectivity K. The choice of regularity of the graph is motivated by the will to simplify the nature of the equations that will be derived within this section; however, the dynamical mean-field theory approach can be extended, in principle, to account for graphs which are not regular: this approach is known in the literature as heterogeneous dynamical mean-field theory(HDMFT)[11].

If the couplings are sampled from some distribution $P(J_{ij})$, it is necessary to extend the approach developed in the previous section; in particular, it is necessary to perform a configurational average of both Z_{ij}^{cav} and Z_i:

$$[Z_{ij}^{cav}] = \int \prod_{k\in\partial i\setminus j} P(J_{ik}) dJ_{ik} Z_{ij}^{cav} \tag{3.32}$$

$$[Z_i] = \int \prod_{k\in\partial i} P(J_{ik}) dJ_{ik} Z_i \tag{3.33}$$

where [...] indicates the configurational average and where the couplings are assumed to be symmetric, namely $J_{ij} = J_{ji}$. The expressions of the partition functions Z_{ij}^{cav} and Z_i that appears in the configurational averages are the ones

obtained just after the small-coupling expansion, so that it is possible to exploit the directly the moments of the chosen distribution $P(J_{ij})$. Therefore, the prescription to find the effective equations of the dynamics in the presence of disorder is the following: first, the partition functions Z_{ij}^{cav} and Z_i are obtained through the MSRJD approach; then the configurational average is taken; at this point the small-coupling expansion is carried out up to the second order and the averages with respect to the cavity marginals are computed, so that the DMFT quantities μ, C and R can be made explicit; now the terms resulting from the expansion can be exponentiated again using the exp-log trick; to conclude the procedure, the average with respect to the noise is performed backwards and the final expressions for Z_{ij}^{cav} and Z_i are obtained.

3.3.2 The homogeneous case

The simplest choice that can be made concerning the couplings consists in setting $P(J_{ik}) = \delta(J_{ik} - J)$.

For what concerns the graph on which the dynamics is simulated, it is interesting to start from the case of the Bethe lattice; in this case the assumptions of the dynamic cavity approach for the derivation of the cavity equations are exact, as the Bethe lattice is a tree-like graph.

The original equation of the dynamics with homogeneous couplings for a given node then becomes:

$$\frac{dx_i}{dt} = f[x_i(t)] + J \sum_{j \in \partial i} x_j(t) + \eta_i(t) \tag{3.34}$$

with:

$$\langle \eta_i(t) \rangle = 0 \tag{3.35a}$$
$$\langle \eta_i(t) \eta_i(t') \rangle = 2D\delta(t - t') \tag{3.35b}$$

Within this simplified picture in which the function $f[x_i(t)]$ and the parameter D are the same on every node and in which the couplings are homogeneous, that is $J_{ij} = J$, the DMFT equations of the dynamics take a simple form. Indeed, the quantities $\{\mu_{k\setminus i}(t)\}_{k \in \partial i \setminus j}$, $\{C_{k\setminus i}(t,t')\}_{k \in \partial i \setminus j}$ and $\{R_{k\setminus i}(t,t')\}_{k \in \partial i \setminus j}$ become the same on every edge: hence, it is possible to replace, in the effective equation, each $\mu_{k\setminus i}(t)$ with the common quantity $\mu_{cav}(t)$, each $C_{k\setminus i}(t,t')$ with the quantity $C_{cav}(t,t')$ and each $R_{k\setminus i}(t,t')$ with $R_{cav}(t,t')$, where the subscript *cav* is a reference to the fact that the reference dynamics for these quantities is the one in which one of the neighboring nodes has been removed. Therefore the effective equations describing the dynamics reduce to:

$$\frac{dx}{dt} = f[x(t)] + (K-1)J\mu_{cav}(t) + (K-1)J^2 \int_0^t dt' R_{cav}(t,t')x(t') + \eta(t) \quad (3.36)$$

with:

$$\langle \eta(t) \rangle = 0 \quad (3.37a)$$
$$\langle \eta(t)\eta(t') \rangle = 2D\delta(t-t') + (K-1)J^2 C_{cav}(t,t') \quad (3.37b)$$

Also for the case of the full dynamics it is possible to rewrite the equation in terms of $\mu_{cav}(t)$, $C_{cav}(t,t')$ and $R_{cav}(t,t')$:

$$\frac{dx}{dt} = f[x(t)] + KJ\mu_{cav}(t) + KJ^2 \int_0^t dt' R_{cav}(t,t')x(t') + \eta(t) \quad (3.38)$$

with:

$$\langle \eta(t) \rangle = 0 \quad (3.39a)$$
$$\langle \eta(t)\eta(t') \rangle = 2D\delta(t-t') + KJ^2 C_{cav}(t,t') \quad (3.39b)$$

In the expressions above the index i has been dropped, since the dynamics of a node is completely equivalent to that of any other node on the graph; the sum on the neighborhood has been substituted by the multiplication by a constant related to K, which is nothing but the connectivity of the Bethe lattice.

Formally, $\mu_{cav}(t)$, $C_{cav}(t,t')$ and $R_{cav}(t,t')$ can be defined as:

$$\mu_{cav}(t) = \langle x(t) \rangle_{K-1} \quad (3.40)$$

$$C_{cav}(t,t') = \langle x(t)x(t') \rangle_{K-1} \quad (3.41)$$

$$R_{cav}(t,t') = \left. \frac{\delta \langle x(t) \rangle_{K-1}}{\delta h(t')} \right|_{h=0} \quad (3.42)$$

where $\langle ... \rangle_{K-1}$ now indicates an average taken by removing one of the neighbors of the chosen node on the Bethe lattice, effectively separating a sub-tree from the rest of the lattice; this means that, to compute empirically averages of the type $\langle ... \rangle_{K-1}$, it is necessary to consider the dynamics of (3.36). The field $h(t)$ is a local external field that can be added to equation (3.34) to compute the response message with a linear response approach.

As a final remark before presenting the algorithm used to compute the quantities $\mu_{cav}(t)$, $C_{cav}(t,t')$ and $R_{cav}(t,t')$, which will be referred to as DMFT messages, it is

important to remember that the coupling J, the connectivity K and the parameters of the function $f[x(t)]$ have to chosen in such a way to avoid an unstable dynamics.

Despite its simplicity, the homogeneous dynamics allows for the introduction of a simple algorithm for the computation of the messages: once they have been obtained, the correctness of the algorithm can be tested by generating trajectories of $x(t)$ according to (3.34) and to (3.38), for a simple dynamics, like that of a linear model in which $f[x(t)] = -\lambda x(t)$, which can be easily analyzed with direct simulations on a random regular graph. Once the validity of the algorithm has been established, it will be possible to study more complex model.

3.4 Algorithm for the derivation of the DMFT messages

Here the general structure of the algorithm for the computation of the DMFT messages of a generic dynamics is presented[10]; the basic idea is the following one: the messages $\mu_{cav}(t)$, $C_{cav}(t,t')$ and $R_{cav}(t,t')$ are initialized in some way, then they are used to generate a certain number of trajectories of $x(t)$, which in conclusion are used to make a self-consistent update of the messages according to the expressions (3.40)-(3.42).

Since in the algorithm it is necessary to integrate numerically the equations of the dynamics to generate the trajectories and to derive the response function $R_{cav}(t,t')$, it is convenient to write (3.36) and (3.38) in discrete time. The equation for the cavity dynamics reads:

$$x^{n+1} = x^n + f[x^n]\Delta + (K-1)J\Delta\mu_{cav}^n + (K-1)J^2\Delta^2 \sum_{n'=0}^{n} R_{cav}^{n,n'} x^{n'} + \Delta\eta^n \quad (3.43)$$

where $\Delta\eta^n = \int_{n\Delta}^{(n+1)\Delta} dt\eta(t)$ and:

$$\langle \Delta\eta^n \rangle = 0 \quad (3.44a)$$

$$\langle \Delta\eta^n \Delta\eta^{n'} \rangle = 2D\Delta\delta_{n,n'} + (K-1)J^2 C_{cav}^{n,n'}\Delta^2 \quad (3.44b)$$

The expressions for the full dynamics in discrete time are similar:

$$x^{n+1} = x^n + f[x^n]\Delta + KJ\Delta\mu_{cav}^n + KJ^2\Delta^2 \sum_{n'=0}^{n} R_{cav}^{n,n'} x^{n'} + \Delta\eta^n \quad (3.45)$$

whit:

$$\langle \Delta\eta^n \rangle = 0 \tag{3.46a}$$

$$\langle \Delta\eta^n \Delta\eta^{n'} \rangle = 2D\Delta\delta_{n,n'} + KJ^2 C_{cav}^{n,n'} \Delta^2 \tag{3.46b}$$

Notice that the equations in discrete time have been derived according to the Euler-Maruyama scheme, which is a relatively good scheme in the case of additive noise. If instead the noise becomes multiplicative, it is necessary to use a different numerical scheme.

Within this discrete time picture, $x(t)$ and $\mu_{cav}(t)$ become the vectors $\mathbf{x}$ and $\mu_{\mathbf{cav}}$, while $C_{cav}(t,t')$ and $R_{cav}(t,t')$ become the matrices C_{cav} and R_{cav}.

The key quantities of the algorithm are:

- $\mu_{\mathbf{cav}}$, C_{cav} and R_{cav}, the desired DMFT quantities
- $\mu_{\mathbf{cav}}^{\mathbf{new}}$, C_{cav}^{new} and R_{cav}^{new}, the new DMFT quantities computed at each iteration of the algorithm
- T, the total number of time steps
- Δ, the size of the time step
- N_{traj}, the number of trajectories that are generated at each iteration for the self-consistent update of the DMFT quantities
- K, the connectivity of the lattice
- α, the parameter for the soft update of $\mu_{\mathbf{cav}}$, C_{cav} and R_{cav} at each iteration of the algorithm
- $(\epsilon_1, \epsilon_2, \epsilon_3)$, threshold values for the convergence of $\mu_{\mathbf{cav}}$, C_{cav} and R_{cav}

3.4.1 Initialization

Step 0: initialization of the DMFT messages

The first thing to do is to initialize $\mu_{\mathbf{cav}}$, C_{cav} and R_{cav}: the way in which this is done depends on the dynamics that is being analyzed; however, for what concerns C_{cav}, it is reasonable to choose a symmetric positive definite matrix, while for R_{cav} the natural choice is some lower triangular matrix, since the analysis is limited to causal dynamics. The initialization of $\mu_{\mathbf{cav}}$ is more subtle, as it can lead to instabilities in the algorithm; some suggestions for the initialization of μ_{cav} can come from a phenomenological analysis of the dynamics under exam.

3.4.2 Iterative step

Step 1: generation of the trajectories

A number N_{traj} of trajectories, that is vectors of length T, is generated according to (3.43) by means of the current values of the DMFT quantities μ^l_{cav}, C^l_{cav} and R^l_{cav}. The first values of each trajectory are chosen according to some distribution $p(x^0)$ to be chosen a priori; the remaining values of the vector are computed according to (3.43): this means that the full trajectory is computed by numerical integration with the Euler-Maruyama approach. Since the trajectories are all independent, it is possible to generate them in parallel to reduce the computational time of the algorithm, if the hardware allows it.

Step 2: derivation of $\mu^{\mathbf{new}}_{\mathbf{cav}}$

The new value of the mean is obtained starting from (3.40); that expression indicates that the new mean $\mu^{\mathbf{new}}_{\mathbf{cav}}$ can be computed by taking the empirical average over the trajectories generated at step 1:

$$\mu^{new,n}_{cav} = \frac{1}{N_{traj}} \sum_{j=1}^{N_{traj}} x^n_j \tag{3.47}$$

for $n \in \{1, ...T\}$.

Step 3: derivation of C^{new}_{cav}

The new covariance matrix C^{new}_{cav} can be computed starting from (3.41); therefore, each element of the matrix is obtained as:

$$C^{new,n,n'}_{cav} = \frac{1}{N_{traj}} \sum_{j=1}^{N_{traj}} x^n_j x^{n'}_j - \mu^{new,n}_{cav} \mu^{new,n'}_{cav} \tag{3.48}$$

for $n, n' \in \{0, ...T\}$.

Step 4: derivation of R^{new}_{cav}

The computation of R^{new}_{cav} is more complicated; one of the possible approaches can be derived starting from (3.42). The idea here is to obtain a differential equation for R_{cav} by taking the average (3.36) and then by computing the functional derivative of the resulting equation with respect to the external field. In the case of a general term $f[x(t)]$, this leads to the following equation in continuous time:

$$\frac{dR_{cav}^{new}(t,t')}{dt} = \left.\frac{\delta\langle f[x(t)]\rangle_{K-1}}{\delta h(t')}\right|_{h=0} + \\ + (K-1)J^2\int_0^t dt'' R_{cav}^{new}(t,t'')R_{cav}^{new}(t'',t') + \delta(t-t') \quad (3.49)$$

This equation has to be considered in discrete time in order to obtain a way to compute all the elements $R_{cav}^{new,n,n'}$; for the computation of the first term on the r.h.s. of (3.49) it is necessary to use the trajectories generated at step 1, if $f[x(t)]$ is not linear in $x(t)$ and approximations are required in this case.

Step 5: check for convergence

At this point μ_{cav}^{new}, C_{cav}^{new} and R_{cav}^{new} can be compared with the current messages μ_{cav}^{l}, C_{cav}^{l} and R_{cav}^{l}. In particular, the algorithm stops if the following conditions are all satisfied:

$$\max_{i\in 1,\dots,T}\{|\mu_{cav}^{new,i} - \mu_{cav}^{l,i}|\} \leq \epsilon_1$$
$$\max_{i,j\in 1,\dots,T}\{|C_{cav}^{new,i,j} - C_{cav}^{l,i,j}|\} \leq \epsilon_2$$
$$\max_{i,j\in 1,\dots,T}\{|R_{cav}^{new,i,j} - R_{cav}^{l,i,j}|\} \leq \epsilon_3$$

If instead these conditions are not satisfied, the algorithm proceeds for a new iteration.

The choice of these constraint is motivated by the observation that having the convergence of large vectors or matrices is hard, in general; therefore, if the largest difference between the old DMFT quantity and the new one is smaller than the chosen tolerance, it is safe to say that the matrix, or the vector, has converged.

Step 6: soft update of the messages

If the check for convergence at step 5 fails, a soft-update of the messages is made, according to:

$$\mu_{cav}^{l+1} = \alpha\mu_{cav}^{l} + (1-\alpha)\mu_{cav}^{new}$$
$$C_{cav}^{l+1} = \alpha C_{cav}^{l} + (1-\alpha)C_{cav}^{new}$$
$$R_{cav}^{l+1} = \alpha R_{cav}^{l} + (1-\alpha)R_{cav}^{new}$$

The choice of performing a soft-update of the messages is motivated by the will to avoid large jumps in the space of the DMFT quantities, which could lead to instabilities in the algorithm.

3.4.3 Conclusion

After the initialization of the messages at step 0, the steps 1 to 6 are repeated iteratively until convergence or until a certain number of iterations is executed. Indeed, if the values ϵ_1, ϵ_2 and ϵ_3 are too small, it is quite difficult to have a complete convergence of the messages, as it could happen that most of the components of the messages reach convergence, but the check still fails due to some isolated component.

It is worth to mention that both the number of trajectories N_{traj} and the soft-update parameter α can vary from step to step: changing N_{traj} affects the precision of the estimates of the DMFT messages, while changing α affects the speed of convergence, apart from the precision of the estimates; moreover, there can be some situations in which a good choice of α allows to avoid convergence issues, which are frequently related to the quantity C_{cav}, which can become non positive definite.

Once $\mu_{\mathbf{cav}}$, C_{cav} and R_{cav} have been computed, they can be used to generate trajectories of $x(t)$ according to (3.45); then, it is possible to exploit them to make a statistical analysis of the model and compare the results with direct numerical simulations.

3.5 Alternative approach for the update of the response function

Let us consider again the way in which the message $R_{cav}(t,t')$ has been computed in the presentation of the fourth step of the algorithm: as it is possible to see from (3.49), the first term on the r.h.s of the equation can be easily computed only if $f[x(t)]$ is linear in $x(t)$; unfortunately, there are many models in which this does not happen. Therefore, there is the need to find a different approach to complete the algorithm, in such a way that it can be used to study also models in which $f[x(t)]$ is non-linear.

To this purpose, it is convenient to remember the definition of the response function as it has been introduced in the explanation of the dynamic cavity approach:

$$R_{i\setminus j}(t,t') = \left.\frac{\delta\langle x_i(t)\rangle_{\setminus j}}{\delta h_i(t')}\right|_{h=0} = \langle x_i(t) i\hat{x}_i(t')\rangle_{\setminus j} \tag{3.52}$$

In the homogeneous case, this expression reduces to:

$$R_{cav}(t,t') = \left.\frac{\delta\langle x(t)\rangle_{K-1}}{\delta h(t')}\right|_{h=0} = \langle x(t) i\hat{x}(t')\rangle_{K-1} \tag{3.53}$$

In order to compute this average, let us consider the partition function of a single node:

$$\mathcal{Z} = \int D\mathbf{x} D\hat{\mathbf{x}} D\eta p(x^0) P[\mathbf{x}|h,\eta] P[\eta] \tag{3.54}$$

where $p(x^0)$ is the probability distribution of the initial value of $x(t)$, $P[\mathbf{x}|h,\eta]$ is the probability distribution associated to a certain trajectory given an external field $h(t)$ and a realization of the noise $\eta(t)$ and $P[\eta]$ is the probability distribution associated to a realization of the noise.

The expressions of the distributions $P[\mathbf{x}|h,\eta]$ and $P[\eta]$ are:

$$P[\mathbf{x}|h,\eta] \propto \exp\left\{ -i \int dt \left[\hat{x}(t) \left(\frac{\partial x}{\partial t} - f[x(t)] - (K-1)\mu_{cav}(t) + \right.\right.\right. \\ \left.\left.\left. - (K-1)J^2 \int_0^t dt' R_{cav}(t,t') x(t') - h(t) - \eta(t) \right) \right] \right\} \tag{3.55}$$

and:

$$P[\eta] \propto \exp\left(-\frac{1}{2} \int dt ds \eta(t) G^{-1}_{cav}(t,s) \eta(s) \right) \tag{3.56}$$

with $G_{cav}(t,t') = 2g[x(t)]\delta(t-t') + (K-1)J^2 C_{cav}(t,t')$ being the covariance matrix of the noise $\eta(t)$.

Hence, one can write:

$$R_{cav}(t,t') = \left[\frac{\delta}{\delta h(t')} \langle x(t) \rangle_{K-1} \right]_{h=0} = \tag{3.57a}$$

$$= \left[\frac{\delta}{\delta h(t')} \int D\mathbf{x} D\hat{\mathbf{x}} D\eta p(x^0) P[\mathbf{x}|h,\eta] P[\eta] x(t) \right]_{h=0} = \tag{3.57b}$$

$$= \left[\int D\mathbf{x} D\hat{\mathbf{x}} D\eta p(x^0) P[\eta] x(t) \frac{\delta P[\mathbf{x}|h,\eta]}{\delta h(t')} \right]_{h=0} \tag{3.57c}$$

It is convenient to notice that taking the functional derivative of $P[\mathbf{x}|h,\eta]$ with respect to $h(t')$ is equivalent to taking the functional derivative with respect to $\eta(t')$, due to the similarity of the term associated to the external field to the term associated to the noise in $P[\mathbf{x}|h,\eta]$. Hence, by making an integration by part, one has:

$$R_{cav}(t,t') = \left[\int D\mathbf{x}D\hat{\mathbf{x}}D\eta p(x^0)P[\eta]x(t)\frac{\delta P[\mathbf{x}|h,\eta]}{\delta\eta(t')}\right]_{h=0} \tag{3.58a}$$

$$= \left[-\int D\mathbf{x}D\hat{\mathbf{x}}D\eta p(x^0)P[\mathbf{x}|h,\eta]x(t)\frac{\delta P[\eta]}{\delta\eta(t')}\right]_{h=0} = \tag{3.58b}$$

$$= \left[\int D\mathbf{x}D\hat{\mathbf{x}}D\eta p(x^0)P[\mathbf{x}|h,\eta]P[\eta]x(t)\int dsG^{-1}_{cav}(t',s)\eta(s)\right]_{h=0} = \tag{3.58c}$$

$$= \left\langle x(t)\int dsG^{-1}_{cav}(t',s)\eta(s)\right\rangle_{K-1} \tag{3.58d}$$

This result provides a practical way to update the response message, without having to deal with the complications arising from the non linearity of the function $f[x(t)]$. Indeed, from a practical point of view, a response message can be computed for each of the trajectories generated in the iterative step and then perform an average. If $R_{j,cav}$ is the response matrix obtained from the j-th trajectory, in discrete time we find the following expression for the elements of the matrix:

$$R^{n,n'}_{j,cav} = x^n_j \sum_{n''=1}^{n} (G^{-1}_{cav})^{n',n''}\Delta\eta^{n''}_j \tag{3.59}$$

In conclusion, the new response message is obtained as:

$$R^{new}_{cav} = \frac{1}{N_{traj}}\sum_{j=1}^{N_{traj}} R_{j,cav} \tag{3.60}$$

This way of computing the response function goes by the name of generating functional approach[10] and it has the perk of being extremely general: the expression of the response function is the same for every model; the only thing that depends on the dynamics under analysis is the way in which the trajectories of the noise and of the degrees of freedom are generated.

This approach, despite being theoretically exact and general, is too heavy from a numerical point of view: indeed, the number of trajectories required to obtain a relatively good approximation of R_{cav} is extremely large, so large that this approach becomes simply too ineffective to be used. For this reason, it is necessary to find alternative approaches to deal with models in which the local term $f[x(t)]$ is non-linear in $x(t)$.

Chapter 4

Numerical implementation of the DMFT algorithm for the analysis of physical models

4.1 Introduction

Here the algorithm that has been outlined at the end of the previous chapter is implemented for various physical models defined on a Bethe lattice: first, the correctness of the algorithm is tested on the linear model; then, the algorithm is applied to the ϕ^4-model, which is characterized by non-trivial features that require the development and the testing of an approximation; after that, the DMFT approach is implemented for the 2-spin model both without and with disorder[12]. For all the models cited above, the results obtained with the DMFT algorithm are compared with those obtained through direct numerical simulations of the model themselves on random regular graphs. The choice of random regular graphs for the simulations of the models is motivated by the fact that these are the finite graphs closest to a Bethe lattice, which has been used in the previous chapter for the derivation of the equations of the dynamic cavity approach; indeed, on a random regular graph, each node has the same number of neighbors and, if the graph is large enough, the effect of loops can be safely neglected. The algorithm and all the code used to obtain the numerical results presented in this chapter have been written using the Julia programming language and it is available at `https://github.com/LorenzoDemichelis99`. Computational resources to run the algorithms were provided by the SmartData@PoliTO interdepartmental center

on Big Data and Data Science.

4.2 The linear model

4.2.1 Presentation of the model

The first model that can be used to test the algorithm is the linear model with homogeneous couplings, in which $f[x_i(t)] = -\lambda x_i(t)$. The reason why this model can be chosen to test the algorithm, apart from it being exactly solvable from an analytical point of view, is that the local term $f[x(t)]$ is linear in $x(t)$; indeed, any model with linear interactions and additive noise can be analyzed without any approximation if the local term $f[x(t)]$ is linear in $x(t)$, so that the cavity response function $R_{cav}(t, t')$ can be computed exactly.

The original equation describing the dynamics of a node i on the Bethe lattice is:

$$\frac{dx_i}{dt} = -\lambda x_i(t) + J \sum_{j \in \partial i} x_j(t) + \eta_i(t) \tag{4.1}$$

with:

$$\langle \eta_i(t) \rangle = 0 \tag{4.2a}$$
$$\langle \eta_i(t) \eta_i(t') \rangle = 2D\delta(t - t') \tag{4.2b}$$

The DMFT equations for this model are readily obtained, as it is enough to make the substitution $f[x(t)] = -\lambda x(t)$ in the effective equations obtained in the previous chapter. Hence, the effective equation for the cavity dynamics reads:

$$\frac{dx}{dt} = -\lambda x(t) + (K-1) J \mu_{cav}(t) + (K-1) J^2 \int_0^t dt' R_{cav}(t, t') x(t') + \eta(t) \tag{4.3}$$

with:

$$\langle \eta(t) \rangle = 0 \tag{4.4a}$$
$$\langle \eta(t) \eta(t') \rangle = 2D\delta(t - t') + (K-1) J^2 C_{cav}(t, t') \tag{4.4b}$$

While for the full dynamics the equation reads:

$$\frac{dx}{dt} = -\lambda x(t) + K J \mu_{cav}(t) + K J^2 \int_0^t dt' R_{cav}(t, t') x(t') + \eta(t) \tag{4.5}$$

with:

$$\langle \eta(t) \rangle = 0 \tag{4.6a}$$
$$\langle \eta(t)\eta(t') \rangle = 2D\delta(t-t') + KJ^2 C_{cav}(t,t') \tag{4.6b}$$

For this dynamics we have $f[x(t)] = -\lambda x(t)$: this term has to balance the term associated to the interaction with the neighbors, characterized by the constant J and by a sum over the neighbors, which can be rewritten just by multiplying by the connectivity K in this particular homogeneous case; hence, to avoid instability, KJ has to be smaller than λ. If this condition is satisfied, we can expect the system to converge to an equilibrium in which the average value of $x(t)$ is equal to zero and its actual value fluctuates around the equilibrium according to the noise $\eta(t)$.

To apply the algorithm presented before it is necessary to specify the full equation for the computation of the cavity response function $R_{cav}(t,t')$. For this trivial model we have:

$$\left.\frac{\delta \langle f[x(t)] \rangle_{K-1}}{\delta h(t')}\right|_{h=0} = -\lambda \left.\frac{\delta \langle x(t) \rangle_{K-1}}{\delta h(t')}\right|_{h=0} = -\lambda R_{cav}(t,t') \tag{4.7}$$

Therefore, the differential equation for R_{cav} reduces to:

$$\frac{dR_{cav}(t,t')}{dt} = -\lambda R_{cav}(t,t') + \\ + (K-1)J^2 \int_0^t dt'' R_{cav}(t,t'') R_{cav}(t'',t') + \delta(t-t') \tag{4.8}$$

As it is possible to notice, $x(t)$ does not appear in the equation: this means that R_{cav} has to be computed just once, right after step 0 of the algorithm, and then it can be used at each iteration to generate the trajectories required for the update of $\mu_{\mathbf{cav}}$ and C_{cav}.

The discrete time version of the equation above is:

$$R_{cav}^{n+1,n'} = (1-\lambda\Delta) R_{cav}^{n,n'} + (K-1)J^2\Delta^2 \sum_{n''=0}^{n} R_{cav}^{n,n''} R_{cav}^{n'',n'} + \delta_{n,n'} \tag{4.9}$$

It is worth to notice that causality can be exploited to simplify the equation above: indeed, a generic element $R_{cav}^{n,n'}$ is different from zero only if $n > n'$. Hence, the expression above can be rewritten as:

$$R_{cav}^{n+1,n'} = (1-\lambda\Delta) R_{cav}^{n,n'} + (K-1)J^2\Delta^2 \sum_{n''=n'+1}^{n-1} R_{cav}^{n,n''} R_{cav}^{n'',n'} + \delta_{n,n'} \tag{4.10}$$

4.2.2 Numerical results

Here some simple results about the trivial dynamics of the linear model are presented; in order to show the validity of the algorithm that has been developed, the results obtained with it can be compared with those obtained by simulating the linear dynamics on a random regular graph. The first thing that can be presented is the relaxation of $\langle x(t) \rangle$ in the stable phase of the linear model, computed by taking the average over a set of 10^5 trajectories generated according to equation 4.5, using the DMFT quantities $\mu_{cav}(t)$, $C_{cav}(t, t')$ and $R_{cav}(t, t')$ obtained with the algorithm. The relaxation is presented in figure 4.1, where the average trajectory is pictured in red, while those in blue are ten trajectories taken from the set used to compute the average.

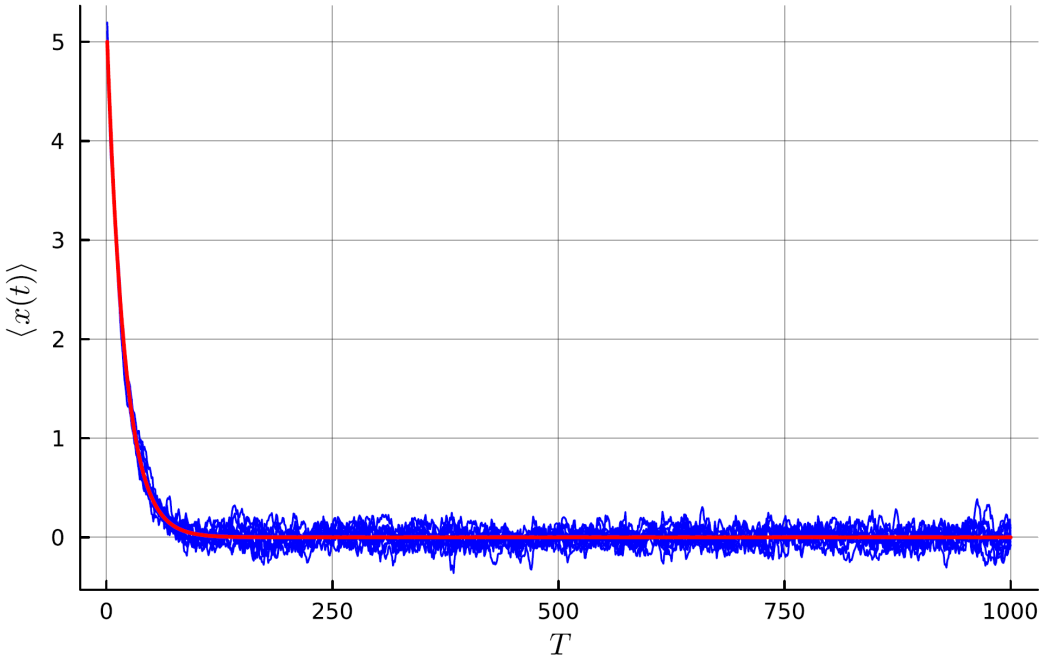

Figure 4.1: Relaxation of $\langle x(t) \rangle$ in the stable phase of the linear model.

These results were obtained by setting $T = 1000$ and $\Delta = 0.01$: this choice is enough to observe the relaxation toward the equilibrium value; moreover, the choice of a small Δ allows to reduce the error due to Euler-Maruyama procedure for the numerical integration of the equations during the generation of the trajectories; such a choice for the integration of the equations allows the algorithm to remain relatively fast and efficient, with a small price to pay in terms of precision of the results. For what concerns the parameters of the model, the following choices were

made: $\lambda = 15.0$, $D = 0.1$, $J = 1.0$ and $K = 10$, so that the dynamics is stable. To generate the trajectories of $x(t)$ according to equation 4.5, the initial condition was set to $x(0) = 5.0 + \delta$, where δ is a Gaussian random variable with mean $\mu = 0.0$ and variance $\sigma^2 = 0.1$. In conclusion, it is necessary to specify the parameters of the algorithm: the soft-update parameter was set to $\alpha = 0.5$; the algorithm made 30 iterations generating 10^3 trajectories, which amounts to a rough step in the space of the DMFT quantities, then it made 10 iterations generating 10^4 trajectories and 20 iterations generating 10^5 trajectories, where these two sets of iterations were used to refine the results obtained in the first set of iterations. In order to check that the choices for the parameters α, N_{traj} and of the number of iterations were good, it is possible to analyze the behavior of the ϵ value of both μ_{cav} and C_{cav} as functions of the iterations. As it is possible to observe in figure 4.2, both ϵ_μ and ϵ_C go to zero already after 20 iterations, so it is safe to say that the algorithm has converged. The DMFT quantities computed by the algorithm are presented in figure 4.3.

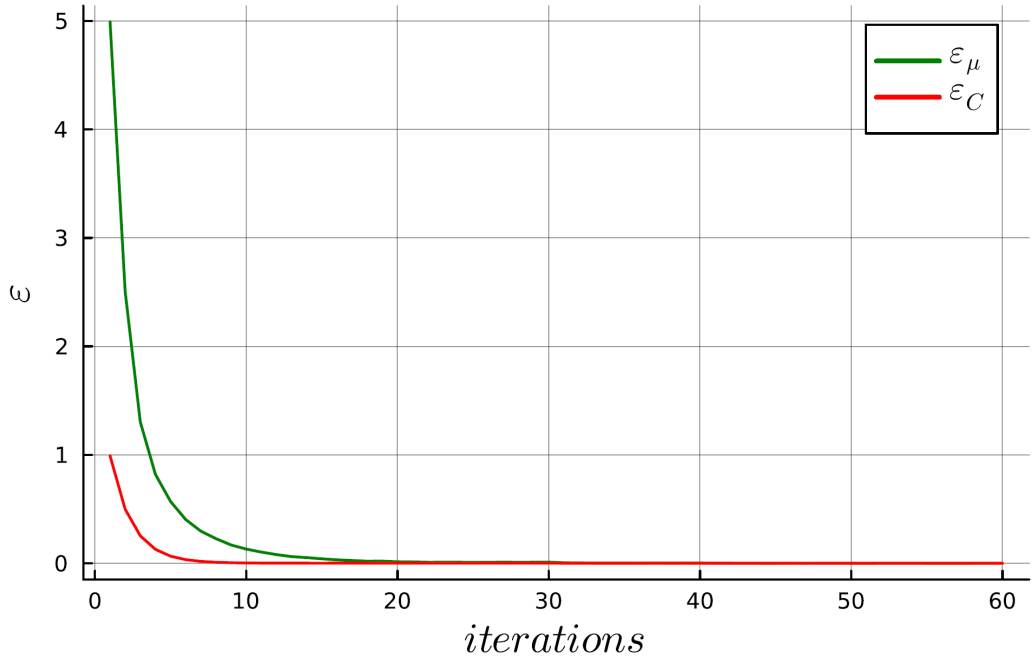

Figure 4.2: ϵ values of the DMFT quantities as a function of the iterations.

To conclude the analysis of the numerical results of the linear model, it is possible to show that the data obtained with the DMFT algorithm are in agreement with those obtained by simulating directly the dynamics. As anticipated in the

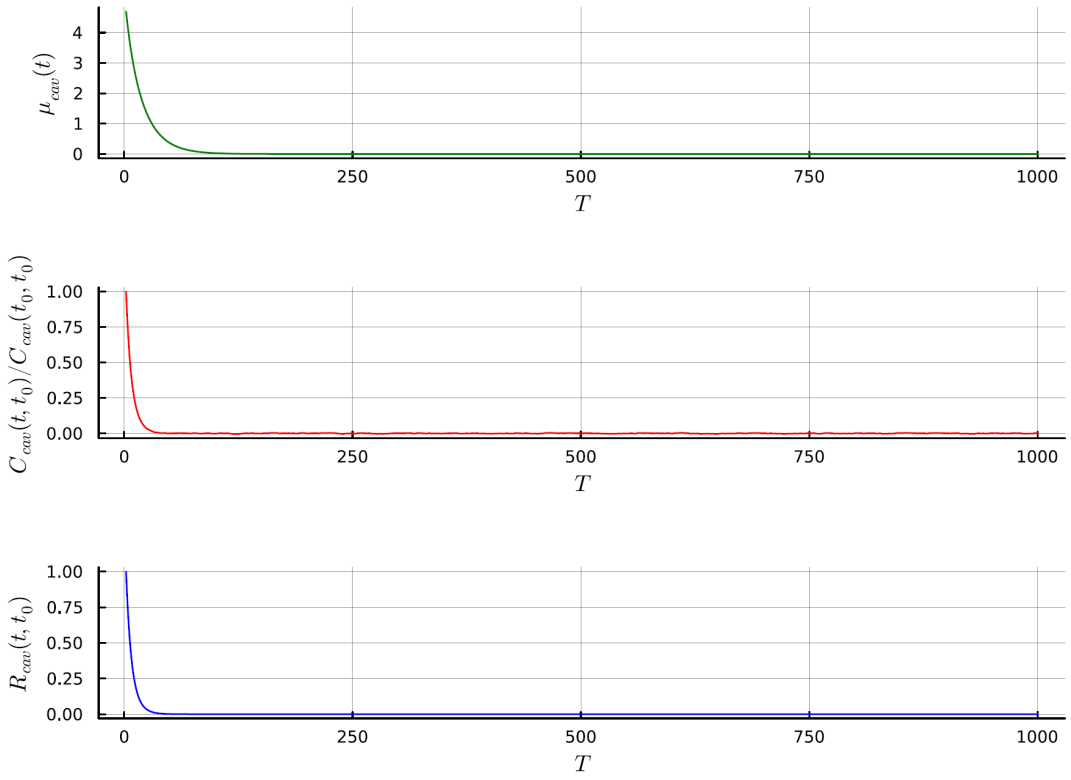

Figure 4.3: DMFT quantities of the linear model.

introduction of the chapter, the dynamics is simulated on a random regular graph with ten thousand node: this choice allows to replicate relatively well the dynamics on a Bethe lattice, if the size of the finite graph is sufficiently large, so that the presence of loops can actually be neglected. To show the validity of the results obtained with the algorithm, it is convenient to compute the quantities $\langle x(t)\rangle_{DS}$ and $C_{DS}(t,t')$ and compare them with the quantities $\langle x(t)\rangle_{DMFT}$ and $C_{DMFT}(t,t')$; these are:

- $\langle x(t)\rangle_{DS} = \frac{1}{N_{nodes}} \sum_{i=1}^{N_{nodes}} x_i(t)$ is the average trajectory computed by simulating the dynamics on the random regular graph, with $x_i(t)$ being the trajectory of the node i on the graph
- $C_{DS}(t,t') = \frac{1}{N_{nodes}} \sum_{i=1}^{N_{nodes}} x_i(t)x_i(t') - \Big(\frac{1}{N_{nodes}} \sum_{i=1}^{N_{nodes}} x_i(t)\Big)\Big(\frac{1}{N_{nodes}} \sum_{i=1}^{N_{nodes}} x_i(t')\Big)$ is the covariance matrix of the trajectories of the nodes of the graph
- $\langle x(t)\rangle_{DMFT}$ is computed by averaging over a set of 10^5 trajectories generated according to equation 4.5 using the DMFT quantities obtained with the

algorithm

- $C_{DMFT}(t, t')$ is the covariance matrix computed using the same set of trajectories used to compute $\langle x(t) \rangle_{DMFT}$

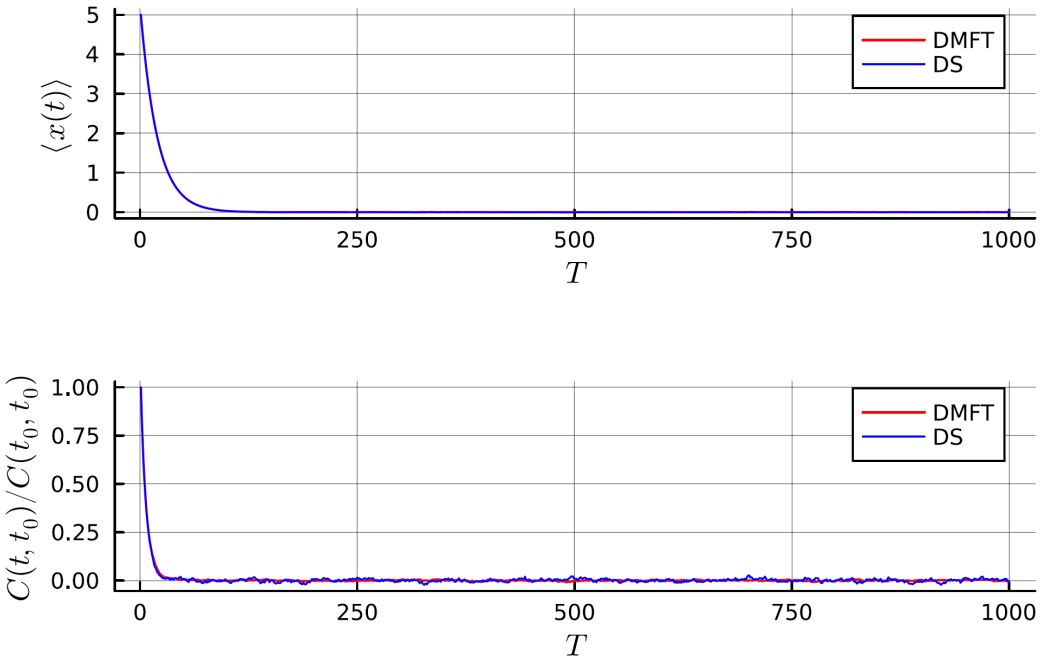

Figure 4.4: Comparison between the data obtained by means of direct simulations of the dynamics and the data obtained with the DMFT algorithm; the covariance function is rescaled by its value at the initial time $t_0 = 0$.

Obviously, to simulate the linear dynamics on the random regular graph the same choices in terms of parameters and initial conditions used to run the DMFT algorithm were made. From figure 4.4 it is possible to see that $\langle x(t) \rangle_{DS}$ perfectly agrees with $\langle x(t) \rangle_{DMFT}$, while, for what concerns the agreement between $C_{DS}(t, t')$ and $C_{DMFT}(t, t')$, it can be seen that $C_{DS}(t, t')$ is affected by small fluctuations which can be imputed to the fact that only 10^4 are used for the estimate in place of the 10^5 trajectories used to estimate $C_{DMFT}(t, t')$.

4.3 The ϕ^4 model

4.3.1 Presentation of the model

One of the simplest non trivial models that can be studied with the DMFT approach is the ϕ^4 model, in which $f[x(t)] = -\lambda x(t) - ux^3(t)$. The equation for the dynamics of a degree of freedom defined on a Bethe lattice with homogeneous couplings reads:

$$\frac{dx_i}{dt} = -\lambda x_i(t) - ux^3(t) + J\sum_{j\in\partial i} x_j(t) + \eta_i(t) \tag{4.11}$$

where $\eta_i(t)$ is the usual Gaussian additive white noise with:

$$\langle \eta_i(t) \rangle = 0 \tag{4.12a}$$
$$\langle \eta_i(t)\eta_i(t') \rangle = 2D\delta(t-t') \tag{4.12b}$$

While in the case of the linear model there was only a single stable phase toward which the system could relax, in the case of the ϕ^4 model the picture is a little bit richer: there is still a phase in which the degrees of freedom relax toward zero value, but, if certain relations between the parameters λ, u, J and D are satisfied, it is possible to observe a spontaneous symmetry breaking in which the degrees of freedom settle around a non zero value.

To grasp something about this dynamics, it is convenient to analyze the model in the absence of noise; in this case, given u and J positives and fixed, there exists a critical $\lambda_c = KJ$ such that: if $\lambda < \lambda_c$, the system possess two symmetric stable states at the values $\pm\sqrt{\frac{JK-\lambda}{u}}$; if instead $\lambda \geq \lambda_c$, the system possess a single stable state at zero value. The presence of the noise enriches this picture, introducing fluctuations in the degrees of freedom, making the phase diagram of the model more complex. To better understand the effect of the parameter D on this model, that is the effect of the noise, it is useful to derive density plots by means of direct simulations, which are pictured in 4.5.

For this model it can be noticed that, since we are considering a case with no disorder, that is $P(J_{ij}) = \delta(J_{ij} - J)$, the effective equations of the dynamics are exactly the same that has been derived in the previous chapter for the homogeneous case; the only thing that changes is the term $f[x(t)]$, which now reads $f[x(t)] = -\lambda x(t) - ux^3(t)$.

The effective equation for the cavity dynamics is:

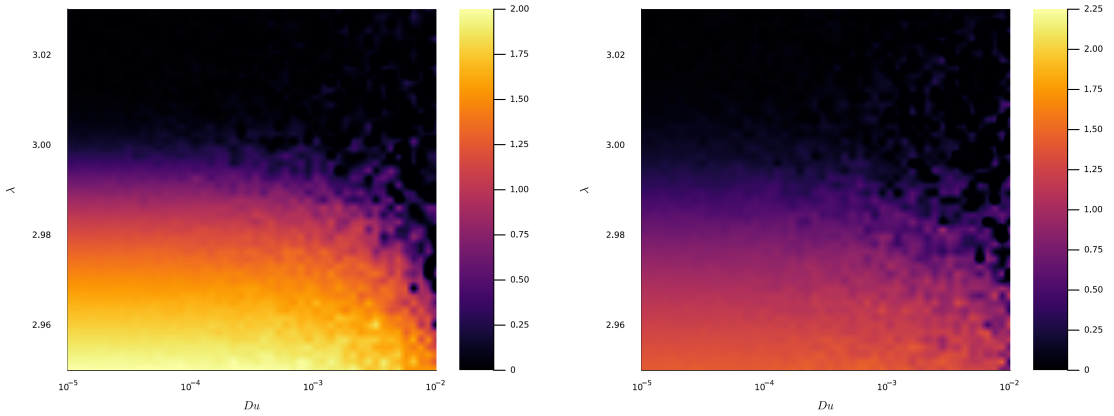

Figure 4.5: Density plots of the ϕ^4 model in the presence of noise: the plot on the left has been obtained for a connectivity $K = 3$, while the plot on the right has been obtained for a connectivity $K = 10$; both density plots have been computed by simulating directly the ϕ^4 model on a random regular graph; the model has been simulated via numerical integration with the Euler-Maruyama approach with a time step $\Delta = 0.1$ and for a number of time steps $T = 3000$, which was enough for the model to relaxe towards equilibrium, starting from an initial condition of $x_i(0) = 1$ for each node on the graph; the model has been simulated with a constant value $u = 0.01$, while varying the parameters λ and D.

$$\frac{dx}{dt} = -\lambda x(t) - ux^3(t) + (K-1)J\mu_{cav}(t) + \\ + (K-1)J^2 \int_0^t dt' R_{cav}(t,t')x(t') + \eta(t) \quad (4.13)$$

with:

$$\langle \eta(t) \rangle = 0 \quad (4.14a)$$
$$\langle \eta(t)\eta(t') \rangle = 2D\delta(t-t') + (K-1)J^2 C_{cav}(t,t') \quad (4.14b)$$

For the full dynamics the equation reads:

$$\frac{dx}{dt} = -\lambda x(t) - ux^3(t) + KJ\mu_{cav}(t) + KJ^2 \int_0^t dt' R_{cav}(t,t')x(t') + \eta(t) \quad (4.15)$$

with:

$$\langle \eta(t) \rangle = 0 \tag{4.16a}$$
$$\langle \eta(t)\eta(t') \rangle = 2D\delta(t-t') + KJ^2 C_{cav}(t,t') \tag{4.16b}$$

4.3.2 Approximation of the cavity response function

For the ϕ^4-model, $f[x(t)]$ is now a non linear function of $x(t)$, therefore there are some issues arising in the computation of the cavity response function. Indeed, in the equation for R_{cav} the following term appears:

$$\left.\frac{\delta\langle f[x(t)]\rangle_{K-1}}{\delta h(t')}\right|_{h=0} = -\lambda \left.\frac{\delta\langle x(t)\rangle_{K-1}}{\delta h(t')}\right|_{h=0} - u \left.\frac{\delta\langle x^3(t)\rangle_{K-1}}{\delta h(t')}\right|_{h=0} \tag{4.17a}$$
$$= -\lambda R_{cav}(t,t') - 3u \left.\left\langle x^2(t)\frac{\delta x(t)}{\delta h(t')}\right\rangle_{K-1}\right|_{h=0} \tag{4.17b}$$

As it is possible to see from the expression above, while the first term simply contains the cavity response function $R_{cav}(t,t')$, the second term is non trivial. From a theoretical point of view this term can be computed using the generating functional approach, which is general and, in principle, exact; however, as it has been pointed out before, that approach requires an extremely large number of trajectories to make a precise estimate. Since the number of trajectories is simply too large for the algorithm to remain efficient, it is necessary to pursue an alternative approach, consisting in the following approximation:

$$\left.\left\langle x^2(t)\frac{\delta x(t)}{\delta h(t')}\right\rangle_{K-1}\right|_{h=0} \approx \left\langle x^2(t)\right\rangle_{K-1}\Big|_{h=0} \left.\left\langle \frac{\delta x(t)}{\delta h(t')}\right\rangle_{K-1}\right|_{h=0} = \tag{4.18a}$$
$$= \langle x^2(t)\rangle_{K-1}\Big|_{h=0} \left.\frac{\delta\langle x(t)\rangle_{K-1}}{\delta h(t')}\right|_{h=0} = \tag{4.18b}$$
$$= \langle x^2(t)\rangle_{K-1}\Big|_{h=0} R_{cav}(t,t') \tag{4.18c}$$

With this approximation in mind, the differential equation for the cavity response function reads:

$$\frac{dR_{cav}(t,t')}{dt} = \Big(-\lambda - 3u\langle x^2(t)\rangle_{K-1}|_{h=0} \Big) R_{cav}(t,t') + $$
$$+ (K-1)J^2 \int_0^t dt'' R_{cav}(t,t'') R_{cav}(t'',t') + \delta(t-t') \tag{4.19}$$

In discrete time, the equation above becomes:

$$R_{cav}^{n+1,n'} = \left(1 - \lambda\Delta - 3u\Delta\langle x^{n2}\rangle_{K-1}|_{h=0}\right)R_{cav}^{n,n'} + \\ + (K-1)J^2\Delta^2 \sum_{n''=0}^{n} R_{cav}^{n,n''} R_{cav}^{n'',n'} + \delta_{n,n'} \quad (4.20)$$

To compute the term $\langle x^{n2}\rangle_{K-1}|_{h=0}$ at each iteration of the algorithm, it is possible to exploit the trajectories generated using the messages at the previous step; the same trajectories that are used to make the self-consistent update of μ_{cav} and C_{cav}.

Now we have everything we need to apply the algorithm to the ϕ^4 model and test the approximation that has been developed to update R_{cav} at each iteration.

4.3.3 Numerical results

To start the numerical analysis of the ϕ^4-model, it is reasonable to check that the DMFT algorithm is capable of reproducing both the equilibrium phases discussed during the presentation of the model, that is the equilibrium phase in which $\langle x(t \to +\infty)\rangle$ tends to zero and also the equilibrium phase in which $\langle x(t \to +\infty)\rangle$ tends to a non zero value. To set the parameters for this preliminary analysis, it is possible to exploit the information obtained during the derivation of the density plots of the ϕ^4-model for different connectivities.

Both pictures in figure 4.6 represent the relaxation of the average value of the degree of freedom $\langle x(t)\rangle$ with $(\lambda = 15.0, J = 1.0, u = 0.01, D = 0.1)$ being the parameters for the first picture and $(\lambda = 5.0, J = 1.0, u = 0.01, D = 0.1)$ being the parameters for the second picture. The dynamics has been simulated with $T = 1000$ and $\Delta = 0.01$. To compute the DMFT quantities, the algorithm performed 30 iterations generating 10^3 trajectories for the update, 10 iterations generating 10^4 trajectories and 20 iterations generating 10^5 trajectories: the first set of iterations correspond to rough steps in the space of the quantities μ_{cav}, C_{cav} and R_{cav}, while the last two sets are used to refine them; to perform all the iterations, a soft-update parameter of $\alpha = 0.5$ was used. At every iteration all the trajectories were generated with the initial condition $x(0) = 1.0 + \delta$, with δ being a Gaussian random variable with mean $\mu = 0.0$ and variance $\sigma^2 = 0.1$, so that it was possible to observe the relaxation dynamics for both phases. After the computation of the DMFT quantities, these have been used to generate trajectories according to the effective stochastic differential equations of the full dynamics to produce the plots of figure 4.6: for both picture, $\langle x(t)\rangle$ is presented in red, while the blue curves are ten trajectories randomly selected from the set used to compute

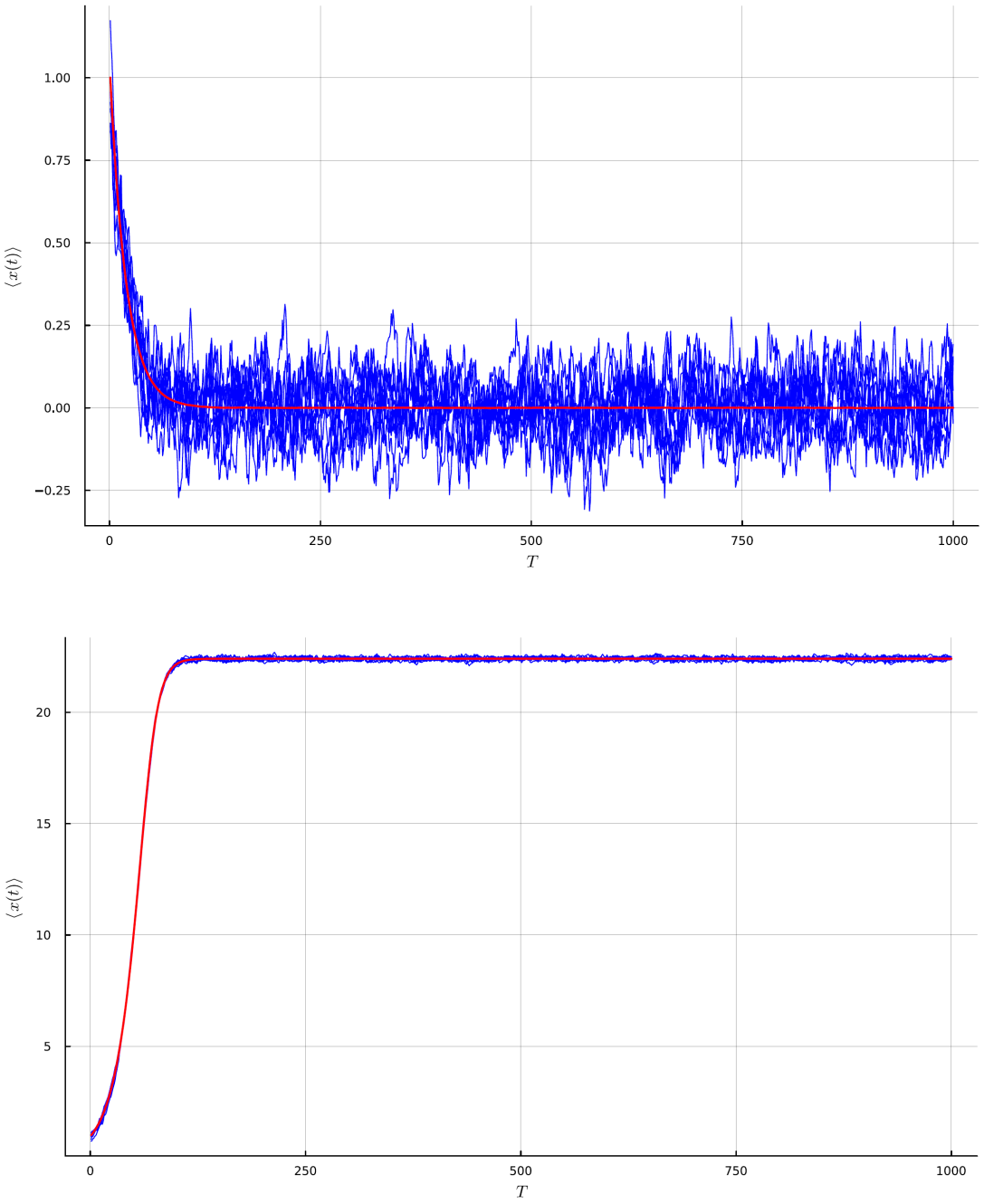

Figure 4.6: Relaxation of $\langle x(t) \rangle$ toward equilibrium: in the picture above the relaxation associated to the phase with zero as the equilibrium value is presented, while in the picture below the relaxation associated to the phase with a non-zero equilibrium value is presented.

$\langle x(t) \rangle$. To verify that the algorithm has converged, it is convenient to analyze the ϵ values of the DMFT quantities as a function of the iterations presented in figure 4.7: from the data of the picture, it can be understood that the algorithm has reached convergence, so that the obtained DMFT quantities can be trusted to generate trajectories according to equation 4.15 and then compare the results with those obtained by means of direct numerical simulations. To complete the presentation of a typical set of results of the DMFT algorithm applied to the ϕ^4-model, it is convenient to show the DMFT quantities $\mu_{cav}(t)$, $C_{cav}(t_1, t_2)$ and $R_{cav}(t_1, t_2)$, which are presented in figure 4.8: as it is possible to see from the picture, both the cavity response function $R_{cav}(t_1, t_2)$ and the cavity correlation function $C_{cav}(t_1, t_2)$ decay to zero after a certain time, with the decay being slightly different in the two phases; instead, for what concern $\mu_{cav}(t)$, it is possible to observe an obvious difference between the two phases, as in one case it decays to zero, while in the other it reaches a non-zero value which is a bit smaller than $\langle x(t \to \infty) \rangle$.

Before proceeding with the analysis of the results, it is worthy to investigate the effects of the approximation that has been chosen for the computation of the response function. To understand these effects, it is reasonable to see the consequences of changing the connectivity K and the coupling constant J on the accuracy of the results obtained with the DMFT algorithm, where the accuracy is verified by comparing the equilibrium value $\langle x(t \to +\infty) \rangle$ obtained by means of direct simulations of the dynamics on a random regular graph and the one obtained with the DMFT algorithm and then by computing the absolute error and the relative error. For both the direct simulations of the dynamics and the DMFT algorithm the values $T = 1000$ and $\Delta = 0.01$ were used, with the trajectories generated starting from the initial condition $x_i(0) = 1.0 \; \forall i \in V$, with $G = (V, E)$ being the random regular graph used simulate the dynamics, and with $x(0) = 1.0$ for the trajectories generated by the DMFT algorithm. For what concern the parameters specific to the DMFT algorithm, that is the soft-update parameter α, the number of trajectories N_{traj} generated for the update of the DMFT quantities and the number of iterations, values similar to those used to obtain the data represented in figure 4.6 were used. All the data gathered for this analysis were obtained in a setting where the parameter D of the noise was set to a small value, in order to reduce the effect of the noise on the error and to simplify the analysis of the approximation. If $\langle x(t \to +\infty) \rangle_{DS} = \frac{1}{|V|} \sum_{i \in V} x_i(t \to +\infty)$ is the average equilibrium value obtained by simulating directly the dynamics and $\langle x(t \to +\infty) \rangle_{DMFT} = \frac{1}{N_{traj}} \sum_{j=1}^{N_{traj}} x_j(t \to +\infty)$, with $\{x_j(t) : j \in \{1, ..., N_{traj}\}\}$ being the set of trajectories simulated with the DMFT algorithm, the errors are computed as:

$$\epsilon_{abs} = |\langle x(t \to +\infty) \rangle_{DS} - \langle x(t \to +\infty) \rangle_{DMFT}| \tag{4.21}$$

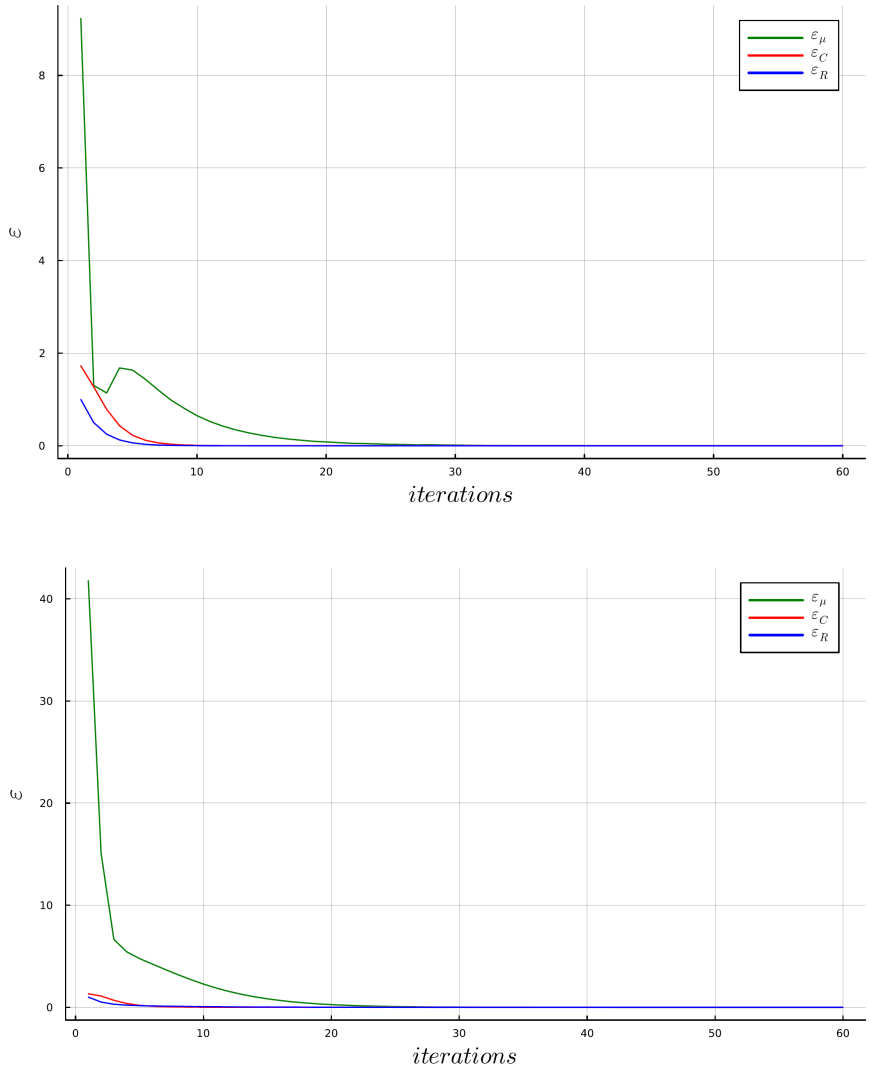

Figure 4.7: ϵ values of the DMFT quantities as a function of the iterations: the picture at the top shows the ϵ values obtained during the derivation of the results for the phase in which $\langle x(t) \rangle$ relaxes toward zero, while the picture at the bottom shows the ϵ values obtained during the derivation of the results for the other phase.

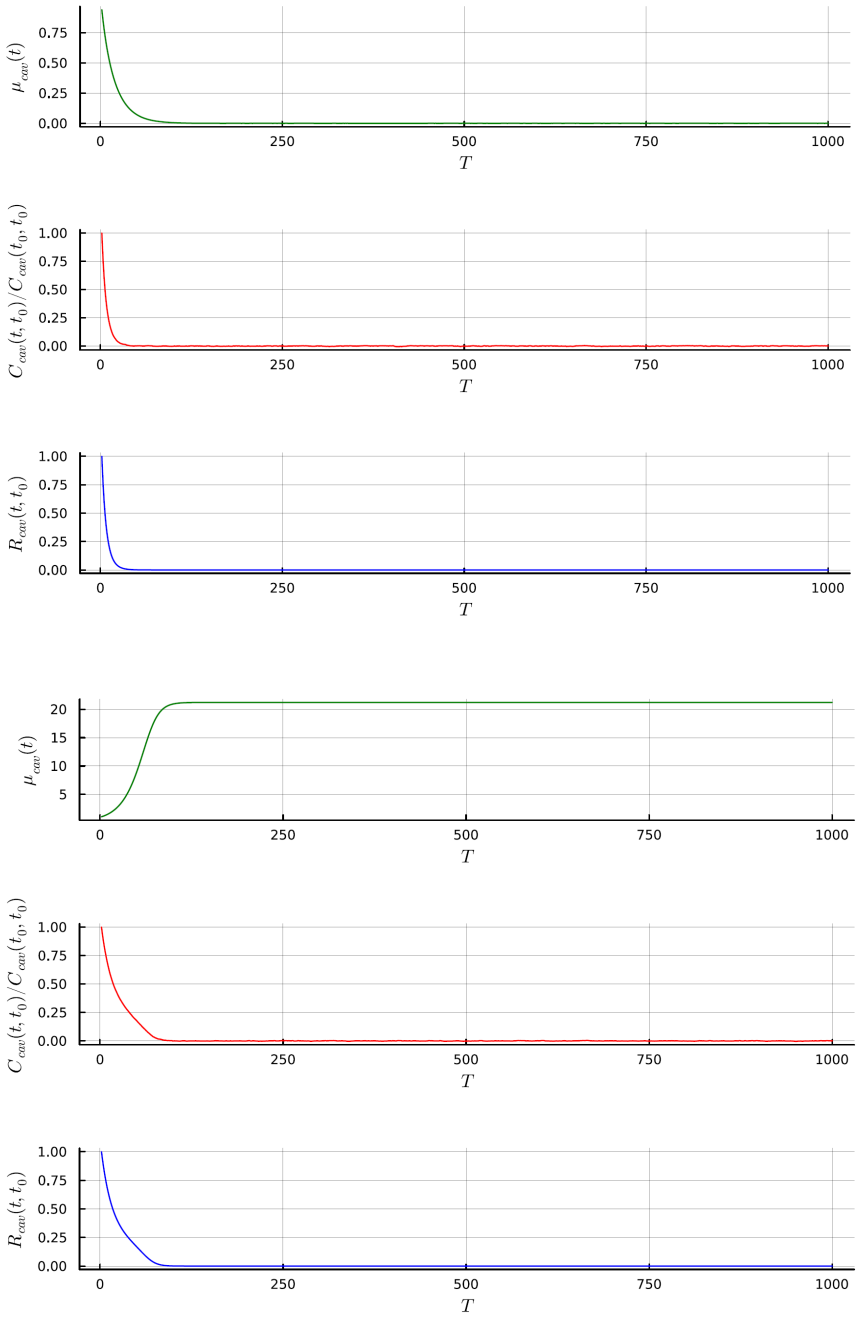

Figure 4.8: DMFT quantities: here the DMFT quantities computed by the algorithm are presented for both the phases of the model, where the function $C_{cav}(t, t_0)$ has been rescaled by the initial value $C_{cav}(t_0, t_0)$; the value t_0 is simply the the initial value on the time axis.

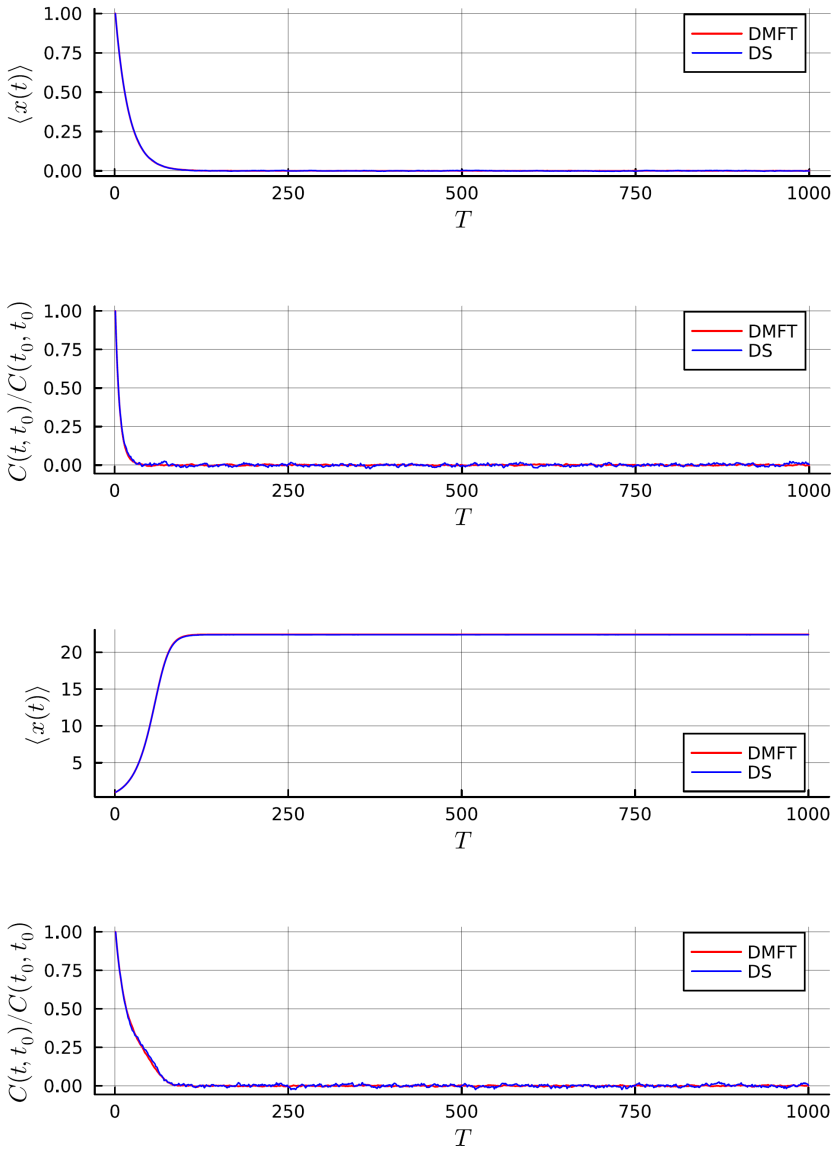

Figure 4.9: Comparison of the results between direct simulations (DS) and DMFT algorithm (DMFT): the two plots at the top were obtained in the phase with $\langle x(t \to +\infty) \rangle = 0$, while the two at the bottoms were obtained in the phase with $\langle x(t \to +\infty) \rangle$ different from zero. The covariance functions are showed rescaled by the value $C(t_0, t_0)$.

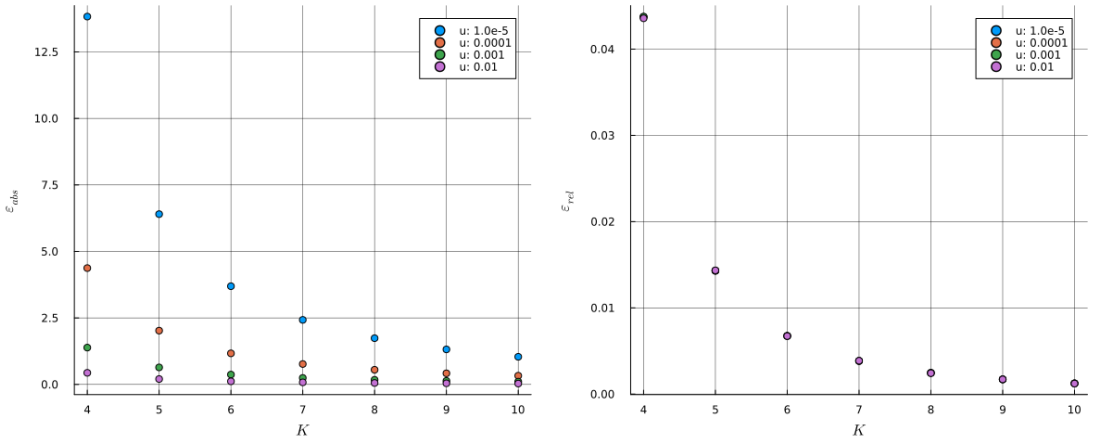

Figure 4.10: Absolute error ϵ_{abs} and relative error ϵ_{rel} as a function of the connectivity K and for different values of the parameter u; the coupling constant and the parameter of the local term chosen here are $J = 1.0$ and $\lambda = 3.0$; the parameter of the fluctuations is set to $D = 0.01$.

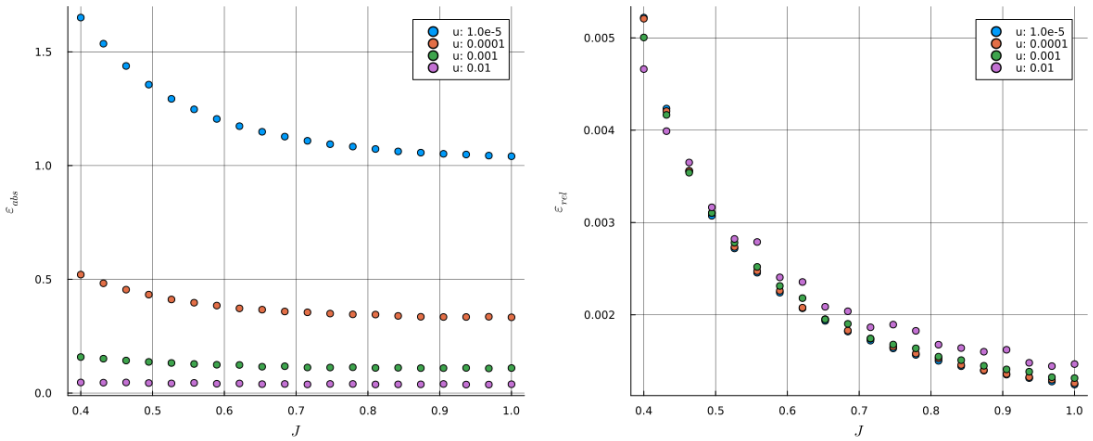

Figure 4.11: Absolute error ϵ_{abs} and relative error ϵ_{rel} as a function of the coupling constant J and for different values of the parameter u; the connectivity and the parameter of the local term chosen here are $K = 10$ and $\lambda = 3.0$; the parameter of the fluctuations is set to $D = 0.01$.

$$\epsilon_{rel} = \left| \frac{\langle x(t \to +\infty) \rangle_{DS} - \langle x(t \to +\infty) \rangle_{DMFT}}{\langle x(t \to +\infty) \rangle_{DS}} \right| \tag{4.22}$$

As it is possible to see in figure 4.10, both the absolute error and the relative error decrease as a the connectivity K increases; this can be easily explained: the

effective equations that are implemented in the algorithm have been derived starting from the assumption that the coupling constant is small, or equivalently, that the connectivity of the graph is large; as a consequence, it is reasonable to expect that the results obtained with the algorithm are affected by a non negligible error if the connectivity is small, and it is also reasonable to observe that this error decreases as the connectivity increases, as the effective equations of the DMFT approach becomes better at capturing the real behavior of the dynamics under exam. From figure 4.10 it can seen that the absolute error decreases as u increases at a fixed value of K, but this is due to the fact that the absolute error does not take into account the increase of $\langle x(t \to +\infty) \rangle$ as u decreases; when this is considered, as it happens in the relative error, the error itself becomes independent in the value of u. The most important conclusion that can be made observing figure 4.10 is that the relative error becomes smaller than 1% already for $K = 6$, signaling that despite its crudeness, the approximation used in the differential equation of the cavity response function is good enough to obtain acceptable numerical results.

The analysis of the approximation can be concluded by analyzing the results presented in figure 4.11: here the absolute error and the relative error are computed by keeping the constant the connectivity K while varying u and the coupling constant J. As it is possible to see from the picture, the absolute error decreases as J increases up to a point in which it remains constant. Note that it would be reasonable to expect that the error increases as J increases, since it would mean going out of the regime in which the effective description of the dynamics holds; to observe such an increase in the error, it would be necessary to use very large values of J, but this is complicated by stability issues in the process of numerical integration of the stochastic differential equations, which could be overcome by reducing the connectivity K. In conclusion, it is possible to see that by increasing J while remaining in the regime of validity of the effective description of the dynamics, both the absolute error and the relative error decreases, but this is decrease is very small: indeed, by observing the relative error, it can be seen that it decreases from the 0.5 % to the 0.2 %.

A further proof of the effectiveness of the approximation used for the cavity response function can be provided by comparing the values of $\langle x(t \to +\infty) \rangle$ obtained with direct simulations and with the algorithm in proximity of the equilibrium phase transition in the plane (Du, J) for different values of the connectivity K. The results of the comparison are presented in figures 4.12 and 4.13: the dots in blue have been obtained by simulating the dynamics on a graph with a thousand nodes many times and by computing the quantity $\langle x(t \to +\infty) \rangle_{DS}$, together with the standard deviation; the dots in red have been obtained with the DMFT algorithm by computing $\langle x(t \to +\infty) \rangle_{DMFT}$ and the standard deviation from a

set of a thousand trajectories. Since the dynamics was analyzed close to a phase boundary, it was necessary to gather a relatively large amount of data from the direct simulations in order to obtain precise estimates of $\langle x(t \to +\infty) \rangle$, due to the presence of fluctuations; for what concern the data acquired with the DMFT algorithm, a relatively small amount of data was more than enough to obtain precise estimates of $\langle x(t \to +\infty) \rangle$, suggesting that the DMFT approach is capable of compensating the effect of fluctuations close to a phase boundary. For both the simulations and the algorithm, the parameters $T = 1000$ and $\Delta = 0.1$ were chosen; for the initial conditions, each initial value of a trajectory ($x_i(0)$ for the simulations or $x(0)$ for a trajectory of the DMFT algorithm) was set equal to $\sqrt{\frac{KJ-\lambda}{u}}$ if $\lambda < \lambda_c$, or equal to zero if $\lambda \geq \lambda_c$, so that the relaxation process to the equilibrium value could be speed up. The parameters α and N_{traj} and the number of iterations of the DMFT algorithm were chosen similar to those used for obtaining the results presented in figure 4.6. Each set of points presented in the figures 4.12 and 4.13 has been obtained by varying λ while keeping all the other parameters constant; moreover, to compare the values of $\langle x(t \to +\infty) \rangle_{DS}$ and $\langle x(t \to +\infty) \rangle_{DMFT}$ along the Du axis, u was kept constant, while D was left to take the values 0.001, 0.01, 0.1 and 1.0.

For what concern the comparison itself, the results can be easily explained. In the case with $K = 3$ there is a discrepancy between the ones obtained with the simulations and the ones obtained with the DMFT algorithm in the phase with $\langle x(t \to +\infty) \rangle$ different from zero, while there is agreement in the phase with $\langle x(t \to +\infty) \rangle$ equal to zero. In the case with $K = 10$ there is instead agreement in both phases, proving once again that the approximation used for the cavity response function is trustworthy if the connectivity is sufficiently large.

4.4 The 2-spin model without disorder

4.4.1 Presentation of the model

An interesting model that can be analyzed without the need of any crude approximation is the 2-spin model. Within this model a set of continuous variables $\{x_i(t)\}_{i \in V}$ is associated to the nodes of a graph $G = (V, E)$; these variable interacts according to the Hamiltonian:

$$H[\vec{x}] = -\frac{1}{2} \sum_{i=1}^{N} \sum_{j \in \partial i} J_{ij} x_i x_j \tag{4.23}$$

and are subjected to the spherical constraint $\sum_{i=1}^{N} x_i^2(t) = N$.

The relaxation dynamics of such a system can be described by considering the following stochastic differential equation for each variable $x_i(t)$:

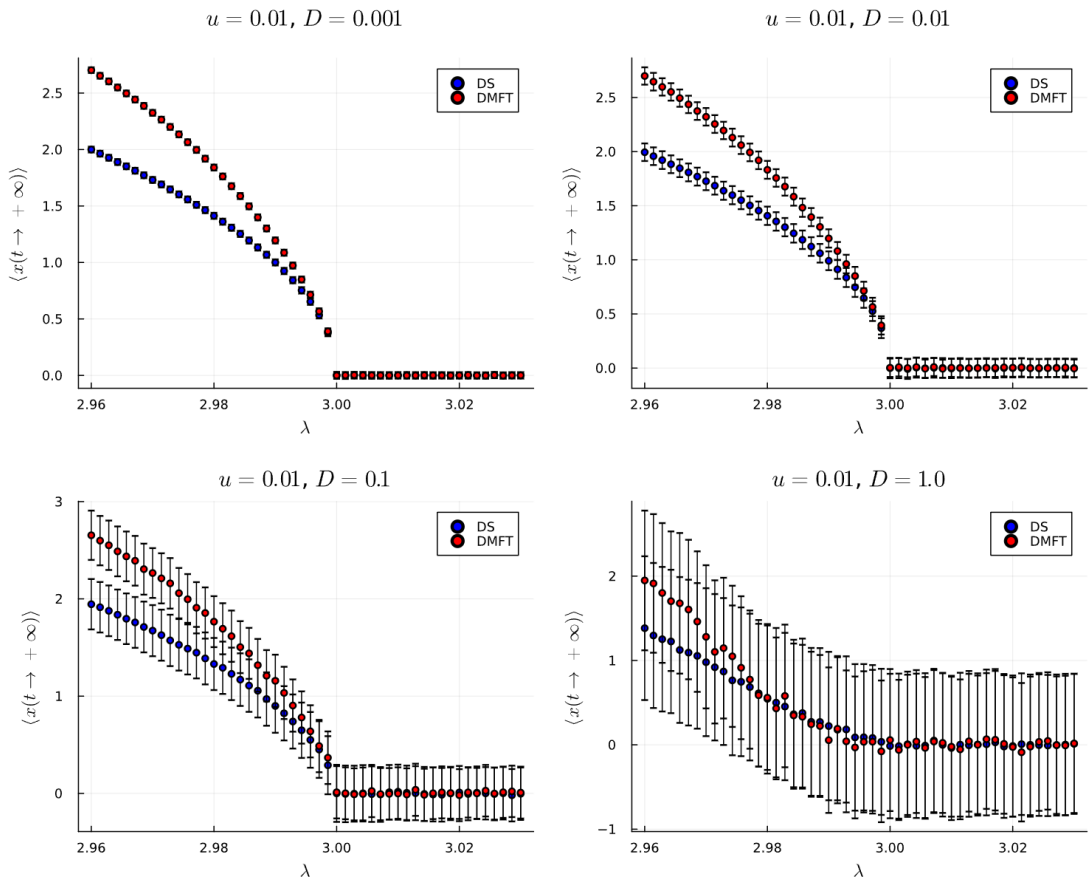

Figure 4.12: Comparison between the results of direct numerical simulations and those obtained with the DMFT algorithm at fixed u and K=3.

$$\frac{dx_i}{dt} = -\frac{\delta H[\vec{x}]}{\delta x_i(t)} - \lambda(t)x_i(t) + \eta_i(t) \tag{4.24}$$

which reduces to:

$$\frac{dx_i}{dt} = \sum_{j \in \partial i} J_{ij}x_j(t) - \lambda(t)x_i(t) + \eta_i(t) \tag{4.25}$$

where $\lambda(t)$ is the Lagrange multiplier enforcing the spherical constraint, whose expression has to be determined self-consistently, and $\eta_i(t)$ is Gaussian noise with zero mean and correlation $\langle \eta_i(t)\eta_j(t') \rangle = 2D\delta_{ij}\delta(t-t')$ modeling the effect of temperature.

If the couplings are positive and homogeneous, that is they are all equal to some value $J > 0$, the behavior of the system is trivial: it presents a low temperature

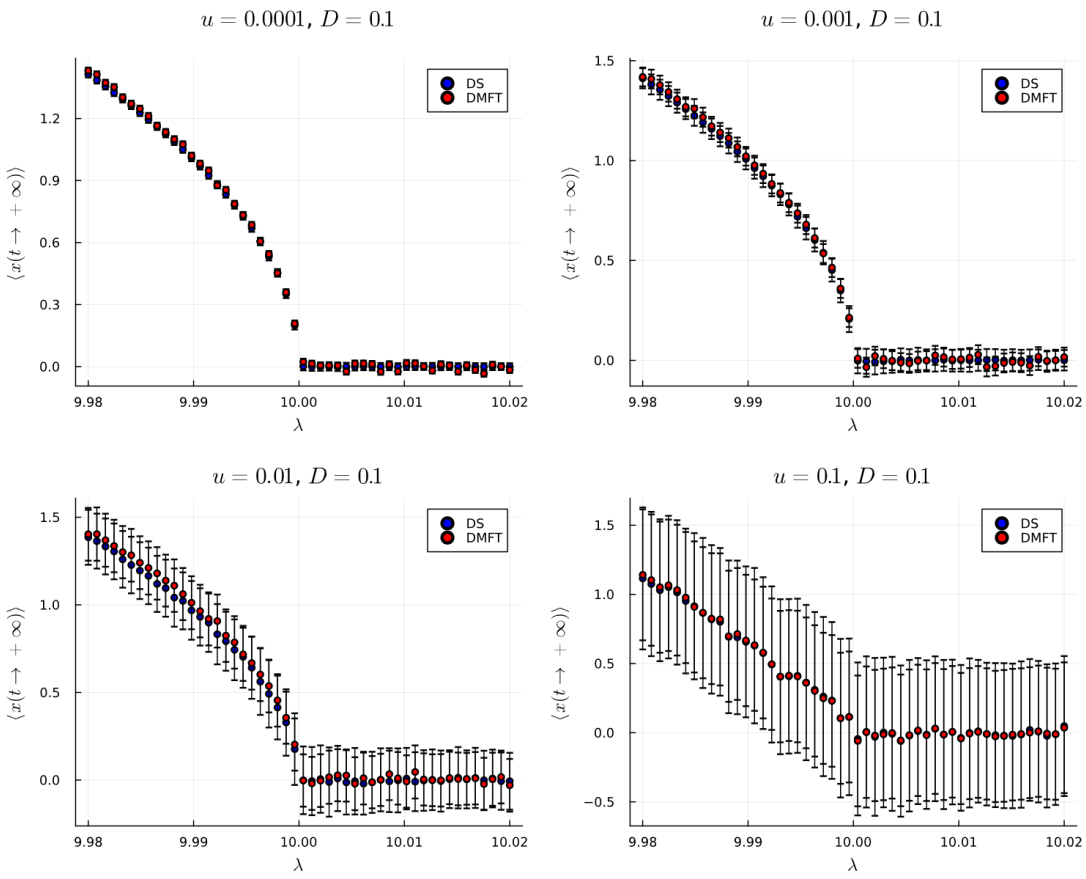

Figure 4.13: Comparison between the results of direct numerical simulations and those obtained with the DMFT algorithm at fixed u and K=10.

ferromagnetic phase, where each variable $x_i(t)$ is equal to one (or to minus one) once the equilibrium is reached, and a high temperature paramagnetic phase where each variable relaxes to zero; as the temperature is modeled by the parameter D, it is reasonable to expect that, for each value of J and K, there exists a critical value D_c separating the high temperature phase from the low temperature phase. Note that if J is too large, the dynamics becomes unstable, as for each degree of freedom the term associated to the Lagrange multiplier is no longer able to compensate the growth of the term associated to the interaction; moreover, J cannot be too large because of the hypothesis on which the effective equations of the dynamics have been derived.

More information about the behavior of the 2-spin model without disorder can be obtained by computing some density plots, like the ones presented in 4.14.

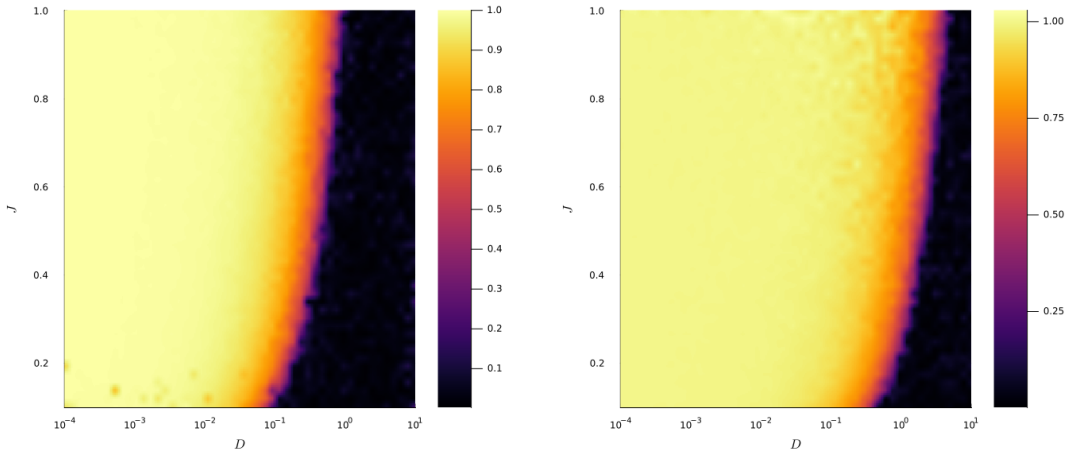

Figure 4.14: Density plots of the 2-spin model in the presence of noise: the plot on the left has been obtained for a connectivity $K = 3$, while the plot on the right has been obtained for a connectivity $K = 10$; both density plots have been computed by simulating directly the 2-spin model on a random regular graph; the model has been simulated via numerical integration with the Euler-Maruyama approach with a time step $\Delta = 0.1$ and for a number of time steps $T = 2000$, which was enough for the model to relaxe towards equilibrium, starting from an initial condition where each degree of freedom on the graph is distributed according to a standard distribution; the model has been simulated with a value of J smaller than one, to ensure the stability of the dynamics.

4.4.2 Derivation of the effective equations of the dynamics in the homogeneous case

Let us here consider the homogeneous case in which the couplings are all the same, that is the case in which the distribution $P(J_{ij})$ is simply a Dirac's delta function, namely $P(J_{ij}) = \delta(J_{ij} - J)$. In this simple case the effective equations of the dynamics can be immediately obtained by substituting the term $f[x(t)]$ in the equations for a general dynamics with homogeneous couplings with the term of the 2-spin model $-\lambda(t)x(t)$.

Therefore, the effective equation for the cavity dynamics reads:

$$\frac{dx}{dt} = -\lambda(t)x(t) + (K-1)J\mu_{cav}(t) + \\ + (K-1)J^2 \int_0^t dt' R_{cav}(t,t')x(t') + \eta(t) \quad (4.26)$$

with:

$$\langle \eta(t) \rangle = 0 \tag{4.27a}$$
$$\langle \eta(t)\eta(t') \rangle = 2D\delta(t-t') + (K-1)J^2 C_{cav}(t,t') \tag{4.27b}$$

For the full dynamics the equation reads:

$$\frac{dx}{dt} = -\lambda(t)x(t) + KJ\mu_{cav}(t) + KJ^2 \int_0^t dt' R_{cav}(t,t')x(t') + \eta(t) \tag{4.28}$$

with:

$$\langle \eta(t) \rangle = 0 \tag{4.29a}$$
$$\langle \eta(t)\eta(t') \rangle = 2D\delta(t-t') + KJ^2 C_{cav}(t,t') \tag{4.29b}$$

4.4.3 Derivation of the equation for the Lagrange multiplier in the homogeneous case

To complete the picture of the 2-spin model in the absence of disorder, it is necessary to derive an explicit equation for the Lagrange multiplier. This can be done by remembering that the correlation function of the degrees of freedom, which can be indicated with $C(t,t') = \langle x(t)x(t') \rangle_K$, has to be equal to one for all $t = t'$. Hence, by exploiting the spherical constraint, we can write:

$$\left[\frac{dC(t,t')}{dt} + \frac{dC(t,t')}{dt'} \right]_{t,t'=s} = 0 \tag{4.30}$$

which results in:

$$\left[\left\langle \frac{dx(t)}{dt} x(t') \right\rangle_K + \left\langle x(t) \frac{dx(t')}{dt'} \right\rangle_K + \right]_{t,t'=s} = 0 \tag{4.31}$$

Here we can compute the two terms of the expression above one by one. For the first term, we have:

$$\left\langle \frac{dx(t)}{dt} x(t') \right\rangle_K = -\lambda(t)\langle x(t)x(t') \rangle_K + KJ\mu_{cav}(t)\langle x(t') \rangle_K + \\ + KJ^2 \int_0^t dt'' R_{cav}(t,t'')\langle x(t'')x(t') \rangle_K + \langle \eta(t)x(t') \rangle_K \tag{4.32}$$

For the second term, we have:

$$\left\langle x(t)\frac{dx(t')}{dt'}\right\rangle_K = -\lambda(t')\langle x(t)x(t')\rangle_K + KJ\mu_{cav}(t')\langle x(t)\rangle_K + \\ + KJ^2\int_0^{t'} dt'' R_{cav}(t',t'')\langle x(t)x(t'')\rangle_K + \langle \eta(t')x(t)\rangle_K \quad (4.33)$$

By plugging these expressions back into the equation (4.31), we get:

$$-\lambda(s)\langle x(s)x(s)\rangle_K + KJ\mu_{cav}(s)\langle x(s)\rangle_K + \\ + KJ^2\int_0^s dt'' R_{cav}(s,t'')\langle x(t'')x(s)\rangle_K + \langle \eta(s)x(s)\rangle_K + \\ -\lambda(s)\langle x(s)x(s)\rangle_K + KJ\mu_{cav}(s)\langle x(s)\rangle_K + \\ + KJ^2\int_0^s dt'' R_{cav}(s,t'')\langle x(t'')x(s)\rangle_K + \langle \eta(s)x(s)\rangle_K = 0 \quad (4.34)$$

By reorganizing the terms and by recalling that $\langle x(s)x(s)\rangle_K = C(s,s) = 1$, we get the following expression for the Lagrange multiplier at any given time:

$$\lambda(s) = KJ\mu_{cav}(s)\langle x(s)\rangle_K + \\ + KJ^2\int_0^s dt'' R_{cav}(s,t'')\langle x(s)x(t'')\rangle_K + \langle \eta(s)x(s)\rangle_K \quad (4.35)$$

4.4.4 DMFT algorithm for the 2-spin model without disorder

The fact that the Lagrange multiplier has to be computed self-consistently is responsible for a modification of the DMFT algorithm presented in the previous chapter. Hence, the steps of the algorithm can be briefly reviewed together with the modifications required to account for the Lagrange multiplier.

The key quantities of the algorithm here reads:

- $\mu_{\mathbf{cav}}$, C_{cav} and R_{cav}, the desired DMFT quantities
- λ is the Lagrange multiplier
- $\mu_{\mathbf{cav}}^{\mathbf{new}}$, C_{cav}^{new} and R_{cav}^{new}, the new messages computed at each iteration of the algorithm
- λ^{new} is the new Lagrange multiplier computed at each iteration of the algorithm
- T, the total number of time steps

- Δ, the size of the time step

- N_{traj}, the number of trajectories that are generated at each iteration for the self-consistent update of the messages and of the Lagrange multiplier

- K, the connectivity of the lattice

- α, the parameter for the soft update of λ, $\mu_{\mathbf{cav}}$, C_{cav} and R_{cav} at each iteration of the algorithm

- $(\epsilon_1, \epsilon_2, \epsilon_3, \epsilon_4)$, threshold values for the convergence of λ, $\mu_{\mathbf{cav}}$, C_{cav} and R_{cav}

Initialization

Step 0: initialization of the messages and of the Lagrange multiplier
Clearly, the first step is the initialization of the messages $\mu_{\mathbf{cav}}$, C_{cav} and R_{cav} and of the Lagrange multiplier λ. For what concerns the initialization of the cavity mean μ_{cav}, it can be set all equal to one in the ferromagnetic phase and all equal to zero in the paramagnetic phase. For both the cavity correlation function C_{cav} and for the cavity response function R_{cav} the standard choices hold: C_{cav} can be initialized with a symmetric positive definite matrix, while R_{cav} can be initialized with a lower triangular matrix. To conclude the initialization, it is necessary to set the Lagrange multiplier λ; this can be achieved with the help of numerical simulations: indeed, the dynamics of the 2-spin model without disorder can be simulated on a small random regular graph, so that the data can be gathered quickly, then the Lagrange multiplier of the DMFT algorithm can be set all equal to the value of the Lagrange multiplier of the direct simulation taken once equilibrium is reached.

Iterative step

Step 1: generation of the trajectories(full dynamics)
A number N_{traj} of trajectories of the noise $\{\boldsymbol{\Delta\eta}_j\}_{j\in\{1,\dots,N_{traj}\}}$ and N_{traj} trajectories of the degree of freedom $\{\boldsymbol{x}_j\}_{j\in\{1,\dots,N_{traj}\}}$ according to the effective equation for the full dynamics:

$$x_j^{n+1} = x_j^n - \lambda^{nn} x_j \Delta + KJ\mu_{cav}^{n\ l} x^n + KJ^2\Delta^2 \sum_{n':n'\leq n} R_{cav}^{n,n'\,l} x_j^{n'} + \Delta\eta_j^n \tag{4.36}$$

with $j \in \{1, ..., N_{traj}\}$ and with μ_{cav}^l, C_{cav}^l and R_{cav}^l being the current values of the DMFT quantities.

Step 2: computation of the new Lagrange multiplier $\lambda^{\mathbf{new}}$
The N_{traj} trajectories of the noise and of the degree of freedom can now be used to compute λ^{new} according to the following equation:

$$\lambda^{n,new} = KJ\mu_{cav}^{n\ \ l}\frac{1}{N_{traj}}\sum_{j=1}^{N_{traj}} x_j^n + \\ + KJ^2\Delta\sum_{n'=0}^{n} R_{cav}^{n,n'l}\frac{1}{N_{traj}}\sum_{j=1}^{N_{traj}} x_j^n x_j^{n'} + \frac{1}{\Delta N_{traj}}\sum_{j=1}^{N_{traj}}\Delta\eta_j^n x_j^n \quad (4.37)$$

where we have exploited the fact that the average $\langle ... \rangle_K$ over the dynamics can be replaced by an average over the trajectories. Note that this is just the discrete time version of equation 4.35.

Step 3: generation of the trajectories(cavity dynamics)
A number N_{traj} of trajectories of the noise $\{\boldsymbol{\Delta\eta}_j\}_{j\in\{1,...,N_{traj}\}}$ and N_{traj} trajectories of the degree of freedom $\{\boldsymbol{x}_j\}_{j\in\{1,...,N_{traj}\}}$ according to the effective equation for the cavity dynamics:

$$x_j^{n+1} = x_j^n - \lambda^{nl}x_j^n\Delta + (K-1)J\Delta\mu_{cav}^{n\ \ l}x^n + \\ + (K-1)J^2\Delta^2\sum_{n':n'\leq n} R_{cav}^{n,n'l}x_j^{n'} + \Delta\eta_j^n \quad (4.38)$$

with $j \in \{1, ..., N_{traj}\}$ and with μ_{cav}^l, C_{cav}^l and R_{cav}^l being the current values of the DMFT quantities.

Step 4: derivation of C_{cav}^{new}
The elements of the matrix C_{cav}^{new} can be computed by means of the trajectories $\{\boldsymbol{x}_j\}_{j\in\{1,...,N_{traj}\}}$ that have been generated as:

$$C_{cav}^{new,n,n'} = \frac{1}{N_{traj}}\sum_{j=1}^{N_{traj}} x_j^n x_j^{n'} - \left(\frac{1}{N_{traj}}\sum_{j=1}^{N_{traj}} x_j^n\right)\left(\frac{1}{N_{traj}}\sum_{j=1}^{N_{traj}} x_j^{n'}\right) \quad (4.39)$$

Step 5: derivation of R_{cav}^{new}
The cavity response function can be computed using the temporal integration approach, which is exact for this particular model. In continuous time the differential equation for $R_{cav}^{new}(t,t')$ reads:

$$\frac{dR_{cav}^{new}(t,t')}{dt} = -\lambda(t)R_{cav}^{new}(t,t') + \\ + (K-1)J^2\int_0^t dt'' R_{cav}^{new}(t,t'')R_{cav}^{new}(t'',t') + \delta(t-t') \quad (4.40)$$

In discrete time the equation becomes:

$$R_{cav}^{new,n+1,n'} = (1-\lambda^n\Delta)R_{cav}^{new,n,n'} + \\ + (K-1)J^2\Delta^2\sum_{n''=0}^{n} R_{cav}^{new,n,n''}R_{cav}^{new,n'',n'} + \delta_{n,n'} \quad (4.41)$$

As a consequence of causality, only the elements R_{cav}^{new,n_1,n_2} with $n_1 > n_2$ are different from zero; hence the equation above can be rewritten as:

$$R_{cav}^{new,n+1,n'} = (1-\lambda^n\Delta)R_{cav}^{new,n,n'} + \\ + (K-1)J^2\Delta^2\sum_{n''=n'+1}^{n-1} R_{cav}^{new,n,n''}R_{cav}^{new,n'',n'} + \delta_{n,n'} \quad (4.42)$$

Step 6: check for convergence
At this point it is necessary to compare the current messages and the current Lagrange multiplier with the one computed at the steps 2, 4 and 5 and check whether the following conditions are satisfied:

$$\max_{i\in 1,\dots,T}\{|\boldsymbol{\lambda}^{new,i} - \boldsymbol{\lambda}^{l,i}|\} \leq \epsilon_1 \quad (4.43a)$$

$$\max_{i\in 1,\dots,T}\{|\boldsymbol{\mu}^{new,i} - \boldsymbol{\mu}^{l,i}|\} \leq \epsilon_1 \quad (4.43b)$$

$$\max_{i,j\in 1,\dots,T}\{|C_{cav}^{new,i,j} - C_{cav}{}^{l,i,j}|\} \leq \epsilon_2 \quad (4.43c)$$

$$\max_{i,j\in 1,\dots,T}\{|R_{cav}^{new,i,j} - R_{cav}{}^{l,i,j}|\} \leq \epsilon_4 \quad (4.43d)$$

If all these conditions are satisfied, the algorithm stops; otherwise, it proceeds to perform a soft-update of the messages and of the Lagrange multiplier.

Step 7: soft-update of the DMFT quantities and of the Lagrange multiplier

If the check for convergence at step 6 fails, a soft-update of the messages is made, according to:

$$\begin{aligned}
\boldsymbol{\lambda}^{l+1} &= \alpha\boldsymbol{\lambda}^{l} + (1-\alpha)\boldsymbol{\lambda}^{new} \\
\boldsymbol{\mu}^{l+1} &= \alpha\boldsymbol{\mu}^{l} + (1-\alpha)\boldsymbol{\mu}^{new} \\
{C_{cav}}^{l+1} &= \alpha{C_{cav}}^{l} + (1-\alpha)C_{cav}^{new} \\
{R_{cav}}^{l+1} &= \alpha{R_{cav}}^{l} + (1-\alpha)R_{cav}^{new}
\end{aligned}$$

The choice of performing a soft-update of the messages is motivated, as for the original algorithm, by the will to avoid large jumps in the space of the messages and of the Lagrange multiplier, which could lead to instabilities in the algorithm.

Conclusion

The algorithm works as follows: it start with the initialization of the quantities of interests; then the steps from 2 to 7 are repeated iteratively, so that the messages and the Lagrange multiplier are updated at each iteration; as soon as the check for convergence succeed, the algorithm stops. If the check for convergence never succeed, the algorithm goes on for a predetermined number of iterations.

4.4.5 Numerical results

To present the numerical results for the 2-spin model without disorder it is convenient to follow the same scheme used for the linear model; this time however, it is necessary to analyze the dynamics in both its phases: the ferromagnetic phase, in which $\langle x(t \to +\infty)\rangle$ is equal to a non zero value, and the paramagnetic phase, in which $\langle x(t)\rangle$ relaxes toward zero at equilibrium. It is important to point out that, in order to avoid the arising of numerical instabilities, the coupling constant J has been rescaled by the connectivity K.

The presentation of the results can start from the ferromagnetic phase, which is obtained by setting $K = 10$, $J = 1.0$ and $D = 0.01$. The dynamics was analyzed with $T = 1500$ and $\Delta = 0.01$, so that the time window is large enough to observe the relaxation of the trajectories to the equilibrium value. The initial conditions were such that $x(0) = 0.5 + \delta$, where δ is a Gaussian random variable with mean $\mu = 0$ and variance $\sigma^2 = 0.01$; in a way similar to that of the ϕ^4-model, the system can relax to a positive equilibrium value and also to symmetric negative value; however, the choice of the initial conditions allow to select the phase characterized by a positive equilibrium value. To derive the DMFT quantities, the algorithm performed 30 iterations generating 10^3 trajectories, 20 iterations generating 10^4 trajectories and then 20 iterations generating 10^5 trajectories; it was convenient to set $\alpha = 0.5$ for the first set of iterations, $\alpha = 0.7$ for the second set of iterations

and $\alpha = 0.8$ for the last set of iterations; the change of the value of α during the various set of iterations can be motivated by the will of reducing "oscillations" in the DMFT quantities during the refinement phase: this way of updating the DMFT quantities was prompted by the analysis of the ϵ values during various runs of the algorithm, where these were seen oscillating after an initial decay, suggesting that an increase in α could help in smoothing out their profiles and increase the precision of the estimates. In the ferromagnetic phase the trajectories relaxed to a non zero value, which for this particular choice of the parameter K, J and D is exactly one, as it can be seen from figure 4.15: as usual, the one in red is the average trajectory, while the ones in blue are ten sample trajectories selected from a set of 10^6 trajectories, generated using the DMFT quantities after the convergence of the algorithm.

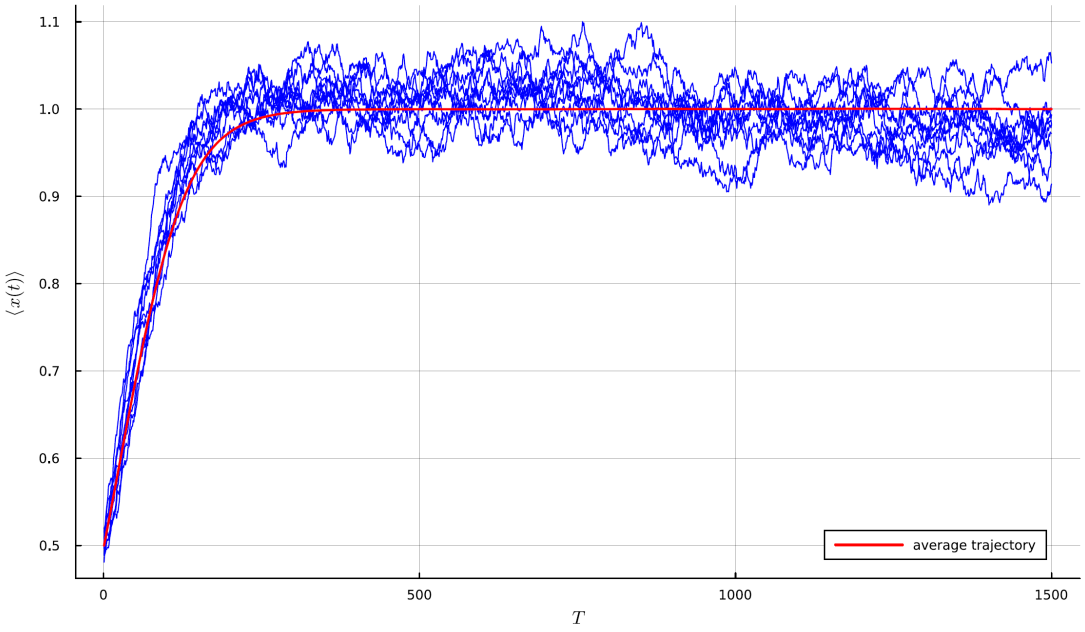

Figure 4.15: Relaxation of $\langle x(t) \rangle$ in the ferromagnetic phase.

As it can be seen in figure 4.16, the ϵ values are quite large during the initial iterations of the algorithm, then decrease to zero as the number of iterations grows; it is safe to say that the algorithm has converged after sixty iterations.

In figure 4.17 the DMFT quantities and the Lagrange multiplier are represented; it can be seen that both the rescaled cavity correlation function and the cavity response function decay to zero, which is a typical behavior for these quantities, as it has been observed also in the previously analyzed dynamics; the cavity mean function and the Lagrange multiplier instead settle to a constant value.

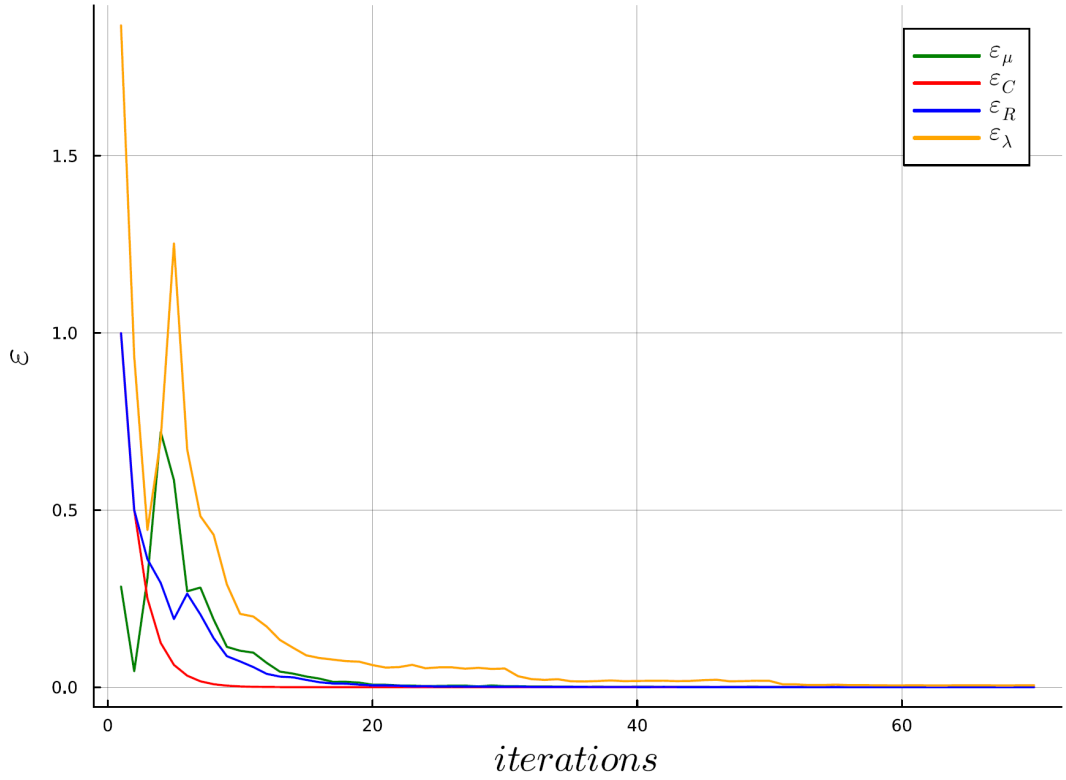

Figure 4.16: ϵ values of the DMFT quantities as a function of the iterations.

To conclude the analysis of the results of the ferromagnetic phase, the results obtained with the DMFT algorithm can be compared with those obtained with direct numerical simulations on random regular graphs. The comparison is presented in figure 4.18: for what concern $\langle x(t) \rangle$ and the Lagrange multiplier, the agreement is perfect; instead, for what concern the correlation function, it is possible to see that the one obtained by direct simulations is affected by fluctuations, but the overall behavior matches the one of the correlation function obtained with the DMFT algorithm. The quality of the results relative to the correlation function could be improved either by simulating the dynamics on a larger graph, or by simulating the dynamics many times on a graph with the same size.

At this point the dynamics of the 2-spin model in the paramagnetic phase can be analyzed; the results in this case have were derived with by choosing the parameters $K = 10$, $J = 1.0$ and $D = 10.0$, with $T = 1500$ and $\Delta = 0.01$. The initial condition for the generation of the trajectories in this phase was set to $x(0) = \delta$, with δ being a value sampled from a standard distribution. The DMFT quantities computed by

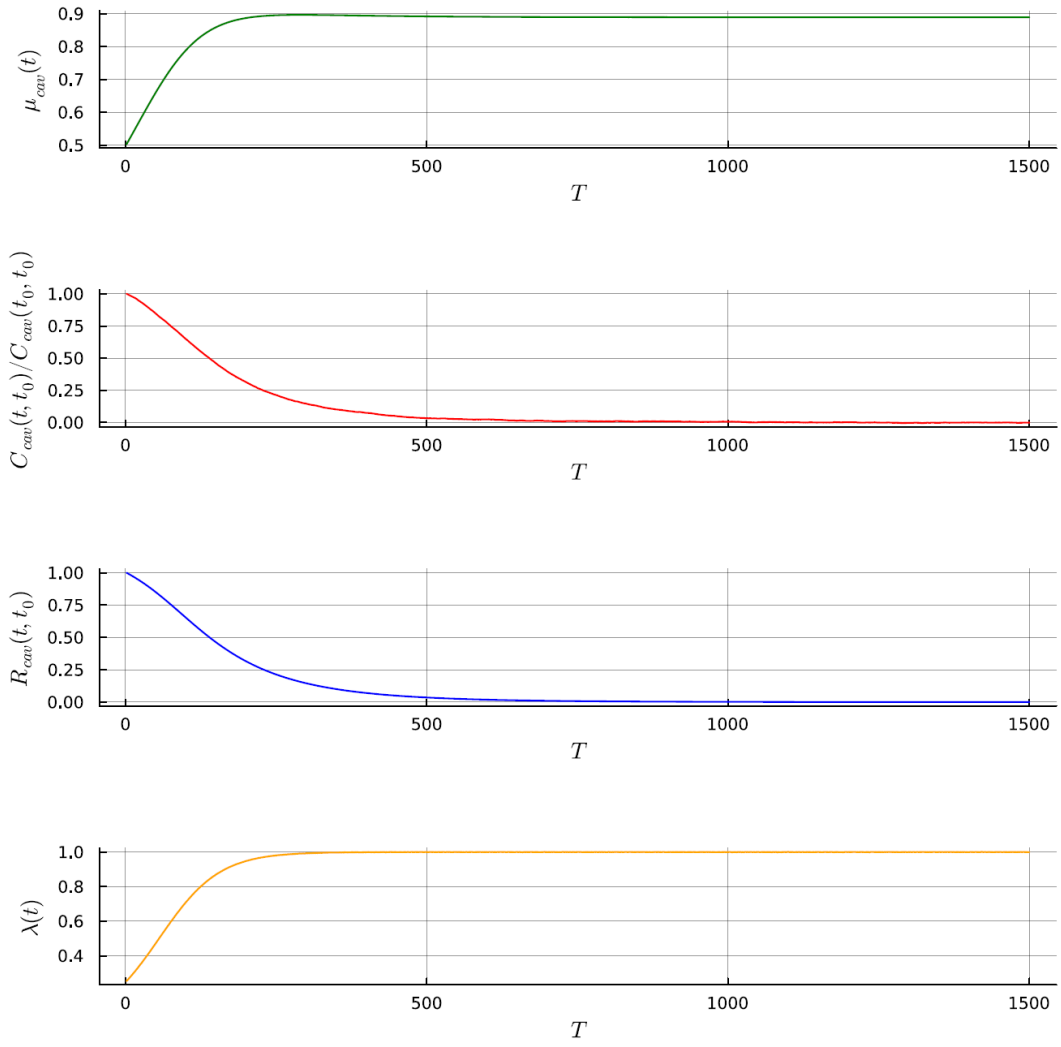

Figure 4.17: DMFT quantities of the 2-spin model in the ferromagnetic phase.

the algorithm were derived with the following settings for what concern α, N_{traj} and the number of iterations: 30 iterations generating 10^3 trajectories with $\alpha = 0.5$; 20 iterations generating 10^4 trajectories with $\alpha = 0.7$; 20 iterations generating 10^4 trajectories with $\alpha = 0.8$; 20 iterations generating 10^4 trajectories with $\alpha = 0.9$; 20 iterations generating 10^5 trajectories with $\alpha = 0.95$. The reason behind these choices for α, N_{traj} and the number of iterations can be found in the the fact that the parameter D is large; this is necessary to observe the paramagnetic phase, as suggested from the density plot on the right of figure 4.14, however, it has important consequences on the convergence process of the algorithm and on the

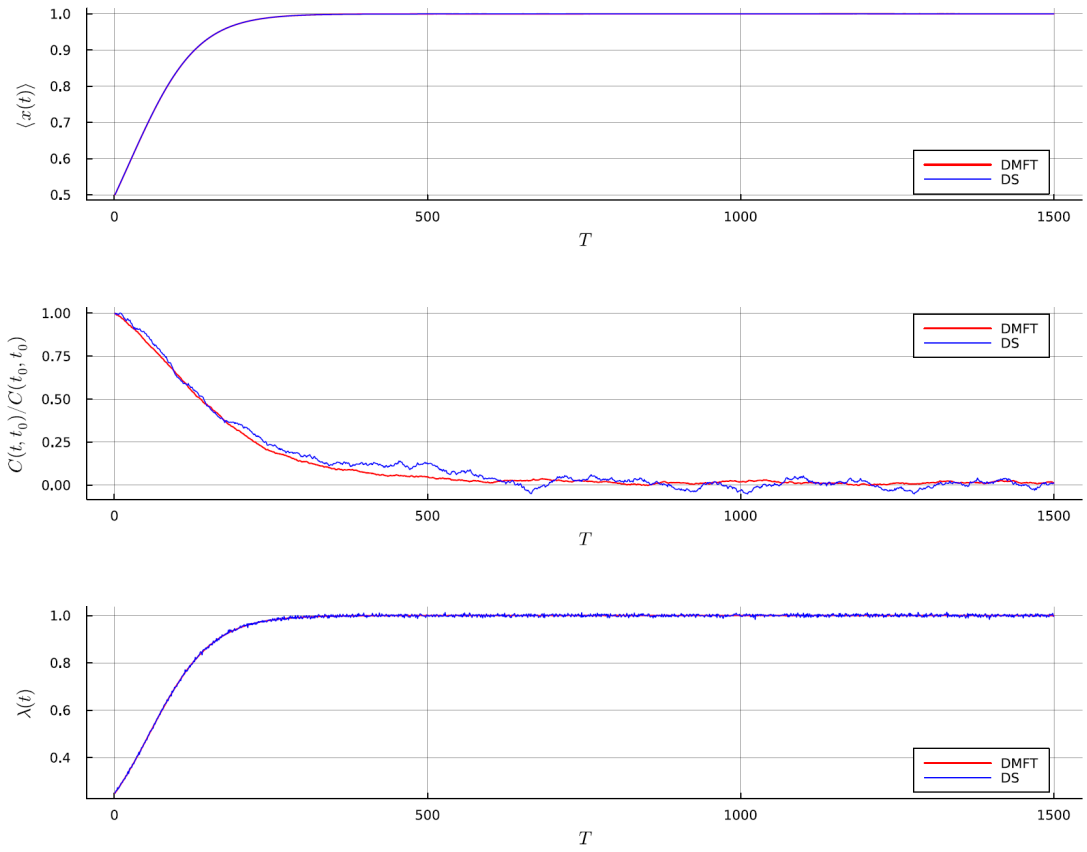

Figure 4.18: Comparison between the data obtained by means of direct simulations of the dynamics and the data obtained with the DMFT algorithm in the ferromagnetic phase; the covariance function is rescaled by its value at the initial time $t_0 = 0$.

quality of the results: large fluctuations associated to the noise are responsible for large fluctuations of the Lagrange multiplier and of the DMFT quantities from iteration to iteration, as it can be seen from the ϵ values showed in figure 4.20; this effect can be mitigated by increasing N_{traj} and by increasing the number of iterations; moreover, it helps to progressively reduce the soft-update parameter α to smooth the variations of the quantities of interests and refine their estimates.

In figure 4.19 the average trajectory is showed in red, while the ones in blue are the usual ten sample trajectories chosen from the set used to obtain the average. As it is possible to see, the trajectories in blue are characterized by very large fluctuations and this is coherent with the fact that the parameter D of the noise was set to a large value. In figure 4.21 the DMFT quantities and the Lagrange

multiplier obtained by the algorithm are presented: the cavity mean, as expected, is very close to zero; both the rescaled cavity correlation function and the cavity response function decay to zero, as observed also in the other analyzed dynamics; the Lagrange multiplier settles to a value close to one, but it is characterized by relatively large fluctuations, which are coherent with the fluctuations of the trajectories. To conclude the analysis, it is possible to consider the comparison of the results pictured in figure 4.22: it can be observed that there is agreement for what concern the average trajectory and the rescaled correlation function; instead, for what concern the Lagrange multiplier, the agreement is less clear to establish, due to the large fluctuations of the results obtained with direct simulations.

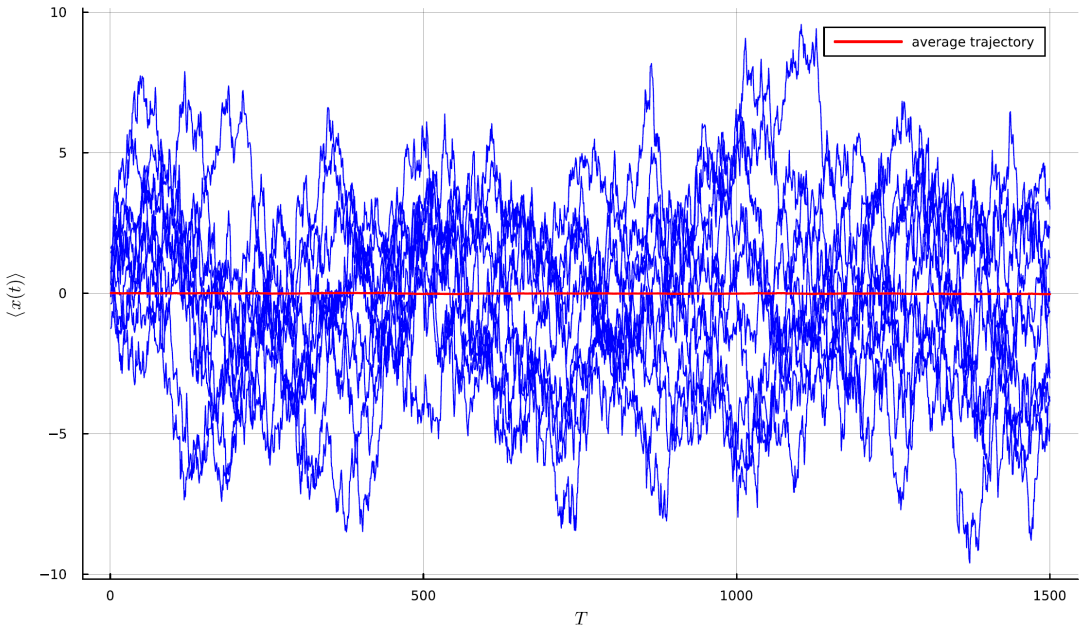

Figure 4.19: Relaxation of $\langle x(t) \rangle$ in the paramagnetic phase.

4.5 The 2-spin model with disorder

4.5.1 Presentation of the model

By introducing disorder in the 2-spin model it is possible to really appreciate the effectiveness of the DMFT approach. The starting point is nothing but the Hamiltonian which has already been introduced during the analysis of the 2-spin model without disorder; therefore, the equation describing the dynamics of a node simply reads:

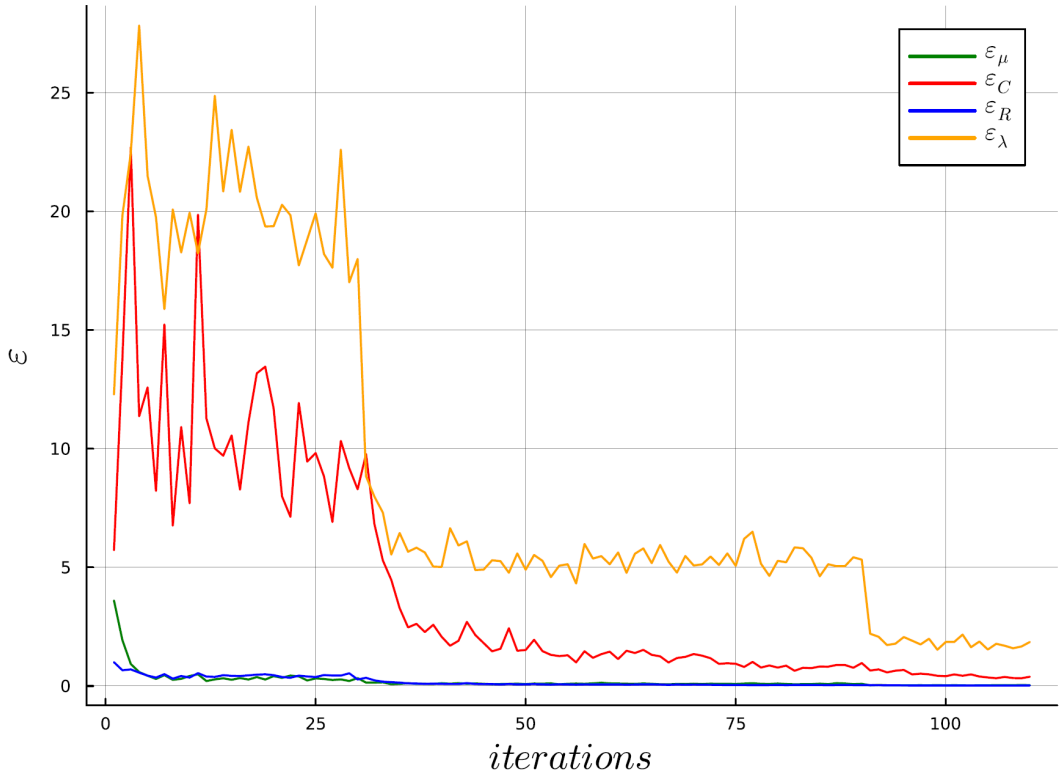

Figure 4.20: ϵ values of the DMFT quantities as a function of the iterations.

$$\frac{dx_i}{dt} = \sum_{j \in \partial i} J_{ij} x_j(t) - \lambda(t) x_i(t) + \eta_i(t) \tag{4.45}$$

where $\lambda(t)$ is once again the Lagrange multiplier, whose expression has to be determined in a way analogous to what has already been done in the case without disorder.

The disorder is introduced in this model by choosing to sample each coupling $J_{ij} = J_{ji}$ independently from a symmetric distribution $P(J_{ij}) = \frac{1}{2}\delta(J_{ij} - J) + \frac{1}{2}\delta(J_{ij} + J)$. For this reason it is necessary to perform explicitly the configurational average over the disorder to obtain the effective equations for the dynamics. The introduction of disorder enriches the physical picture of the standard 2-spin model[9][12]; in particular, the system no longer exhibit the equilibrium phases observed in the case with homogeneous couplings, as the trajectories do not converge to a unique value; moreover, the system starts to show glassy features, the easier to observe and investigate being the aging phenomenon: the rugged energy landscape created by the introduction of disorder is responsible for a slow relaxation

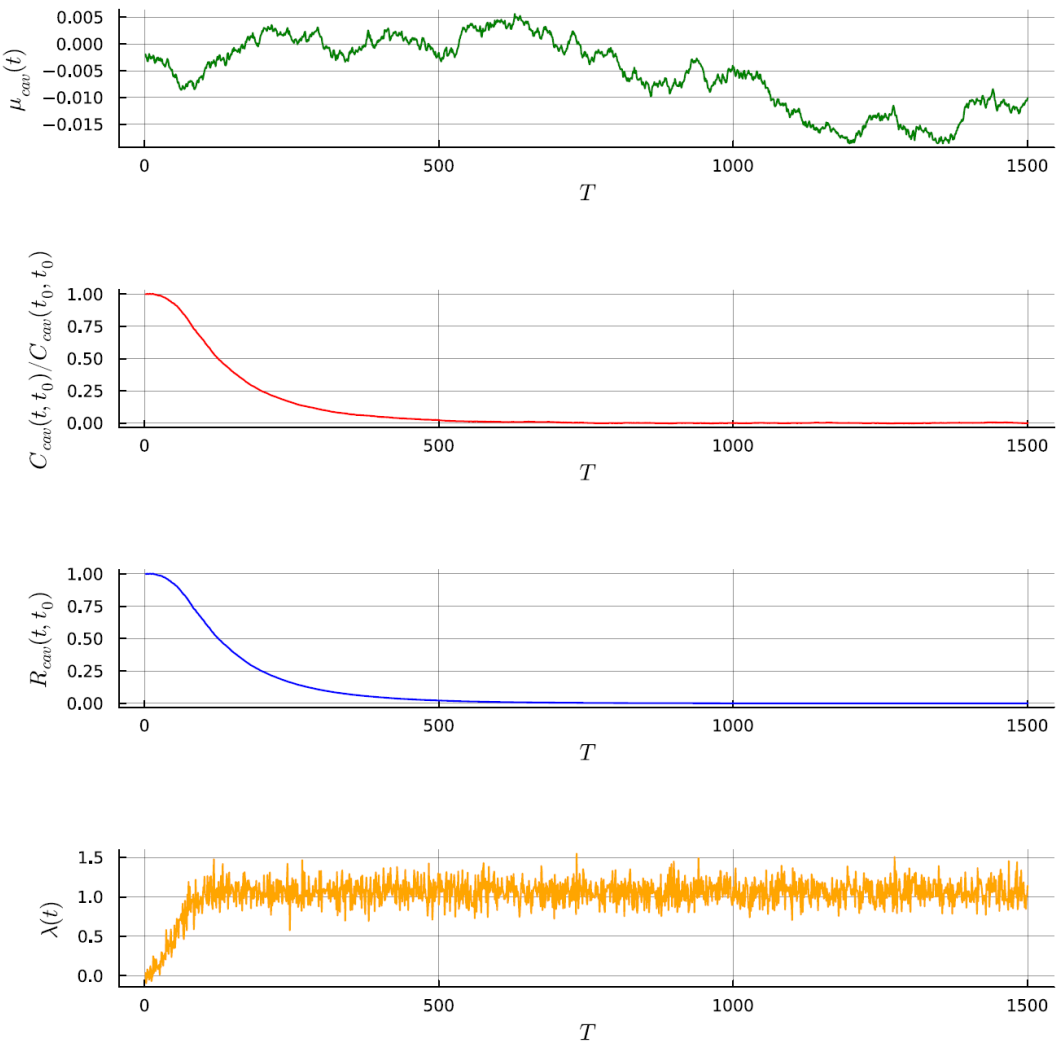

Figure 4.21: DMFT quantities of the 2-spin model in the paramagnetic phase.

dynamics, which keeps memory of how much time the system has already spent in the low temperature phase; the aging behavior can be detected by analyzing the correlation function of the trajectories of the degrees of freedom.

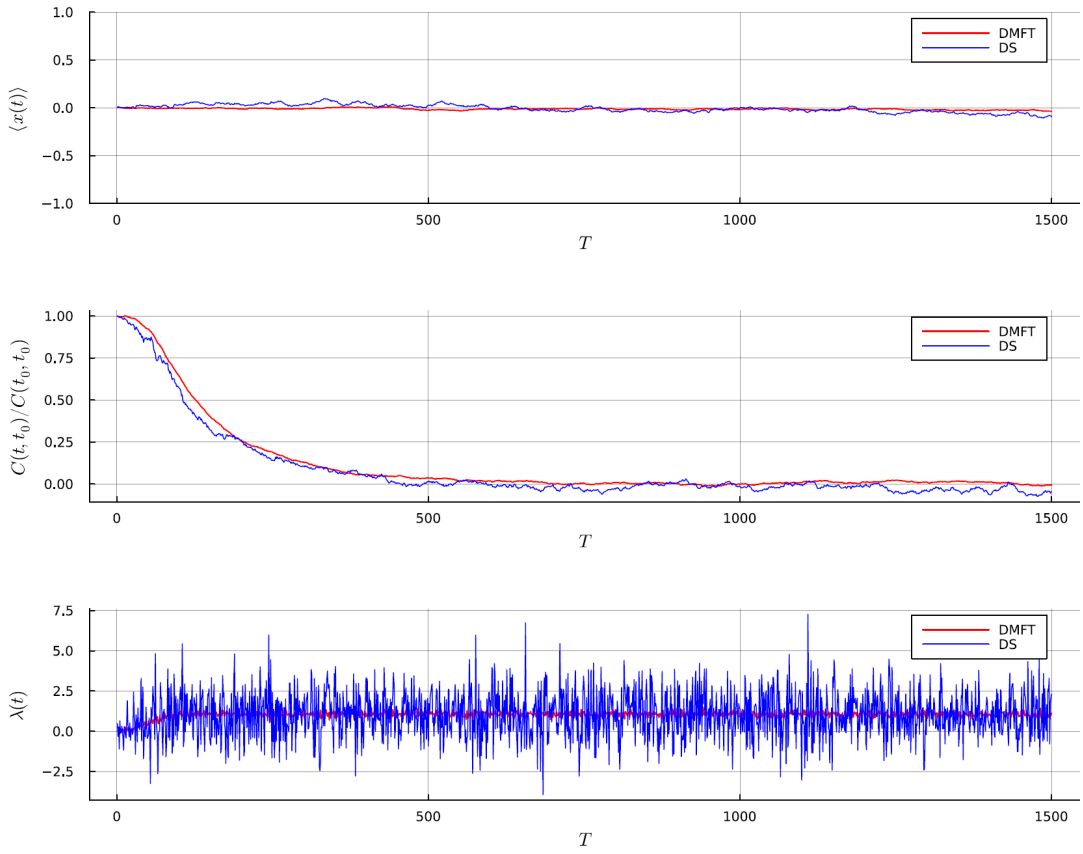

Figure 4.22: Comparison between the data obtained by means of direct simulations of the dynamics and the data obtained with the DMFT algorithm in the paramagnetic phase; the covariance function is rescaled by its value at the initial time $t_0 = 0$.

4.5.2 Derivation of the effective equations of the dynamics in presence of disorder

In order to apply the DMFT algorithm it is necessary to derive a description of the system which is independent on the specific realization of the couplings. To do such a thing, it is necessary to perform a configurational average of the dynamical partition functions Z_{ij}^{cav} and Z_i, before performing the small-coupling expansion, so that the effective equations of the dynamics can be explicitly derived.

As it has been suggested in the previous chapter, one can write:

$$[Z_{ij}^{cav}] = \int \prod_{k \in \partial i \setminus j} dJ_{ik} P(J_{ik}) Z_{ij}^{cav} \tag{4.46}$$

$$[Z_i] = \int \prod_{k\in\partial i} dJ_{ik} P(J_{ik}) Z_i \tag{4.47}$$

For convenience, the general expressions for Z_{ij}^{cav} and Z_i obtained by means of the dynamic cavity approach can be recalled:

$$Z_{ij}^{cav} = \int D\mathbf{x}_i D\hat{\mathbf{x}}_i e^{\sum_n \left\{-i\hat{x}_i^n(x_i^{n+1}-x_i^n-f[x_i^n]\Delta)-g[x_i^n]\Delta(\hat{x}_i^n)^2\right\}} \times \\ \times \prod_{k\in\partial i\setminus j} \int D\mathbf{x}_k D\hat{\mathbf{x}}_k c_{ki}[\mathbf{x}_k,\hat{\mathbf{x}}_k] e^{\alpha\Delta\sum_n (J_{ki} i\hat{x}_k^n x_i^n + J_{ik} i\hat{x}_i^n x_k^n)} \tag{4.48}$$

$$Z_i = \int D\mathbf{x}_i D\hat{\mathbf{x}}_i e^{\sum_n \left\{-i\hat{x}_i^n(x_i^{n+1}-x_i^n-f[x_i^n]\Delta)-g[x_i^n]\Delta(\hat{x}_i^n)^2\right\}} \times \\ \times \prod_{k\in\partial i} \int D\mathbf{x}_k D\hat{\mathbf{x}}_k c_{ki}[\mathbf{x}_k,\hat{\mathbf{x}}_k] e^{\alpha\Delta\sum_n (J_{ki} i\hat{x}_k^n x_i^n + J_{ik} i\hat{x}_i^n x_k^n)} \tag{4.49}$$

where the parameter α appearing in the exponentials associated to the interactions between nearest neighbors is the usual parameter required to perform the small-coupling expansion.

By performing explicitely the configurational averages according to the symmetric distribution, one gets:

$$[Z_{ij}^{cav}] = \int \prod_{k\in\partial i\setminus j} dJ_{ik} \frac{1}{2}\Big(\delta(J_{ik}-J)+\delta(J_{ik}+J)\Big) Z_{ij}^{cav} = \tag{4.50a}$$

$$= \frac{1}{2}\int \prod_{k\in\partial i\setminus j} dJ_{ik}\delta(J_{ik}-J) Z_{ij}^{cav} + \tag{4.50b}$$

$$+ \frac{1}{2}\int \prod_{k\in\partial i\setminus j} dJ_{ik}\delta(J_{ik}+J) Z_{ij}^{cav} = \tag{4.50c}$$

$$= \frac{1}{2} Z_{ij}^{+,cav} + \frac{1}{2} Z_{ij}^{-,cav} \tag{4.50d}$$

$$[Z_i] = \int \prod_{k\in\partial i} dJ_{ik} \frac{1}{2}\Big(\delta(J_{ik}-J)+\delta(J_{ik}+J)\Big) Z_i = \tag{4.51a}$$

$$= \frac{1}{2}\int \prod_{k\in\partial i} dJ_{ik}\delta(J_{ik}-J) Z_i + \tag{4.51b}$$

$$+ \frac{1}{2}\int \prod_{k\in\partial i} dJ_{ik}\delta(J_{ik}+J) Z_i = \tag{4.51c}$$

$$= \frac{1}{2} Z_i^{+} + \frac{1}{2} Z_i^{-} \tag{4.51d}$$

where the expressions of $Z_{ij}^{+,cav}$, $Z_{ij}^{-,cav}$, Z_i^+ and Z_i^- are respectively:

$$Z_{ij}^{+,cav} = \int D\mathbf{x}_i D\hat{\mathbf{x}}_i e^{\sum_n \left\{-i\hat{x}_i^n(x_i^{n+1}-x_i^n-f[x_i^n]\Delta)-g[x_i^n]\Delta(\hat{x}_i^n)^2\right\}} \times \\ \times \prod_{k\in\partial i\setminus j} \int D\mathbf{x}_k D\hat{\mathbf{x}}_k c_{ki}[\mathbf{x}_k,\hat{\mathbf{x}}_k] e^{\alpha\Delta\sum_n (Ji\hat{x}_k^n x_i^n + Ji\hat{x}_i^n x_k^n)} \tag{4.52}$$

$$Z_{ij}^{-,cav} = \int D\mathbf{x}_i D\hat{\mathbf{x}}_i e^{\sum_n \left\{-i\hat{x}_i^n(x_i^{n+1}-x_i^n-f[x_i^n]\Delta)-g[x_i^n]\Delta(\hat{x}_i^n)^2\right\}} \times \\ \times \prod_{k\in\partial i\setminus j} \int D\mathbf{x}_k D\hat{\mathbf{x}}_k c_{ki}[\mathbf{x}_k,\hat{\mathbf{x}}_k] e^{-\alpha\Delta\sum_n (Ji\hat{x}_k^n x_i^n + Ji\hat{x}_i^n x_k^n)} \tag{4.53}$$

$$Z_{i}^{+} = \int D\mathbf{x}_i D\hat{\mathbf{x}}_i e^{\sum_n \left\{-i\hat{x}_i^n(x_i^{n+1}-x_i^n-f[x_i^n]\Delta)-g[x_i^n]\Delta(\hat{x}_i^n)^2\right\}} \times \\ \times \prod_{k\in\partial i} \int D\mathbf{x}_k D\hat{\mathbf{x}}_k c_{ki}[\mathbf{x}_k,\hat{\mathbf{x}}_k] e^{\alpha\Delta\sum_n (Ji\hat{x}_k^n x_i^n + Ji\hat{x}_i^n x_k^n)} \tag{4.54}$$

$$Z_{i}^{-} = \int D\mathbf{x}_i D\hat{\mathbf{x}}_i e^{\sum_n \left\{-i\hat{x}_i^n(x_i^{n+1}-x_i^n-f[x_i^n]\Delta)-g[x_i^n]\Delta(\hat{x}_i^n)^2\right\}} \times \\ \times \prod_{k\in\partial i} \int D\mathbf{x}_k D\hat{\mathbf{x}}_k c_{ki}[\mathbf{x}_k,\hat{\mathbf{x}}_k] e^{-\alpha\Delta\sum_n (Ji\hat{x}_k^n x_i^n + Ji\hat{x}_i^n x_k^n)} \tag{4.55}$$

At this point, to derive the effective equations, it is necessary to perform the small-coupling expansion. The procedure can be done for Z_{ij}^{cav} only, as for Z_i it would almost the same. Hence, it is possible to write:

$$Z_{ij}^{+,cav} = \int D\mathbf{x}_i D\hat{\mathbf{x}}_i e^{\sum_n \left\{-i\hat{x}_i^n(x_i^{n+1}-x_i^n-f[x_i^n]\Delta)-g[x_i^n]\Delta(\hat{x}_i^n)^2\right\}} \times \tag{4.56a}$$

$$\times \prod_{k\in\partial i\setminus j} \int D\mathbf{x}_k D\hat{\mathbf{x}}_k c_{ki}[\mathbf{x}_k,\hat{\mathbf{x}}_k] \Bigg(1 + \alpha\Delta \sum_n (Ji\hat{x}_k^n x_i^n + Ji\hat{x}_i^n x_k^n) + \tag{4.56b}$$

$$+ \frac{1}{2}\alpha^2\Delta^2 \sum_{n,n'} (J^2 i\hat{x}_k^n x_i^n i\hat{x}_k^{n'} x_i^{n'} + J^2 i\hat{x}_i^n x_k^n i\hat{x}_i^{n'} x_k^{n'} + \tag{4.56c}$$

$$+ J^2 i\hat{x}_k^n x_i^n i\hat{x}_i^{n'} x_k^{n'} + J^2 i\hat{x}_i^n x_k^n i\hat{x}_k^{n'} x_i^{n'}) + o(\alpha^2) \Bigg) \tag{4.56d}$$

$$Z_{ij}^{-,cav} = \int D\mathbf{x}_i D\hat{\mathbf{x}}_i e^{\sum_n \left\{-i\hat{x}_i^n(x_i^{n+1}-x_i^n-f[x_i^n]\Delta)-g[x_i^n]\Delta(\hat{x}_i^n)^2\right\}} \times \tag{4.57a}$$

$$\times \prod_{k\in\partial i\setminus j} \int D\mathbf{x}_k D\hat{\mathbf{x}}_k c_{ki}[\mathbf{x}_k,\hat{\mathbf{x}}_k]\Bigg(1-\alpha\Delta\sum_n (Ji\hat{x}_k^n x_i^n + Ji\hat{x}_i^n x_k^n) + \tag{4.57b}$$

$$+\frac{1}{2}\alpha^2\Delta^2\sum_{n,n'}(J^2 i\hat{x}_k^n x_i^n i\hat{x}_k^{n'} x_i^{n'} + J^2 i\hat{x}_i^n x_k^n i\hat{x}_i^{n'} x_k^{n'} + \tag{4.57c}$$

$$+ J^2 i\hat{x}_k^n x_i^n i\hat{x}_i^{n'} x_k^{n'} + J^2 i\hat{x}_i^n x_k^n i\hat{x}_k^{n'} x_i^{n'}) + o(\alpha^2)\Bigg) \tag{4.57d}$$

Therefore, Z_{ij}^{cav} reads:

$$Z_{ij}^{cav} = \frac{1}{2}\Bigg\{\int D\mathbf{x}_i D\hat{\mathbf{x}}_i e^{\sum_n \left\{-i\hat{x}_i^n(x_i^{n+1}-x_i^n-f[x_i^n]\Delta)-g[x_i^n]\Delta(\hat{x}_i^n)^2\right\}} \times \tag{4.58a}$$

$$\times \prod_{k\in\partial i\setminus j} \int D\mathbf{x}_k D\hat{\mathbf{x}}_k c_{ki}[\mathbf{x}_k,\hat{\mathbf{x}}_k]\Bigg(1+\alpha\Delta\sum_n (Ji\hat{x}_k^n x_i^n + \tag{4.58b}$$

$$+ Ji\hat{x}_i^n x_k^n) + \frac{1}{2}\alpha^2\Delta^2\sum_{n,n'}(J^2 i\hat{x}_k^n x_i^n i\hat{x}_k^{n'} x_i^{n'} + J^2 i\hat{x}_i^n x_k^n i\hat{x}_i^{n'} x_k^{n'} + \tag{4.58c}$$

$$+ J^2 i\hat{x}_k^n x_i^n i\hat{x}_i^{n'} x_k^{n'} + J^2 i\hat{x}_i^n x_k^n i\hat{x}_k^{n'} x_i^{n'})\Bigg)\Bigg\} + \tag{4.58d}$$

$$+\frac{1}{2}\Bigg\{\int D\mathbf{x}_i D\hat{\mathbf{x}}_i e^{\sum_n \left\{-i\hat{x}_i^n(x_i^{n+1}-x_i^n-f[x_i^n]\Delta-g[x_i^n]\Delta(\hat{x}_i^n)^2)\right\}} \times \tag{4.58e}$$

$$\times \prod_{k\in\partial i\setminus j} \int D\mathbf{x}_k D\hat{\mathbf{x}}_k c_{ki}[\mathbf{x}_k,\hat{\mathbf{x}}_k]\Bigg(1-\alpha\Delta\sum_n (Ji\hat{x}_k^n x_i^n + \tag{4.58f}$$

$$+ Ji\hat{x}_i^n x_k^n) + \frac{1}{2}\alpha^2\Delta^2\sum_{n,n'}(J^2 i\hat{x}_k^n x_i^n i\hat{x}_k^{n'} x_i^{n'} + J^2 i\hat{x}_i^n x_k^n i\hat{x}_i^{n'} x_k^{n'} + \tag{4.58g}$$

$$+ J^2 i\hat{x}_k^n x_i^n i\hat{x}_i^{n'} x_k^{n'} + J^2 i\hat{x}_i^n x_k^n i\hat{x}_k^{n'} x_i^{n'})\Bigg)\Bigg\} + o(\alpha^2) \tag{4.58h}$$

By grouping together the terms Z_{ij}^{cav} becomes:

$$Z_{ij}^{cav} = \int D\mathbf{x}_i D\hat{\mathbf{x}}_i e^{\sum_n \left\{ -i\hat{x}_i^n (x_i^{n+1} - x_i^n - f[x_i^n]\Delta) - g[x_i^n]\Delta(\hat{x}_i^n)^2 \right\}} \times \tag{4.59a}$$

$$\times \prod_{k \in \partial i \setminus j} \int D\mathbf{x}_k D\hat{\mathbf{x}}_k c_{ki}[\mathbf{x}_k, \hat{\mathbf{x}}_k] \Bigg(1 + \tag{4.59b}$$

$$+ \frac{1}{2}\alpha^2 \Delta^2 \sum_{n,n'} (J^2 i\hat{x}_k^n x_i^n i\hat{x}_k^{n'} x_i^{n'} + J^2 i\hat{x}_i^n x_k^n i\hat{x}_i^{n'} x_k^{n'} + \tag{4.59c}$$

$$+ J^2 i\hat{x}_k^n x_i^n i\hat{x}_i^{n'} x_k^{n'} + J^2 i\hat{x}_i^n x_k^n i\hat{x}_k^{n'} x_i^{n'}) \Bigg) \tag{4.59d}$$

By recalling that the local statistical averages are defined as:

$$\langle \mathcal{O}[\mathbf{x}_k, \hat{\mathbf{x}}_k] \rangle_{\setminus i} = \int D\mathbf{x}_k D\hat{\mathbf{x}}_k c_{ki}[\mathbf{x}_k, \hat{\mathbf{x}}_k] \mathcal{O}[\mathbf{x}_k, \hat{\mathbf{x}}_k] \tag{4.60}$$

and the definition of the messages, it is possible to write:

$$[Z_{ij}^{cav}] = \int D\mathbf{x}_i D\hat{\mathbf{x}}_i \exp\Bigg(\sum_n \Big\{ -i\hat{x}_i^n (x_i^{n+1} - x_i^n - f[x_i^n]\Delta) - g[x_i^n]\Delta(\hat{x}_i^n)^2 \Big\} +$$
$$+ \frac{1}{2}\alpha^2 \sum_{n,n'} \sum_{k \in \partial i \setminus j} J^2 C_{k\setminus i}^{n,n'} i\hat{x}_i^n i\hat{x}_i^{n'} \Delta^2 + \alpha^2 \sum_{n \geq n'} \sum_{k \in \partial i \setminus j} J^2 R_{k\setminus i}^{n,n'} i\hat{x}_i^n x_i^{n'} \Delta^2 \Bigg) \tag{4.61}$$

Similarly for Z_i we have:

$$[Z_i] = \int D\mathbf{x}_i D\hat{\mathbf{x}}_i \exp\Bigg(\sum_n \Big\{ -i\hat{x}_i^n (x_i^{n+1} - x_i^n - f[x_i^n]\Delta) - g[x_i^n]\Delta(\hat{x}_i^n)^2 \Big\} +$$
$$+ \frac{1}{2}\alpha^2 \sum_{n,n'} \sum_{k \in \partial i} J^2 C_{k\setminus i}^{n,n'} i\hat{x}_i^n i\hat{x}_i^{n'} \Delta^2 + \alpha^2 \sum_{n \geq n'} \sum_{k \in \partial i} J^2 R_{k\setminus i}^{n,n'} i\hat{x}_i^n x_i^{n'} \Delta^2 \Bigg) \tag{4.62}$$

The final step for the derivation of the effective equation consists in performing backward the Gaussian integrals associated to the noise term; once that is done, we get the following expressions for the partition functions averaged over all the possible realizations of the couplings:

$$[Z_{ij}^{cav}] = \Bigg\langle \int D\mathbf{x}_i D\hat{\mathbf{x}}_i \exp\Bigg(\sum_n \Big\{ -i\hat{x}_i^n (x_i^{n+1} - x_i^n - f[x_i^n]\Delta +$$
$$- \sum_{n' : n' \leq n} \sum_{k \in \partial i \setminus j} J^2 R_{k\setminus i}^{n,n'} x_i^{n'} \Delta^2 - \Delta\eta_i^n) \Big\} \Bigg) \Bigg\rangle_{\vec{\Delta\eta}} \tag{4.63}$$

$$[Z_i] = \left\langle \int D\mathbf{x}_i D\hat{\mathbf{x}}_i \exp\left(\sum_n \Big\{ -i\hat{x}_i^n (x_i^{n+1} - x_i^n - f[x_i^n]\Delta + \right. \right.$$
$$\left. \left. - \sum_{n':n'\leq n} \sum_{k\in\partial i} J^2 R_{k\setminus i}^{n,n'} x_i^{n'} \Delta^2 - \Delta\eta_i^n) \Big\} \right) \right\rangle_{\vec{\Delta\eta}} \tag{4.64}$$

Finally, the expressions for the effective equations of the 2-spin model, after having averaged over disorder, can be written in discrete time. The equation for the cavity dynamics reads:

$$x_i^{n+1} = x_i^n + f[x_i^n]\Delta + \sum_{n':n'\leq n} \sum_{k\in\partial i\setminus j} J^2 R_{k\setminus i}^{n,n'} x_i^{n'} \Delta^2 + \Delta\eta_i^n \tag{4.65}$$

where the properties of the noise are:

$$\langle \Delta\eta_i^n \rangle = 0 \tag{4.66a}$$
$$\langle \Delta\eta_i^n \Delta\eta_i^{n'} \rangle = 2g[x_i^n]\Delta\delta_{n,n'} + \sum_{k\in\partial i\setminus j} J^2 C_{k\setminus i}^{n,n'} \Delta^2 \tag{4.66b}$$

The equation for the full dynamics instead reads:

$$x_i^{n+1} = x_i^n + f[x_i^n]\Delta + \sum_{n':n'\leq n} \sum_{k\in\partial i} J^2 R_{k\setminus i}^{n,n'} x_i^{n'} \Delta^2 + \Delta\eta_i^n \tag{4.67}$$

where the properties of the noise now are:

$$\langle \Delta\eta_i^n \rangle = 0 \tag{4.68a}$$
$$\langle \Delta\eta_i^n \Delta\eta_i^{n'} \rangle = 2g[x_i^n]\Delta\delta_{n,n'} + \sum_{k\in\partial i} J^2 C_{k\setminus i}^{n,n'} \Delta^2 \tag{4.68b}$$

The parameter α has been set equal to one in the expressions above, as it is no longer necessary.

The equations in continuous time are readily obtained; for the cavity case, one has:

$$\frac{dx_i}{dt} = f[x_i(t)] + \sum_{k\in\partial i\setminus j} \int_0^t dt' J^2 R_{k\setminus i}(t,t') x_i(t') + \eta_i(t) \tag{4.69}$$

where $\eta_i(t)$ is now a colored Gaussian noise with the following moments:

$$\langle \eta_i(t) \rangle = 0 \tag{4.70a}$$
$$\langle \eta_i(t)\eta_i(t') \rangle = 2g[x_i(t)]\delta(t-t') + \sum_{k \in \partial i \setminus j} J^2 C_{k\setminus i}(t,t') \tag{4.70b}$$

For the full case, one has:

$$\frac{dx_i}{dt} = f[x_i(t)] + \sum_{k \in \partial i} \int_0^t dt' J^2 R_{k\setminus i}(t,t') x_i(t') + \eta_i(t) \tag{4.71}$$

where $\eta_i(t)$ is once again a colored Gaussian noise with the following moments:

$$\langle \eta_i(t) \rangle = 0 \tag{4.72a}$$
$$\langle \eta_i(t)\eta_i(t') \rangle = 2g[x_i(t)]\delta(t-t') + \sum_{k \in \partial i} J^2 C_{k\setminus i}(t,t') \tag{4.72b}$$

Since only regular graphs will be considered in the following, it is possible to notice that, taken any node in the graph, the incoming messages from the various edges are exactly the same. Hence, the effective equations of the dynamics introduced above can be simplified; in continuous time the equation for the cavity dynamics reads:

$$\frac{dx}{dt} = -\lambda(t)x(t) + (K-1)\int_0^t dt' J^2 R_{cav}(t,t') x(t') + \eta(t) \tag{4.73}$$

where the properties of the noise are:

$$\langle \eta(t) \rangle = 0 \tag{4.74a}$$
$$\langle \eta(t)\eta(t') \rangle = 2D\delta(t-t') + (K-1)J^2 C_{cav}(t,t') \tag{4.74b}$$

To obtain the equation for the full dynamics it is enough to replace $K-1$ with K:

$$\frac{dx}{dt} = -\lambda(t)x(t) + K\int_0^t dt' J^2 R_{cav}(t,t') x(t') + \eta(t) \tag{4.75}$$

where the properties of the noise are:

$$\langle \eta(t) \rangle = 0 \tag{4.76a}$$
$$\langle \eta(t)\eta(t') \rangle = 2D\delta(t-t') + KJ^2 C_{cav}(t,t') \tag{4.76b}$$

In the expressions above the index i has been dropped, as it is now irrelevant which node is under consideration; moreover, two things have been specified: the term $f[x(t)]$ has been substituted by the typical term of the 2-spin model, where $\lambda(t)$ is the Lagrange multiplier whose explicit expression has to be determined self-consistently; the term $g[x(t)]$ of the noise has been substituted by a constant D.

4.5.3 Derivation of the equation for the Lagrange multiplier in presence of disorder

To analyze this model with the DMFT algorithm it is crucial to derive an expression for the Lagrange multiplier $\lambda(t)$. Let $C(t,t')$ be the two-point correlation function of $x(t)$ in the full dynamics case; namely, $C(t,t') = \langle x(t)x(t')\rangle_K$. The spherical constraint of the 2-spin model forces the correlation function to be equal to one when $t = t'$, that is $C(t,t) = 1$; this translates into the following expression:

$$\left[\frac{dC(t,t')}{dt} + \frac{dC(t,t')}{dt'}\right]_{t,t'=s} = 0 \tag{4.77}$$

which results in:

$$\left[\left\langle \frac{dx(t)}{dt}x(t')\right\rangle_K + \left\langle x(t)\frac{dx(t')}{dt'}\right\rangle_K\right]_{t,t'=s} = 0 \tag{4.78}$$

The two terms can be analyzed one by one:

$$\begin{aligned}\left\langle \frac{dx(t)}{dt}x(t')\right\rangle_K &= -\lambda(t)\langle x(t)x(t')\rangle_K + \\ &+ KJ^2\int_0^t dt''R_{cav}(t,t'')\langle x(t')x(t'')\rangle_K + \langle \eta(t)x(t')\rangle_K\end{aligned} \tag{4.79}$$

For the second term, we have:

$$\begin{aligned}\left\langle x(t)\frac{dx(t')}{dt'}\right\rangle_K &= -\lambda(t')\langle x(t)x(t')\rangle_K + \\ &+ KJ^2\int_0^{t'} dt''R_{cav}(t',t'')\langle x(t'')x(t')\rangle_K + \langle \eta(t')x(t')\rangle_K\end{aligned} \tag{4.80}$$

Hence, by plugging back these two results into (4.78), one gets:

$$-\lambda(s)\langle x(s)x(s)\rangle_K + KJ^2\int_0^s dt''R_{cav}(s,t'')\langle x(s)x(t'')\rangle_K + \langle\eta(s)x(s)\rangle_K +$$
$$-\lambda(s)\langle x(s)x(s)\rangle_K + KJ^2\int_0^s dt''R_{cav}(s,t'')\langle x(t'')x(s)\rangle_K + \langle\eta(s)x(s)\rangle_K = 0 \quad (4.81)$$

By reorganizing the terms and by noticing that $\langle x(s)x(s)\rangle_K = C(s,s) = 1$, we finally obtain the explicit expression for the Lagrange multiplier $\lambda(s)$:

$$\lambda(s) = KJ^2\int_0^s dt''R_{cav}(s,t'')\langle x(s)x(t'')\rangle_K + \langle\eta(s)x(s)\rangle_K \quad (4.82)$$

4.5.4 DMFT algorithm for the 2-spin model in presence of disorder

The algorithm that can be used to analyze the 2-spin model in the presence of disorder is clearly similar to the one outlined for the analysis of the 2-spin model in the absence of disorder; the main difference is that in this case the message μ_{cav} is no longer present, so the steps involving it are obviously modified.

The key quantities of the algorithm here reads:

- C_{cav} and R_{cav}, the desired messages
- λ is the Lagrange multiplier
- C_{cav}^{new} and R_{cav}^{new}, the new messages computed at each iteration of the algorithm
- λ^{new} is the new Lagrange multiplier computed at each iteration of the algorithm
- T, the total number of time steps
- Δ, the size of the time step
- N_{traj}, the number of trajectories that are generated at each iteration for the self-consistent update of the messages and of the Lagrange multiplier
- K, the connectivity of the lattice
- α, the parameter for the soft update of λ, C_{cav} and R_{cav} at each iteration of the algorithm
- $(\epsilon_1, \epsilon_2, \epsilon_3)$, threshold values for the convergence of λ, C_{cav} and R_{cav}

Initialization

Step 0: initialization of the messages and of the Lagrange multiplier
The first step is the initialization of the messages C_{cav} and R_{cav} and of the Lagrange multiplier λ. The initialization of C_{cav} and R_{cav} is trivial: the first can be initialized as a positive definite matrix, while the second can be initialized as a lower triangular matrix. The initialization of the Lagrange multiplier λ can be done with the same approach used for the 2-spin model without disorder: the dynamics can be directly simulated on a small random regular graph, so that the results can be gathered quickly, and then the Lagrange multiplier of the DMFT algorithm can be initialized by setting all its components equal to the value that the Lagrange multiplier computed with the simulation takes after the initial relaxation phase.

Iterative step

Step 1: generation of the trajectories(full dynamics)
A number N_{traj} of trajectories of the noise $\{\boldsymbol{\Delta\eta}_j\}_{j\in\{1,...,N_{traj}\}}$ and N_{traj} trajectories of the degree of freedom $\{\boldsymbol{x}_j\}_{j\in\{1,...,N_{traj}\}}$ according to the effective equation for the full dynamics:

$$x_j^{n+1} = x_j^n - \lambda^{nl} x_j^n \Delta + KJ^2\Delta^2 \sum_{n':n'\leq n} R_{cav}^{n,n'^l} x_j^{n'} + \Delta\eta_j^n \tag{4.83}$$

with $j \in \{1, ..., N_{traj}\}$ and with λ^l, R_{cav}^l and C_{cav}^l being the current values of the Lagrange multiplier and of the DMFT quantities.

Step 2: computation of the new Lagrange multiplier $\lambda^{\mathbf{new}}$
The N_{traj} trajectories of the noise and of the degree of freedom can now be used to compute λ^{new} according to the following equation:

$$\lambda^{n,new} = KJ^2\Delta \sum_{n'=0}^{n} R_{cav}^{n,n'} \frac{1}{N_{traj}} \sum_{j=1}^{N_{traj}} x_j^n x_j^{n'} + \frac{1}{\Delta N_{traj}} \sum_{j=1}^{N_{traj}} \Delta\eta_j^n x_j^n \tag{4.84}$$

where we have exploited the fact that the average $\langle ... \rangle_k$ over the dynamics can be replaced by an average over the trajectories.

Step 3: generation of the trajectories(cavity dynamics)
A number N_{traj} of trajectories of the noise $\{\boldsymbol{\Delta\eta}_j\}_{j\in\{1,...,N_{traj}\}}$ and N_{traj} trajectories of the degree of freedom $\{\boldsymbol{x}_j\}_{j\in\{1,...,N_{traj}\}}$ according to the effective equation for the cavity dynamics:

$$x_j^{n+1} = x_j^n - \lambda^{nl} x_j^n \Delta + (K-1) J^2 \Delta^2 \sum_{n':n' \leq n} R_{cav}^{n,n'^l} x_j^{n'} + \Delta \eta_j^n \tag{4.85}$$

with $j \in \{1, ..., N_{traj}\}$ and with λ^l, R_{cav}^l and C_{cav}^l being the current values of the Lagrange multiplier and of the DMFT quantities.

Step 4: derivation of C_{cav}^{new}
The elements of the matrix C_{cav}^{new} can be computed by means of the trajectories $\{\boldsymbol{x}_j\}_{j \in \{1,...,N_{traj}\}}$ that have been generated as:

$$C_{cav}^{new,n,n'} = \frac{1}{N_{traj}} \sum_{j=1}^{N_{traj}} x_j^n x_j^{n'} - \left(\frac{1}{N_{traj}} \sum_{j=1}^{N_{traj}} x_j^n \right) \left(\frac{1}{N_{traj}} \sum_{j=1}^{N_{traj}} x_j^{n'} \right) \tag{4.86}$$

Step 5: derivation of R_{cav}^{new}
The cavity response function can be computed using the temporal integration approach, which is exact for this particular model. In continuous time the differential equation for $R_{cav}^{new}(t, t')$ reads:

$$\frac{dR_{cav}^{new}(t,t')}{dt} = -\lambda(t) R_{cav}^{new}(t,t') + \\ + (K-1) J^2 \int_0^t dt'' R_{cav}^{new}(t,t'') R_{cav}^{new}(t'',t') + \delta(t-t') \tag{4.87}$$

In discrete time the equation becomes:

$$R_{cav}^{new,n+1,n'} = (1 - \lambda^n \Delta) R_{cav}^{new,n,n'} + \\ + (K-1) J^2 \Delta^2 \sum_{n''=0}^{n} R_{cav}^{new,n,n''} R_{cav}^{new,n'',n'} + \delta_{n,n'} \tag{4.88}$$

Step 6: check for convergence
At this point it is necessary to compare the current messages and the current Lagrange multiplier with the one computed at the steps 2, 4 and 5 and check whether the following conditions are satisfied:

$$\max_{i \in 1,...,T} \{ |\boldsymbol{\lambda}^{new,i} - \boldsymbol{\lambda}^{l,i}| \} \leq \epsilon_1 \tag{4.89a}$$

$$\max_{i,j \in 1,...,T} \{ |C_{cav}^{new,i,j} - {C_{cav}}^{l,i,j}| \} \leq \epsilon_2 \tag{4.89b}$$

$$\max_{i,j \in 1,...,T} \{ |R_{cav}^{new,i,j} - {R_{cav}}^{l,i,j}| \} \leq \epsilon_3 \tag{4.89c}$$

If all these conditions are satisfied, the algorithm stops; otherwise, it proceeds to perform a soft-update of the messages and of the Lagrange multiplier.

Step 7: soft-update of the DMFT quantities and of the Lagrange multiplier
If the check for convergence at step 6 fails, a soft-update of the messages is made, according to:

$$\begin{aligned}\boldsymbol{\lambda}^{l+1} &= \alpha\boldsymbol{\lambda}^{l} + (1-\alpha)\boldsymbol{\lambda}^{new} \\ {C_{cav}}^{l+1} &= \alpha {C_{cav}}^{l} + (1-\alpha)C_{cav}^{new} \\ {R_{cav}}^{l+1} &= \alpha {R_{cav}}^{l} + (1-\alpha)R_{cav}^{new}\end{aligned}$$

The choice of performing a soft-update of the messages is motivated, as for the original algorithm, by the will to avoid large jumps in the space of the messages and of the Lagrange multiplier, which could lead to instabilities in the algorithm.

Conclusion

The algorithm works as follows: it start with the initialization of the quantities of interests; then the steps from 2 to 7 are repeated iteratively, so that the messages and the Lagrange multiplier are updated at each iteration; as soon as the check for convergence succeed, the algorithm stops. If the check for convergence never succeed, the algorithm goes on for a predetermined number of iterations.

4.5.5 Numerical results

The structure for the presentation of the results is the same used for the previous analyzed models, but this time only one set of results has to be showed, since this model is not characterized by different equilibrium phases. However, despite its simplicity, the disordered 2-spin model presents glassy features like that of the aging behavior, which can be investigated using the DMFT algorithm. To see that this model fails to reach an equilibrium, it is enough to see the trajectories presented in figure 4.23; these were obtained by choosing the parameters $K = 10$, $J = 1.0$ and $D = 0.01$, with the coupling constant being rescaled by $\sqrt{K}$. The parameters for the integration of the equations were set to $T = 1500$ and $\Delta = 0.01$. For what concerns the parameters α, N_{traj} and the number of iterations, the following choices were made: 100 iterations were made while generating 10^3 trajectories and then 20 iterations while generating 10^4 trajectories; all the iterations were made using $\alpha = 0.9$. The choice of a relatively large soft-update parameter was forced by the fact that any other smaller value caused either the noise covariance matrix G or the cavity correlation matrix C_{cav} to become non positive definite; this choice for

α was responsible for a slower convergence of the algorithm, hence the increase in the number of iterations with respect to the other analyzed models.

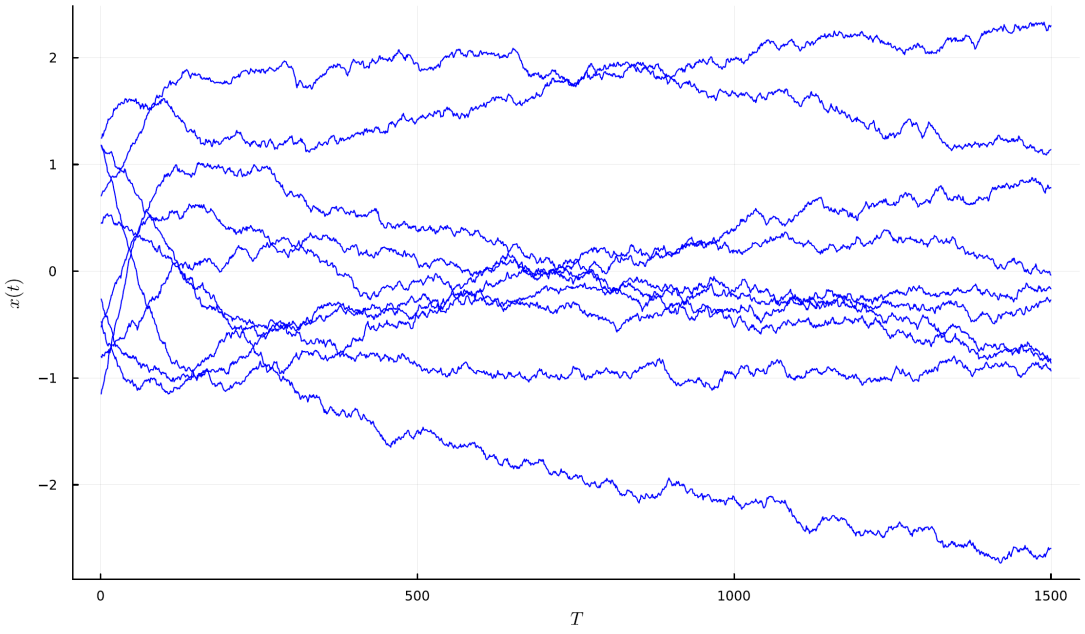

Figure 4.23

As usual, the convergence of the algorithm can be checked by observing the behavior of the ϵ values of the DMFT quantities in figure 4.24: after large variations in the initial fifty iterations, all the ϵ went to zero; hence, it is safe to say that the algorithm has converged.

For what concerns the DMFT quantities computed by the algorithm, it is possible to see in figure 4.25 that both the rescaled cavity correlation function and the cavity response function are characterized by the usual profile in which they decay to zero; instead, for what concerns the Lagrange multiplier, it has reached a constant value with a smooth profile.

To validate the results obtained by the algorithm, it is useful to compare the correlation function of the trajectories generated by the algorithm at convergence and the Lagrange multiplier with the ones obtained by direct numerical simulations; as it is possible to see from figure 4.26, the agreement between the results is almost perfect.

To conclude the analysis of the 2-spin model with disorder, the results obtained investigating the aging phenomenon presented in figure 4.27 can de discussed. To obtain these result. the DMFT algorithm was run for different values of the

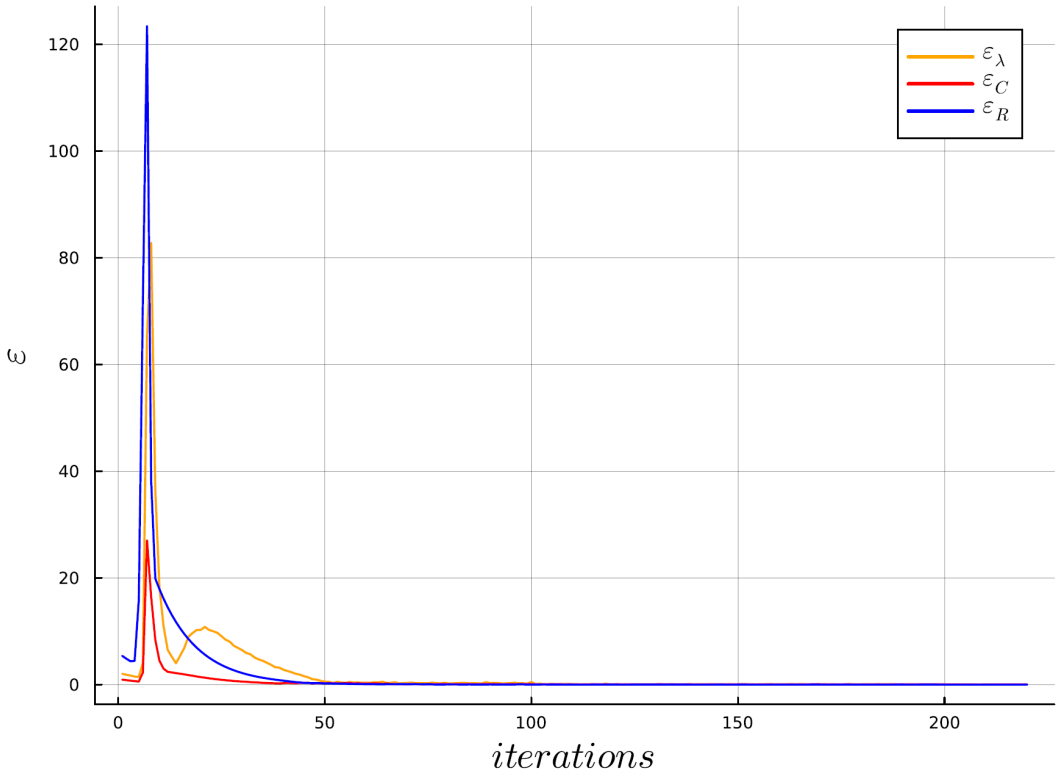

Figure 4.24: ϵ values of the DMFT quantities as a function of the iterations.

connectivity K, while keeping the same coupling constant, which was fixed to $J = 1.0$. In order to observe aging, it was necessary to consider a relatively large Δ and also a large T, so that the value of τ could range from 10^{-1} up to at least 10^2; to do this, it was necessary to modify the algorithm by implementing a time-slicing approach: this means that the convergence is not reached directly on the entire time window of length T, but starting from a much smaller time window which is progressively increased up to the value T. The procedure can be clarified as follows: the original time window T was partitioned in a number Q of smaller slices $\{T_1, ..., T_Q : \sum_{q=1}^{Q} T_q = T\}$; the algorithm started from the initial slice T_1 by generating the trajectories and by updating the DMFT quantities until convergence was reached on this first slice; then, the trajectories were generated over the new increased time slice $T_1 + T_2$ and the DMFT quantities were updated as well until convergence was reached over $T_1 + T_2$; the procedure went on until convergence was reached over the entire time window of interest $T = \sum_{q=1}^{Q} T_q$. To obtain the results presented in figure 4.27, the full time window was set to $T = 1500$, with $\Delta = 0.1$; the time window pas partitioned into smaller slices, with $T_q = 100$ for each

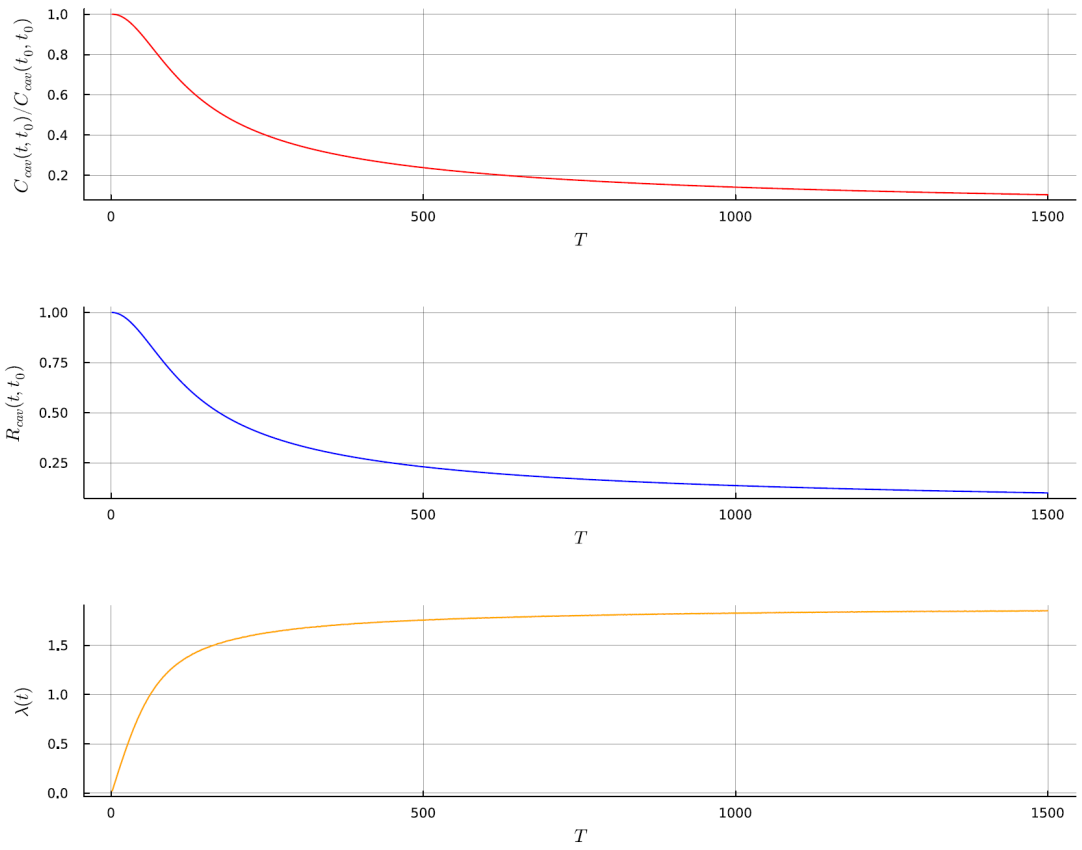

Figure 4.25: DMFT quantities of the disordered 2-spin model.

$q \in \{1, ..., Q\}$; in each time slice, the soft-update parameter was set to $\alpha = 0.95$ for 80 iterations generating 10^3 trajectories and to $\alpha = 0.99$ for 50 iterations generating 10^4 trajectories. The parameter of the noise was set to $D = 0.3$ and the initial conditions for the trajectories were chosen as $x(0) = \delta$, with δ being a normal standard random variable.

To make the figure 4.27, the DMFT quantities computed by the algorithm were used to generate 10^6 trajectories according to the full dynamics defined by equation 4.75, and then these were used to compute the correlation matrix. The curves in the picture are nothing but the correlation function $C(t_w + \tau, t_w)$, where t_w is the waiting time, that is the time spent in the low-temperature frozen phase. As it is possible to see, for each value of the connectivity showed in the figure, the rate at which the correlation function decay decreases as the waiting time increases, which is coherent with the expectations. Moreover, it is possible to notice that, at

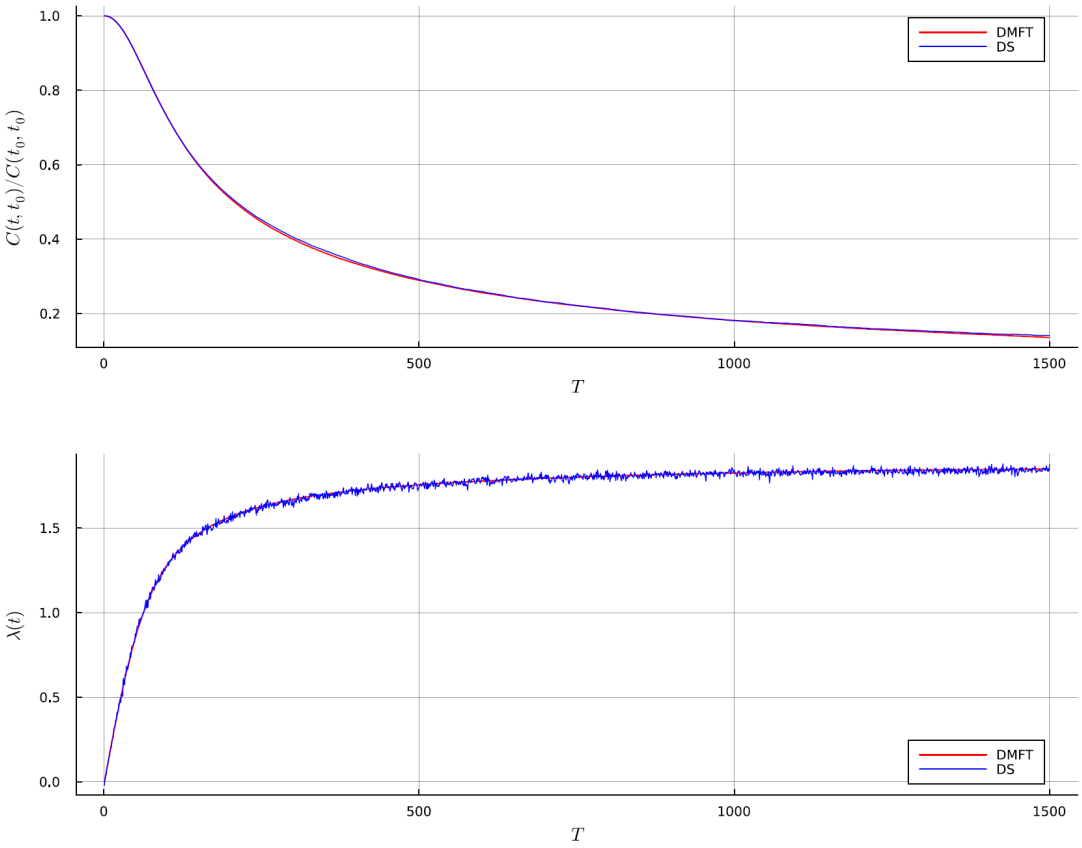

Figure 4.26: Comparison between the data obtained by means of direct simulations of the dynamics and the data obtained with the DMFT algorithm; the covariance function is rescaled by its value at the initial time $t_0 = 0$.

fixed waiting time, the correlation function decays at a rate which decreases as the connectivity of the lattice increases.

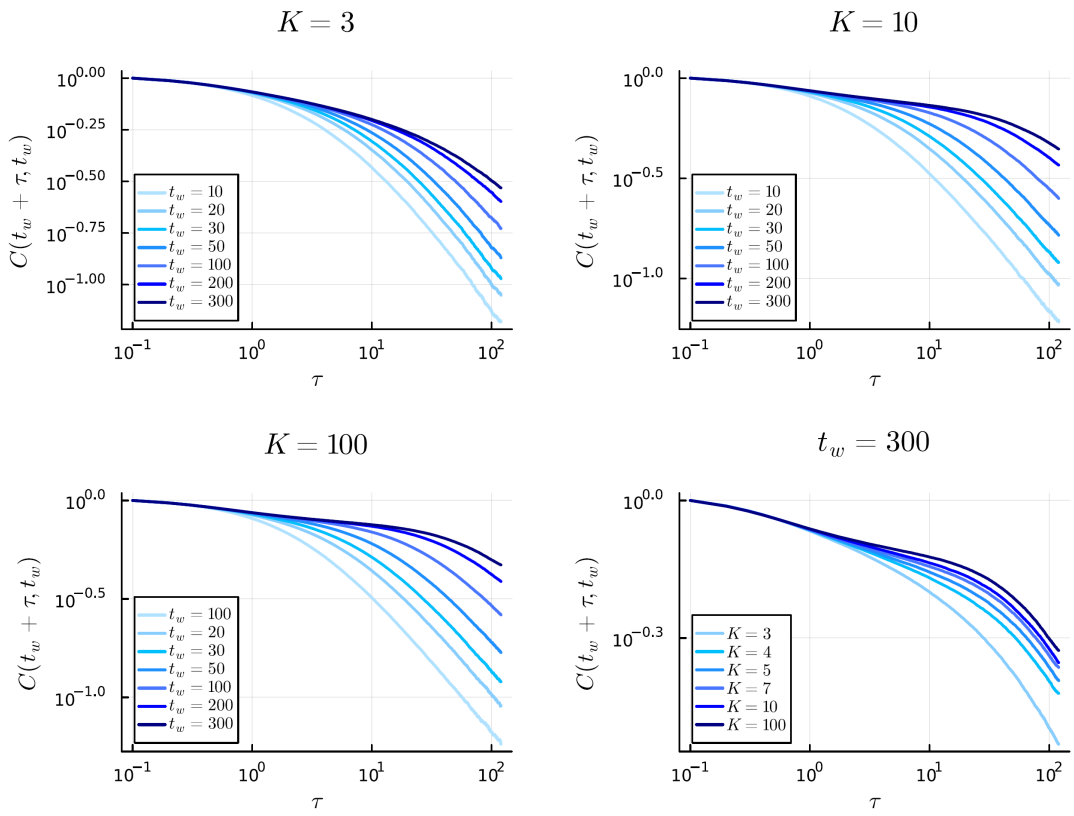

Figure 4.27: Aging in the 2-spin model with disorder: $C(t_w + \tau, t_w)$ is the correlation function computed using the trajectories generated using the DMFT quantities at convergence; $C(t_w + \tau, t_w)$ is presented at fixed connectivity K for different values of the waiting time t_w in the top-left, top-right and bottom-left corners; $C(t_w + \tau, t_w)$ is presented for different connectivity K at fixed waiting time t_w in the bottom-right corner.

Chapter 5

Conclusions and Outlooks

With this last chapter it is possible to sum up the results of this thesis work and make some considerations about further developments. From a theoretical point, it has been showed that cavity approaches allow to analyze classical and quantum systems defined on various lattices at equilibrium, in a way which is theoretically exact and prone to the derivation of intuitive numerical algorithms for the computation of useful local distributions and observables. Moreover, it has been showed that the methodologies of dynamical mean-field approaches can be successfully applied to quantum systems at equilibrium (B-DMFT and F-DMFT) and to classical systems out of equilibrium. For this last class of systems, it has been showed that the recipe based on the dynamical cavity approach and on a small-coupling expansion (or equivalently large connectivity expansion) allows to derive an effective description of the system based on a set of cavity mean functions, cavity correlation functions and cavity response functions.

Depending on the properties of the dynamics that is being analyzed and on also on the properties of the graph, different paths are available. If the dynamics is sufficiently simple and the underlying graph is regular, the system can be described by using a single cavity mean function, a single cavity correlation function and a single cavity response function; these can be computed using the algorithm developed in this thesis, but sometimes approximations are required to compute the cavity response function in closed form, as pointed out during the analysis of the ϕ^4-model. If instead the graph is not regular or the dynamics is not simple enough, it is not possible to make the reductions of the sets of cavity quantities to their respective single quantity; in these cases it is convenient to define distributions for the cavity quantities, which in principle can be obtained using a population dynamics algorithm, deploying similar, but more general, ideas to the ones of the algorithm presented in this thesis.

Now some considerations about the algorithm developed in this thesis can be summed up: it is important to remember that effective equations which provide the theoretical starting point of the algorithm itself have been derived under the assumptions of small-coupling constant or large connectivity; choosing proper values of T and Δ is crucial to avoid divergences of the generated trajectories, but this issue can be overcome by means of the time-slicing approach, at the expense of the efficiency of the algorithm; setting the soft-update parameter is non trivial and requires an analysis based on trial and errors to obtain the optimal value. In conclusion, the algorithm is sufficiently simple and general, so that it can be applied to various dynamics. From a theoretical point of view, exact results could be obtained also for non-linear dynamics, if the generating functional approach could be efficiently implemented; for the moment, approximations are still required, in such a way that the cavity response function can be easily estimated.

A possible improvement in the framework of interest of this thesis could be the development of a population dynamic algorithm able to derive the distributions of the cavity mean function, the cavity correlation function and the cavity response function for the effective description of a dynamics on a graph with a generic connectivity. Such an algorithm would provide a more general approach to tackle problems involving degree heterogeneity and also disorder; however, such an algorithm would require approximation for what concerns the cavity response function; hence, further investigation in the numerical implementation of the generating functional approach are worthy of interest.

Bibliography

[1] G. Semerjian, M. Tarzia, and F. Zamponi. «Exact solution of the Bose-Hubbard model on the Bethe lattice». In: *Physical Review B* (2009) (cit. on pp. 1, 25, 29, 35).

[2] O. Dimitrova and M. Mézard. «The cavity method for quantum disordered systems: from transverse random field ferromagnets to directed polymers in random media». In: *Journal of Statistical Mechanics: Theory and Experiment* volume 2011 (2011) (cit. on pp. 1, 7–9, 19, 22).

[3] F. Krzakala, A. Rosso, G. Semerjian, and F. Zamponi. «Path-integral representation for quantum spin models: Application to the quantum cavity method and Monte Carlo simulations». In: *Physical Review B* (2008) (cit. on pp. 1, 9, 15, 24).

[4] C. Laumann, A. Scardicchio, and S.L. Sondhi. «On quantum spin glasses with finite connectivity: cavity method and applications». In: *Journal of Physics: Conference Series* volume 143 (2009) (cit. on pp. 1, 7, 9).

[5] K. Byczuk and D. Vollhardt. «Correlated bosons on a lattice: Dynamical mean-field theory for Bose-Einstein condensed and normal phases». In: *Physical Review B* (2008) (cit. on pp. 24, 29, 35).

[6] A. Hubener, M. Snoek, and W. Hofstetter. «Magnetic phases of two-component ultracold bosons in an optical lattice». In: *Physical Review B* (2009) (cit. on pp. 24, 29, 35).

[7] P. Anders, E. Gull, L. Pollet, M. Troyer, and P. Werner. «Dynamical mean-field theory for bosons». In: *New Journal of Physics* (2011) (cit. on pp. 24, 29, 35, 42).

[8] A. Altland and B. Simons. *Condensed Matter Field Theory*. Third Edition. Cambridge University Press, 2023 (cit. on pp. 25, 50).

[9] M. Tarabolo and L. Dall'Asta. «Gaussian approximation of dynamic cavity equations for linearly-coupled stochastic dynamics» (cit. on pp. 43, 96).

[10] F. Roy, G. Biroli, G. Bunin, and C. Cammarota. «Numerical implementation of dynamical mean field theory for disordered systems: application to the Lotka-Volterra model of ecosystems». In: *Journal of Physics A: Mathematical and Theoretical* volume 52.48 (2019) (cit. on pp. 43, 56, 62).

[11] F. Aguirre-López. «Heterogeneous mean-field analysis of the generalized Lotka-Volterra model on a network». In: *Journal of Physics A: Mathematical and Theoretical* volume 57.34 (2024) (cit. on p. 53).

[12] L.F. Cugliandolo. «Recent Applications of Dynamical Mean-Field Methods». In: *Annual Review of Condensed Matter Physics* volume 15 (2024) (cit. on pp. 63, 96).